

**Immunohistochemical Localization of I<sub>h</sub> Channel  
Subunits, HCN1-4, in the Rat Brain**

Takuya Notomi

DOCTOR OF PHILOSOPHY

Department of Physiological Sciences

School of Life Science

The Graduate University for Advanced Studies

2003

## CONTENTS

Summary -----	3
Introduction -----	6
Material and Methods -----	10
Results -----	15
Discussion -----	31
Literature Cited -----	40
Figures and Table -----	49

## Summary

Hyperpolarization-activated cation currents, termed  $I_h$ , were discovered in the heart and brain. These currents contribute to various physiological properties and functions, including neuronal pacemaker activity, the setting of resting potential and dendritic integration. The Hyperpolarization-activated and Cyclic-Nucleotide-gated nonselective cation channels (HCNs: HCN1-4), which generate  $I_h$ , have been cloned recently. To understand the functional diversity of  $I_h$  in the brain, precise immunohistochemical localization of all four HCNs is needed. Here I present the distribution and subcellular localization of immunoreactivity for HCNs in the rat brain using newly raised guinea pig polyclonal antibodies against fusion proteins containing rat HCN sequences. Immunoblot analyses of the rat brain with these antibodies showed single bands, which disappeared after adsorption of the antibodies with the respective antigens, suggesting specificity of these antibodies to each HCN subunit.

Then, I performed immunohistochemical investigation of HCNs in the rat brain. Immunoreactivity for all HCN subunits was detected with various intensities in neuropil throughout the brain. For HCN3 and HCN4 but not for HCN1 and HCN2, immunoreactive neuronal cell bodies and processes were clearly visible in light microscopic level in many brain regions. HCN1: Intense HCN1-like immunoreactivity (LI) was observed in the main olfactory bulb, cerebral cortex, lacunosum moleculare (LM) of the hippocampal CA areas, superior colliculus, inferior olive, area postrema, hypoglossal nucleus and molecular layer of the cerebellum. HCN2: HCN2-LI was widely distributed throughout the brain being most intense in the cerebral cortex, thalamus, inferior colliculus, brain stem and granular layer of the cerebellum. The immunoreactivities for HCN1 and HCN2 were overlapped in layer I of the neocortex and the LM of CA areas. In electron microscopic level, immunogold particles for HCN1 and HCN2 were found dense along the plasma membrane of distal dendrites of pyramidal cells in the neocortex and CA1 area. The HCN2-immunopositive small glia-like cells were observed throughout the brain including the white matter. HCN3:

HCN3-LI was mainly distributed in the main and accessory olfactory bulbs, piriform cortex, preoptic area, habenular nuclei, hypothalamus, interpeduncular nuclei and inferior olivary complex. In the flocculus of the cerebellum, intense HCN3-LI was observed in the cholinergic terminal and axon. HCN4: The distribution pattern of HCN4-LI was restricted to the thalamic nuclei and some other regions such as the external plexiform layer of the main olfactory bulb, nucleus of the olfactory tract, fasciculus retroflexus, lateral lemniscus, ventral cochlear nucleus, superior olivary complex and area postrema.

I found that all four HCN-LIs were localized to presynaptic elements as well as to postsynaptic elements. In presynaptic elements, immunoreactivity for HCNs was often found in preterminal and axonal parts rather than axon terminals. For example, in cerebellar basket cells, most of immunogold particles for HCN1 were found in the pons of the basket cell, but only rarely localized to their terminals with symmetrical synapses. I also found immunoreactivity for HCNs in plasma membrane of myelinated axons in various regions including the fasciculus retroflexus and hippocampus.

Next, to identify HCN2-immunopositive small cells, I tried double immunostaining using the guinea pig anti-HCN2 antibody and mouse or rabbit antibodies for various markers including NeuN for matured neurons, GFAP for astrocytes, NG2 for oligoprogenitors, Iba1 for microglia-macrophages, and GST- $\pi$  for oligodendrocytes. I found that all of the HCN2-positive cells were labeled only for GST- $\pi$  throughout the brain except the amygdaloid areas and cingulate, piriform, and lateral entorhinal cortices, where I found only single labeled cells GST- $\pi$ . In addition, some of the double-immunopositive cells were particularly close to neuronal cell bodies and processes in the hippocampal pyramidal cell layer and cerebellar granule cell layer. In electron microscopic level, the HCN2-immunopositive cells had some clumps of heterochromatin along nuclear membrane and those clumps were eccentrically located in the soma, having similar properties to those of previously described perineuronal oligodendrocytes. These results suggest that HCN2-immunopositive small

cells belong to a subpopulation of oligodendrocytes, including perineuronal oligodendrocytes.

In conclusion four HCNs have distinct distribution patterns in neuropil and neuronal cell bodies throughout the brain consistent with the reported patterns of distribution of mRNAs for HCNs. My results indicate that HCNs are localized not only in somato-dendritic compartments, but also in axonal compartments of neurons. The HCN1 and HCN2 are co-localized in the hippocampus and neocortex and had similar distribution patterns in electron microscopic level, suggesting that these subunits could form the heteromeric channels. Interestingly, HCN2 is extensively expressed in a subpopulation of oligodendrocytes including perineuronal oligodendrocytes. These results support previous electrophysiological findings and further suggest diversified roles of  $I_h$  channels in the brain, which are not yet fully identified.

## Introduction

Hyperpolarization-activated cation currents ( $I_h$ ) are observed in the heart (DiFrancesco, 1993) and brain (Pape, 1996). In spontaneously firing nerve and muscle cells,  $I_h$  contributes to the pacemaker depolarization that generates rhythmic activity (Luthi and McCormick, 1998). In nonpacing cells, such as hippocampal stratum lucidum interneurons (Chapman and Lacaille, 1999) and hypoglossal nucleus neurons (Thoby-Brisson et al., 2000),  $I_h$  plays a significant role in determining the resting membrane potential of neurons (Pape, 1996; Robinson and Siegelbaum, 2002). In the crayfish neuromuscular junction, presynaptic  $I_h$  has been postulated to enhance transmitter release by increasing the readily releasable vesicle pool by means of cAMP modulation (Beaumont and Zucker, 2000). Moreover, Mellor et al. put forward the provocative idea that the presynaptic  $I_h$  channels are necessary for hippocampal mossy fiber long-term potentiation (LTP) (Mellor et al., 2002). In hippocampal CA1 pyramidal cells,  $I_h$  channels are highly expressed in the distal dendrites and participate in regulating cable properties (Magee, 1998) and temporal summation of excitatory postsynaptic potentials (Magee, 1999).

$I_h$  is a mixed nonselective cation current that typically activates with hyperpolarizing steps to potentials negative to -50 to -70mV and slowly depolarizes the cell toward the equilibrium potential (Pape, 1996). The electrophysiological characterization of  $I_h$  has been prevented by its small magnitude, combined with the presence of overlapping ionic currents that activate over a similar range of potentials, such as inward rectifier  $K^+$  currents, hyperpolarization- $Cl^-$  currents and transient A-type  $K^+$  currents (Pape, 1996; Robinson and Siegelbaum, 2002). Thus,  $I_h$  has often been identified by its sensitivity to low concentrations of external  $Cs^+$ , which produce substantial blockade at a concentration of 1-2 mM. Since  $Cs^+$  inhibits a part of  $K^+$  channels at that concentration, more selective blockers, ZD-7288 and DK-AH269, have been widely used to block  $I_h$  specifically (Robinson and Siegelbaum, 2002). The identified  $I_h$  has been shown to have

differential activation kinetics depending on cell types (Magee, 1998; Santoro et al., 2000). Another characteristic property of  $I_h$  channels is the enhancement of the rate of activation by direct binding of cAMP to the  $I_h$  channels, providing a powerful means to regulate excitability of various neurons (DiFrancesco, 1993; Pape, 1996; Gasparini and DiFrancesco, 1999).

Four members of a gene family encoding the mammalian Hyperpolarization-activated and Cyclic-Nucleotide-gated nonselective cation channels (HCNs: HCN1-4), which generate  $I_h$ , have been cloned (Ludwig et al., 1998; Santoro et al., 1998; Ishii et al., 1999; Seifert et al., 1999). Structurally, each HCN subunit consists of six transmembrane domains with a pore region between S5 and S6 and a cyclic nucleotide-binding domain in the cytoplasmic C-terminal region, having a structure similar to those of cyclic nucleotide-gated channels (Santoro et al., 1998; Ludwig et al., 1999; Santoro et al., 2000; Robinson and Siegelbaum, 2002). Previous studies have suggested that each HCN subunit can form homomeric channels with different functional properties; homomeric channels of HCN1 activate rapidly on hyperpolarization (in tens of milliseconds) and show a minimal response to cAMP (Santoro et al., 1998), while those of HCN2 activate more slowly (hundreds of milliseconds) and are modulated strongly by cAMP (Ludwig et al., 1998). Activation of HCN3 homomeric channels is even slower (Moosmang et al., 2001), and that of HCN4 channels is the slowest (seconds) (Ishii et al., 1999). Homomeric channels of HCN4 also show a strong response to cAMP (Ishii et al., 1999; Seifert et al., 1999). In addition, different HCN subunits can coassemble to form functional heteromers (Chen et al., 2001; Ulens and Tytgat, 2001). Expression of a HCN1-HCN2 tandem dimer (Ulens and Tytgat, 2001) or co-injection of recombinant HCN1 and HCN2 cRNAs to *Xenopus* oocytes (Chen et al., 2001) leads to the formation of  $I_h$  channels with novel properties that are different from the linear sum of independent populations of HCN1 and HCN2 homomers. These HCN1+HCN2 heteromeric channels have more similar properties to native  $I_h$  in CA1 pyramidal neurons than homomeric

HCN1 or HCN2 channels expressed in HEK293 cells (Chen et al., 2001), suggesting that HCN1 and HCN2 coassemble in these neurons.

In situ hybridization studies demonstrate that all four HCN isoforms are expressed in the adult mouse and rat brains with different regional expression patterns (Ludwig et al., 1998; Santoro et al., 1998; Moosmang et al., 1999; Monteggia et al., 2000; Santoro et al., 2000; Bender et al., 2001). The mRNA expression for HCN2 is extensively observed throughout the brain, while those for the other three HCNs are limited and generally complementary to each other. For example, HCN1 mRNA is strongly expressed in the neocortex, hippocampus, cerebellar cortex and superior colliculus, whereas HCN3 mRNA is expressed most prominently in the hypothalamus and HCN4 mRNA is in the medial habenula, thalamus and ventral cochlear nucleus. These differential expression patterns of HCNs may underlie the heterogeneity in native  $I_h$ .

Immunohistochemical localization of HCNs has also been reported in some regions in the brain. In the hippocampus and neocortex, HCN1-like immunoreactivity (LI) is very strong in distal dendrites of pyramidal cells (Santoro et al., 1997; Brauer et al., 2001; Brewster et al., 2002; Lorincz et al., 2002; Vasilyev and Barish, 2002), and was also suggested to be present in axon terminals of hippocampal and cerebellar basket cells (Santoro et al., 1997). The results for HCN2 immunoreactivity are somewhat inconsistent; HCN2-LI was found to be intense in the molecular layer of the dentate gyrus and stratum lucidum of the CA3 area in one report (Vasilyev and Barish, 2002), but only weak to moderate in another (Brewster et al., 2002). Immunoreactivity for HCN4 was generally weak in the hippocampus (Vasilyev and Barish, 2002).

To understand the functional diversity of  $I_h$  in the brain, precise immunohistochemical localization of all four HCNs is needed. In this study,

we present a detailed mapping and subcellular localization of immunoreactivity for HCN1-4 isoforms in the rat brain.

## **Material and Methods**

### **Antibody production and purification**

I developed guinea pig polyclonal antibodies for HCN1 (N12), HCN2 (N21), HCN3 (N31) and HCN4 (N43) using glutathione S-transferase fusion proteins containing the C-terminals of rat HCNs (amino acid residues 850-910 of HCN1 (Accession#: Q9JKB0), 797-862 of HCN2 (Q9JKA9), 719-780 of HCN3 (Q9JKA8) and 1114-1198 of HCN4 (Q9JKA7)) as described earlier (Shigemoto et al., 1997). For immunization, these fusion proteins were purified by sodium dodecyl sulphate-polyacrylamide gel electrophoresis (SDS-PAGE). The gel fragments containing the purified fusion protein were emulsified with Freund's complete (first immunization) or incomplete (second immunization) adjuvant (Nacalai tesque, Kyoto, Japan) and injected subcutaneously into guinea pigs (50-100 µg fusion protein per animal) at intervals of 4 weeks. From antisera collected 2 weeks after the second injection, HCN antibodies were affinity purified, first using Protein G-Sepharose (Amersham Pharmacia Biotech, Upsala, Sweden) and then CNBr-activated Sepharose 4B (Amersham Pharmacia Biotech) coupled to the fusion proteins. Characterization of the HCN1 antibody was also reported previously (Lorincz et al., 2002).

### **Immunoblotting**

Crude membrane fractions of the whole brain were prepared from adult male rats (Sprague-Dawley (SD), Charles River, Yokohama, Japan) as described (Shigemoto et al., 1997). The fractions were separated by 7.0% or 9.0% SDS-PAGE and transferred to polyvinylidene difluoride (PVDF, BioRad, Hercules, CA, USA) membranes. The membranes were blocked with Block-Ace (Dainippon Pharmaceutical, Suita, Japan) and then reacted for 1hr at room temperature with the affinity-purified antibodies for HCNs (0.5µg/ml) or with antibodies adsorbed with respective antigens (10-100µg/ml). The ECL chemiluminescence detection system (Amersham) was used to visualize the reaction.

### **Immunocytochemistry**

To test cross-reactivity of the HCN antibodies to other HCN subunits, we transfected COS-7 cells with cDNA s of mouse HCN1, human HCN2, mouse HCN3 and rabbit HCN4 (HCN1, HCN2 and HCN4 cDNAs: generous gifts from Dr. T. Ishii, Kyoto University; HCN3 cDNA: a generous gift from Dr. K. Kimura, Kyoto University) using Lipofectamine reagent (Invitrogen, CA, USA). Cells were fixed with 4% paraformaldehyde, washed in 25mM phosphate-buffered saline (PBS), pH7.4, and then incubated overnight at 4 °C with HCN antibodies (0.5µg/ml) in PBS containing 0.5% normal goat serum (NGS) and 0.1% TritonX-100. After washes in PBS, the cells were incubated with a goat anti-guinea pig IgG antibody conjugated to Alexa488 (1:500; Molecular Probes, OR, USA) in PBS. All images were obtained using an Olympus Fluoview confocal microscope (FV300-IX; Olympus, Tokyo, Japan).

### **Tissue for immunohistochemistry**

In this study, 15 adult male SD rats, 5-10 weeks of age, were used. The protocol was approved by National Institute for Physiological Sciences's Animal Care and Use Committee. For light microscopy, twelve rats were deeply anesthetized with pentobarbital (50mg/kg body weight), perfused through the aorta with 25mM PBS for 1min, followed by an ice-cold fixative, containing 4% paraformaldehyde, 0.05% glutaraldehyde and 15% saturated picric acid made up in 0.1M phosphate buffer (PB, pH 7.4) for 15-30min. The brains were immediately removed and cut into several blocks.

For electron microscopic observation, the other 3 rats were perfused with 0.9% saline for 1min, followed by a fixative containing 4% paraformaldehyde and 0.05% glutaraldehyde in 0.1M sodium acetate buffer (pH 6.0) for 2 min, and then a fixative containing 4% paraformaldehyde and 0.05% glutaraldehyde in 0.1M sodium borate buffer (pH 8.0) for 1hr. This fixation method gave acceptable ultrastructure and was partly responsible for the

improved sensitivity of detection of GABA and HCN1, as previously described (Sloviter et al., 2001; Lorincz et al., 2002). After the perfusion, the brains were left in the skull for 24h at 4 °C.

### **Immunohistochemistry**

For light microscopy, sections were cut on a freezing microtome at a thickness of 40µm after cryoprotection in 30% sucrose in 0.1M PB at 4°C for 2 overnights and then incubated at 4 °C with the HCN antibodies (1.0µg/ml) in PBS containing 0.1% Triton X-100, 0.25%λ-carrageenan, and 0.5% NGS. After several washes in PBS, the sections were incubated with biotinylated goat anti-guinea pig IgG antibodies (1:200, Vector, CA, USA) at room temperature for 1hr and then with avidin-biotin peroxidase complex (1:100 ABC-Elite; Vector) at room temperature for 1hr. Subsequently, the sections were incubated in 50mM Tris-HCl (pH 7.4) containing 0.025% 3-3-diaminobenzidine tetrahydrochloride (DAB; Dojindo, Kumamoto, Japan), 0.05% nickel chloride and 0.003% hydrogen peroxide.

For fluorescence double labeling experiments, the guinea pig HCN2 (N21) antibody was combined with each of rabbit antibodies to neuronal nuclei (1:500, NeuN; Chemicon, CA, USA), Iba-I (1:500; a generous gift from Dr. S. Kohsaka, National Institute of Neurosciences) and HCN1 (1:200 Alomone, Jerusalem, Israel ), and mouse antibodies to NG-2 (1:500; a generous gift from Dr. J. M. Levine, State University of New York at Stony Brook), GFAP (1:250, Chemicon, CA, USA ) and GST- π (1:500, BD Biosciences, CA, USA). I also used the guinea pig anti-HCN3 (N31) with mouse anti-choline acetyltransferase (1:500, ChAT; Chemicon) or goat anti-vesicular acetylcholine transporter (1:500, VAcHT; Chemicon) antibodies. Secondary antibodies used were Alexa594-conjugated goat anti-guinea pig IgG (1:500), Alexa488-conjugated goat anti-rabbit IgG (1:500) or anti-mouse IgG (1:500), and Alexa488-conjugated donkey anti-goat IgG (1:500). All images were obtained using an Olympus Fluoview confocal microscope (FV300-IX; Olympus). The rabbit anti-HCN1 antibody exhibited the similar

immunostaining to the guinea pig anti-HCN1 (N12) as described in my previous report (Lorincz et al., 2002). One of the primary antibodies was omitted or replaced with normal IgG or serum for control experiments, and no immunofluorescence for the omitted or replaced antibody was detected.

For electron microscopy, coronal sections (50µm thick) were prepared with a microslicer (DTK-1000; Dosaka, Kyoto, Japan), and washed several times in 0.1M PB. PBS, containing 10% NGS and 0.05% Triton-X100, was used to block non-specific binding at room temperature for 1hr, followed by incubation in the primary and secondary antibodies as previously described (Shigemoto et al., 1997; Lorincz et al., 2002). The guinea pig antibodies to HCNs were diluted in PBS containing 10% NGS at final concentrations of 2.0-4.0µg/ml. After washes, the sections were incubated with biotinylated secondary antibodies (1:100; Vector) for immunoperoxidase reaction, or with 0.8nm gold-coupled secondary antibodies (1:100; Aurion, Netherlands) for immunogold reaction, then reacted with the ABC-Elite (Vector) or R-Gent SE-EM (Aurion), respectively. For double immunostaining, the sections were incubated sequentially with (1) a mixture of the guinea pig anti-HCN1 or anti-HCN2 antibodies (2.0-4.0µg/ml) and a mouse antibody to glutamic acid decarboxylase (1:500, GAD; Chemicon) in PBS containing 10% NGS and (2) a mixture of goat anti-guinea pig antibody conjugated with 0.8nm gold particles (1:100; Aurion) and biotinylated goat anti-mouse antibody (1:100; Vector). Subsequently, the sections were reacted with (3) R-Gent SE-EM (Aurion), (4) the ABC-Elite (1:100; Vector) and (5) the DAB-H<sub>2</sub>O<sub>2</sub> solution. After treatment with 1% OsO<sub>4</sub> in 0.1M PB, the sections were stained with uranyl-acetate, dehydrated and flat embedded in Durcupan resin (Fluka, Switzerland). Ultrathin sections were prepared (Ultracut S; Leica, Germany) and examined with a 1200EX electron microscope (JEOL, Tokyo, Japan).

As controls for immunostaining specificity, sections were incubated with the omission of each of the primary antibodies or with antibodies adsorbed

with respective antigens (10-100µg/ml) for 1hr at room temperature. Under these conditions, no specific immunostaining for the respective molecules was observed (data not shown). The anatomic nomenclature of Paxinos and Watson (Paxinos and Watson, 1998) was adopted in most regions of the nervous system.

## Results

### Antibody specificity

The specificity of the affinity-purified antibodies to HCNs was assessed with an immunoblot analysis of crude membrane fractions from the adult rat brain (Fig. 1). The HCN1 and HCN2 antibodies labeled broad bands with a molecular mass of 120 kDa consistent with the previous studies (Lorincz et al., 2002; Ludwig et al., 2003). The HCN3 and HCN4 antibodies gave rise to broad bands around molecular masses of 85 and 140 kDa, respectively, which are consistent with the previous study (Muller et al., 2003). All of the immunoreactivity described here was adsorbed completely by preincubation of the primary antibodies with an excess amount of the respective antigens (Fig. 1; lane Ads). Thus, these antibodies were judged to bind specifically to the respective HCN channel subunits.

To confirm the lack of cross-reactivity of the antibodies among four HCNs, we used HCN-expressing COS-7 cells (Fig. 2). Each HCN antibody reacted only with the corresponding subtype-expressing COS-7 cells.

### Distribution of HCN-LI in the brain

#### General Remarks

The overall distribution patterns of HCN-like immunoreactivity (LI) are shown in parasagittal brain sections (Fig. 3), and the intensity of immunostaining for each HCN in neuropil of brain regions is summarized in Table.1. For HCN3 and HCN4, but not for HCN2, immunoreactive neuronal cell bodies and processes were clearly visible in many brain regions (indicated with C in Table. 1, examples shown in Fig. 4). For HCN2, immunopositive cells smaller than typical neurons were observed throughout the brain (Fig. 4) including the white matter. These cells are oligodendrocytes as shown later.

HCN1: Intense HCN1-LI in neuropil was observed in the main olfactory bulb, cerebral cortex, stratum lacunosum moleculare of the hippocampus,

fornix, superior colliculus, inferior olivary complex, area postrema, hypoglossal nucleus, spinal trigeminal nuclei and cochlear nuclei.

HCN2: HCN2-LI was widely distributed throughout the brain. Intense HCN2-LI in neuropil was observed in the main olfactory bulb, cerebral cortex, globus pallidus, thalamus and extensive regions in the brain stem, especially in the inferior colliculus, superior olivary complex, hypoglossal nucleus, spinal trigeminal nuclei and cochlear nuclei.

HCN3: Intense HCN3-LI in neuropil was found in relatively restricted regions such as the main and accessory olfactory bulbs, piriform cortex, preoptic area, habenular nuclei, hypothalamic regions including the paraventricular nucleus, mammillary nuclei and lateral hypothalamic area, interpeduncular nuclei, tegmental nuclei, raphe nuclei, inferior olivary complex and dorsal cochlear nucleus. Neuronal cell bodies immunopositive for HCN3 were densely found in the amygdaloid nuclei, caudate putamen, ventral pallidum, supraoptic nucleus, paraventricular nucleus, anterodorsal pretecal nucleus and ventral cochlear nuclei.

HCN4: The distribution pattern of HCN4-LI was restricted to some regions including the main olfactory bulb, nucleus of the lateral olfactory tract, thalamus, fasciculus retroflexus and ventral cochlear nucleus. The HCN4-immunopositive cell bodies were dense in the ventral pallidum, lateral and medial substantia nigra, reticular thalamic nucleus, supraoptic nucleus, paraventricular nucleus, arcuate hypothalamic nucleus, lateral hypothalamic area, anterior pretecal nuclei, ventral cochlear nuclei, inferior colliculus, lateral lemniscus, anterior tegmental nucleus, median raphe nuclei, interpeduncular nuclei and red nuclei.

### **Olfactory bulbs and associated regions**

In the glomerular layer of the main olfactory bulb, all HCN-LI except HCN4-LI was intense (Fig. 5). HCN2-LI was found diffusely in the glomeruli, whereas HCN1- and HCN3-immunopositive fine dendritic processes and somata were clearly visible in the glomerular layer. My results for HCN1 was identical to the previous report (Holderith et al.,

2003), describing HCN1-positive periglomerular cells with a thin, aspiny dendrite that branched in one glomerulus. In the external plexiform layer, HCN4-LI was intense and HCN2-LI was moderate. Immunoreactivity for HCN4 had a gradient increasing towards the glomerular layer (Fig. 5). Axon bundle-like structures were strongly labeled for HCN2 and HCN3 in the internal plexiform layer. HCN3-immunopositive axon bundles were also scattered in the granule cell layer (Fig. 5; arrowheads). In the accessory olfactory bulb, all HCN-LI were weak and/or moderate, except for intense HCN3-LI in the internal plexiform layer.

The anterior olfactory nucleus and island of Calleja showed intense HCN1- and HCN2-LIs (Fig. 6). The superficial layer of the border between the dorsal peduncular cortex and tenia tecta, close to the rhinal incisula, showed intense HCN1-LI (Fig. 6). In the piriform cortex, HCN2- and HCN3-LIs were intense in layer Ia, whereas HCN1-LI was intense in layer Ib, II and III (Fig. 6). Interestingly, the nucleus of lateral olfactory tract selectively showed intense HCN4-LI especially in layer I, whereas superficial layers of all regions receiving projections from the main olfactory bulb showed intense HCN3-LI (Fig. 14). Similarly in the olfactory tubercle, intense immunoreactivity for HCN2 and HCN3 was observed in the most superficial layer, which is a continuity of the layer Ia of the piriform cortex, while that for HCN1 was intense in neuropil of the deeper layer (Fig. 12).

### **Cerebral cortex**

In the neocortex, apical dendrites of pyramidal cells were strongly immunopositive for HCN1 and HCN2 in superficial layers (Figs. 7 and 8). The HCN1-labeling intensity increased in distal parts of the dendrites, with dendritic tufts showing the strongest labeling in layer I. Double immunofluorescence revealed extensive colocalization of HCN1 and HCN2 in the distal dendrites (Fig. 8). At the electron microscopic level, immunogold particles for HCN1 (Lorincz et al., 2002) and HCN2 were diffusely distributed to dendritic plasma membrane of pyramidal cells (Fig. 9a). Density of immunogold particles for HCN2 was lower in spines than in

dendritic shafts as found for HCN1 (Lorincz et al., 2002). The cingulate and retrosplenial cortices also showed intense HCN1- and HCN2-LIs in the superficial layers. In the lateral and medial entorhinal cortices, HCN1-LI was intense in layer I. Both HCN3- and HCN4-LIs were weak to moderate in the cortical region.

### **Hippocampus and related regions**

In the CA1 area of the hippocampus, intense HCN1- and HCN2-LIs were observed in the stratum lacunosum moleculare (Fig. 10). Similar to the distance-dependent immunolabeling pattern of cortical pyramidal cells, intense HCN1- (Lorincz et al., 2002) and HCN2-LIs were observed along plasma membrane of the apical dendrites of CA1 pyramidal cells (Fig. 9). The density of labeling was higher in dendritic shafts than in spines. In the CA3 area, intense HCN1-LI and moderate HCN2-LI was observed in the stratum lacunosum moleculare. The pyramidal cell layer of all hippocampal regions exhibited moderate to intense immunoreactivity for HCN1 and HCN2 (Fig. 10), which was extensively overlapped (Fig. 8). At the electron microscopic level, this labeling was found in axons and axon terminals of basket cells making symmetrical synapses on soma of pyramidal cells (Fig. 11). Immunogold particles for HCN1 were often found in preterminal and terminal parts of axons distant from symmetrical synapses (Fig. 11). The stratum lucidum of the CA3 area was immunonegative for all HCNs. In addition, HCN3-immunopositive interneurons were observed in the CA areas being densest in the border of the alveus and CA1 stratum oriens. Interestingly, in the molecular layer of the dentate gyrus, diffuse HCN1-LI in neuropil was observed in the outer two third, whereas HCN3-LI was found in the inner one third (Fig. 10; arrowheads). In the subiculum, intense HCN1- and HCN2-LIs were observed in the superficial portion of the molecular layer. In the presubiculum and parasubiculum, HCN1-LI was intense throughout all layers.

### **Septal, preoptic and amygdaloid regions**

In the lateral septal nucleus, HCN1-LI was intense, and other three HCN-LIs were weak to moderate (Fig. 12). In the medial septal nucleus, immunoreactivity was intense for HCN2 and HCN3, and moderate for HCN1 and HCN4. In the bed nucleus of the stria terminalis, HCN1-LI was moderate to intense. In the nucleus of the diagonal band, immunoreactivity was intense for HCN2 and HCN3, and moderate for HCN1. Intense HCN2-LI was found in the septohippocampal nucleus.

In the preoptic region, distinct immunostaining patterns were found among HCN subtypes. Moderate HCN1-LI was found in the anterodorsal preoptic nucleus. Moderate to intense HCN2-LI was found in the lateral preoptic area and magnocellular preoptic nucleus. Intense HCN3-LI was observed in the anterodorsal preoptic nucleus, lateral preoptic area and magnocellular preoptic nucleus (Fig. 14). For HCN4, the magnocellular preoptic nucleus showed moderate immunoreactivity. Other preoptic regions showed no or weak immunoreactivity for all HCNs.

In the amygdaloid regions, HCN1-LI was moderate to intense in neuropil of all amygdaloid nuclei while other HCN-LIs were generally weak. HCN3-positive cell bodies and processes were found in the medial, cortical and lateral amygdaloid nuclei.

### **Basal ganglia and associated regions**

In the caudate putamen, immunoreactivity in neuropil was intense for HCN2, and moderate for HCN1 and HCN3 (Fig. 12). Some axon bundles penetrating the caudate-putamen were strongly immunostained for HCN1 especially in the medial part (arrow in Fig. 12). For HCN3, some large neuronal cell bodies and processes were strongly immunopositive throughout the caudate putamen while the majority of neuronal cell bodies, presumably medium spiny cells, were labeled only weakly (Fig. 13). Cholinergic interneurons in the caudate putamen are known to express robust  $I_h$  (Kawaguchi, 1992; Momiyama and Koga, 2001). To confirm the identity of the HCN3-positive neurons, we examined colocalization of HCN3

and choline acetyltransferase (ChAT) in these cells (Fig. 13). All of the strongly HCN3-positive cells were also labeled for ChAT and all ChAT-positive cells were labeled for HCN3.

The ventral pallidum showed intense HCN2- and HCN3-LIs, and moderate to intense HCN4-LI. In this region, HCN3- and HCN4-immunoreactive neuronal cell bodies and processes were found. However, in the lateral globus pallidus, only HCN2-LI was intense and other three HCN-LIs were weak to moderate (Fig. 15). The medial globus pallidus showed intense HCN2-LI and moderate to intense HCN3-LI. Intense HCN1-LI was observed in the claustrum. In the substantia nigra pars compacta, immunoreactivity was intense for HCN3, and moderate for other HCNs, while in the substantia nigra pars reticulata, intense HCN2-LI was observed (Figs. 18 and 19). In the lateral and medial parts of the substantia nigra, immunoreactivity in neuropil was intense for HCN2, and moderate for other HCNs. In this region, HCN4- immunoreactive neuronal cell bodies and processes were observed. The ventral tegmental area showed weak to moderate HCN2-LI. In the subthalamic nucleus, immunoreactivity was intense for HCN2 and HCN3, and moderate for HCN4.

### **Thalamic region**

Differential distribution patterns of HCN-LI were observed in neuropil of the thalamic nuclei (Figs. 15-18).

### **Midline group**

The paraventricular nucleus showed intense HCN3-LI and the neighboring paratenial nucleus had intense HCN2- and HCN4-LIs (Figs. 15 and 16). In the reuniens nucleus, intense HCN2-LI, and moderate HCN1-LI were found.

### **Anterior group**

In the anteroventral and laterodorsal nuclei, intense HCN1- and HCN2-LIs were observed (Figs. 15 and 16). The anteromedial nucleus showed intense immunoreactivity for HCN4 especially in the ventral part (Fig. 15). In the

anterodorsal nucleus, immunoreactivity in neuropil was intense for HCN1, HCN2 and HCN3, and moderate for HCN4. In the interanterodorsal, interanteromedial and intermediodorsal nuclei, all four HCN-LIs were moderate to weak.

### **Medial group**

The mediodorsal nucleus had intense HCN2- and HCN4-LIs, and moderate HCN1- and HCN3-LIs (Fig. 16). In the submedius nucleus, HCN2- and HCN4-LIs were intense but no HCN3-LI was detected (Fig. 16).

### **Intralaminar nuclei**

In the centralmedial nucleus and rhomboid nucleus, HCN3-LI was intense, and HCN2-LI was moderate (Figs. 15 and 16). Other intralaminar nuclei showed generally weak to moderate immunoreactivity for HCNs.

### **Lateral group**

In the lateral posterior nucleus, immunoreactivity in neuropil was intense for HCN 1, and moderate for HCN2 and HCN4 (Figs. 17 and 18). Ventrally, it was confluent with the posterior thalamic nuclear group, which exhibited moderate immunoreactivity for HCN1, HCN2 and HCN4. HCN3-LI was generally very weak in the lateral and ventral groups and found moderate only in the suprageniculate nucleus.

### **Ventral group**

The ventral anterior, ventral lateral and ventral posterolateral nuclei showed intense immunoreactivity for all HCNs, except for HCN3 (Figs. 15-17). In the ventral medial nucleus, intense HCN4-LI, and moderate HCN1- and HCN2-LIs were observed. In the ventral posteromedial nucleus, immunoreactivity was intense for HCN2 and HCN4, and moderate for HCN1. The parvicellular part of the ventral posterior nucleus had the most intense HCN4-LI in the brain (Fig. 17), and showed intense HCN2-LI and moderate HCN1-LI.

### **Geniculate complex**

The medial and the dorsal lateral geniculate nuclei showed intense HCN2- and HCN4-LIs, and intense to moderate HCN1-LI (Fig. 18). In the ventral lateral geniculate nucleus, immunoreactivity in neuropil was intense for HCN2. In the intergeniculate leaflet, intense HCN3-LI separated less stained dorsal and ventral parts of the lateral geniculate complex (Fig. 18).

### **Epithalamus**

Intense HCN3-LI was observed throughout the medial and lateral habenula (Figs. 10, 16 and 17). The lateral habenula also had intense HCN2-LI, and the medial edge of the medial habenula showed very strong HCN4-LI (Fig. 17). In the border zone between the medial and lateral habenula, patches of intense HCN1-LI was found (arrow in Figs. 10 and 17). Some moderately immunostained cells were observed for HCN4 in the medial habenula.

### **Ventral thalamus**

The reticular thalamic nucleus showed intense HCN2-LI and moderate HCN3- and HCN4-LIs (Figs. 15 and 16). In this region, HCN4-immunoreactive neuronal cell bodies and processes were found. The zona incerta had intense HCN3-LI and moderate HCN2-LI (Fig. 16).

### **Hypothalamic region**

Most hypothalamic nuclei showed intense immunoreactivity for HCN3 while other HCN-LI was intense only in limited nuclei in the hypothalamus (Figs. 14-18)

The supraoptic nucleus exhibited intense immunoreactivity for HCN3 (Fig. 14), and moderate for HCN2 and HCN4. In this nucleus, some moderately immunostained cell bodies and processes were observed for HCN3 and HCN4.

In the paraventricular nucleus, some intensely immunostained cell bodies and processes as well as neuropil were found for HCN3. The anterior and lateral hypothalamic areas had intense HCN3-LI (Fig. 15). In the suprachiasmatic nucleus, intense HCN3- and HCN4-LIs were observed (Fig. 14).

HCN3-LI was moderate in the ventromedial hypothalamic nucleus and posterior hypothalamic area (Figs. 16 and 17). Intense HCN1-LI was observed around the ventromedial hypothalamic nucleus (Fig. 16). The dorsomedial hypothalamic nucleus showed intense HCN3-LI and moderate HCN1- and HCN2-LIs (Fig. 16). In the arcuate hypothalamic nucleus, the cell bodies and processes showed moderate HCN4-LI.

In the premammillary nucleus, intense immunoreactivity in neuropil was observed for HCN2 and HCN3 (Fig. 17). In the mammillary nuclei, stronger immunoreactivity was observed in the lateral than medial nucleus for HCN2 and HCN3 (Fig. 18). The supramammillary nucleus showed intense immunoreactivity for HCN3 and moderate for HCN2.

## **Sensory brain stem systems**

### **Visual**

Nuclei involved in visual sensory information processing showed various diffuse patterns of HCN-LI (Figs. 19 and 21-25). In the superficial gray layer of the superior colliculus (SC), immunoreactivity in neuropil was intense for HCN1 and HCN3, and moderate for HCN2 and HCN4 (Fig. 19). Interestingly, HCN1-LI in this layer had a gradient increasing towards the surface of the superficial layer, similar to the HCN1 immunostaining pattern in the LM of the hippocampus and layer I of the neocortex. The optic nerve layer showed weak labeling for all HCNs. In the intermediate gray layer of the SC, intense HCN2-LI was homogeneously observed while HCN3-LI exhibited dense network processes (arrows in Fig. 19). This

patch-like staining pattern of the dense network processes is similar to that of serotonergic fibers (Sefton and Dreher, 1995). The intermediate white layer showed moderate HCN2-LI.

In the parabigeminal nucleus, moderate HCN2- and HCN3-LIs were observed. In the nucleus of the optic tract, all HCN-LIs were weak while moderate HCN1- and HCN4-LIs were observed in the medial terminal nucleus of the accessory optic tract. The olivary pretectal nucleus exhibited intense HCN4-LI and moderate HCN3-LI. In the anterior pretectal nucleus, intense immunoreactivity was observed for HCN1 and HCN2 in the dorsal part (Fig. 18). In these regions, intense HCN3 and HCN4-immunoreactive neuronal cell bodies and processes were found (Figs. 4 and 18). The medial pretectal nucleus showed intense HCN3-LI, and moderate HCN2-LI.

### **Somatosensory**

In the somatosensory regions in the brain stem, intense HCN1- and HCN2-LIs were seen in most nuclei.

In the trigeminal mesencephalic nucleus, cell bodies of large neurons were intensely immunoreactive for both HCN1 and HCN2 (Fig. 8). The principal sensory trigeminal nucleus showed intense immunoreactivity for HCN1 (Fig. 22), while the spinal trigeminal nuclei showed intense HCN1- and HCN2-LIs (Figs. 22-25). Dorsally, these HCN-LIs were confluent with those in the paratrigeminal nucleus. Moderate HCN3-LI was concentrated in the marginal layer of the caudal part of the spinal trigeminal nucleus. In the external cuneate, cuneate and gracile nuclei, intense HCN1- and HCN2-LIs and moderate HCN3- and HCN4-LIs were observed.

### **Auditory**

Most nuclei involved in the auditory sensory information exhibited strong HCN-LI. These regions were unique in that the all four HCN-LIs were strongly co-observed.

Intense immunoreactivity in neuropil was observed for all HCNs in the dorsal cochlear nucleus (Fig. 23). Also, distinctly stained cell bodies with

processes for all HCNs were seen in this nucleus. In the ventral cochlear nucleus, large numbers of intensely stained cell bodies for HCN1, HCN3 and HCN4 were observed in the anterior and posterior parts, and all HCN-LIs were intense in neuropil (Figs. 22 and 23). In the granular layer of the cochlear nuclei, immunoreactivity in neuropil was intense for HCN1 and HCN2, and moderate for HCN 3 and HCN4.

The inferior colliculus exhibited intense and homogeneous immunoreactivity for HCN1 and HCN2, and moderate for HCN4 (Fig. 21). HCN3-LI showed a patchy staining pattern of neuropil especially in the dorsal and caudal parts of the inferior colliculus (Fig. 21). The lateral lemniscus and superior olivary complex exhibited intense immunoreactivity for all HCNs (Figs. 21 and 22). In these regions, HCN4-like immunoreactive neuronal cell bodies and processes were found. The nucleus of the trapezoid body showed intense HCN2-LI, and moderate HCN1-, HCN3- and HCN4-LIs. I also observed HCN4-immunopositive neuronal cell bodies and processes in this region. Electron microscopic observation revealed peroxidase reaction endproducts for HCN1 and HCN2 along plasma membrane of cell bodies in this nucleus but no immunoreactivity for these HCNs was observed in the terminal of calyx of Held (data not shown).

### **Vestibular**

Throughout the vestibular nuclei, intense HCN2-LI and moderate HCN1-LI were observed in neuropil, while intense HCN3-LI was restricted to the superior and medial vestibular nuclei (Figs. 22-24). In the medial vestibular nucleus, all HCN-LIs were moderate in the magnocellular part, whereas intense HCN1-, HCN2- and HCN3-LIs were observed in the parvicellular part.

### **Gustatory and visceral**

The nuclei relaying gustatory and visceral information including the nucleus of the solitary tract, parabrachial nuclei and area postrema exhibited intense HCN3-LI (Figs. 24 and 25). In the lateral parabrachial

nucleus, intense HCN1- and HCN2-LI was also observed. The area postrema showed intense immunoreactivity for HCN1 and HCN4 as well as for HCN3.

### **Motor brain stem systems**

In motor nuclei for the eye movement including the abducens, oculomotor and trochlear nuclei, intense HCN2-LI and moderate HCN1- and HCN3-LIs were observed in neuropil. The Edinger-Westphal nucleus showed moderate HCN2-LI. In the facial nucleus, intense HCN1- and HCN2-LIs were observed (Fig. 23). The motor nucleus of the trigeminal nerve had moderate HCN1-LI. In the hypoglossal nucleus, intense immunoreactivity for both HCN1 and HCN2 was observed (Fig. 25). However, no clear colocalization of HCN1 and HCN2 was found in double fluorescence (Fig. 8). In the ambiguous nucleus, intense immunoreactivity for HCN1 and HCN3 in neuropil, and intense HCN1-positive cell bodies and processes were observed. The dorsal motor nucleus of vagus showed intense HCN3-LI.

### **Reticular core**

#### **Periaqueductal gray**

Intense to moderate HCN2-LI was observed throughout the periaqueductal gray (Figs. 19 and 21). In the dorsolateral periaqueductal gray, HCN3-LI was prominently observed (Fig. 19). In the anterior tegmental nucleus, intense HCN4- immunoreactive cell bodies were observed. In the ventral and laterodorsal tegmental nuclei, immunoreactivity in neuropil was intense for HCN3, and moderate for HCN1. In the dorsal tegmental nucleus, intense HCN2- and HCN3-LIs were observed. In the peduncle-pontine tegmental nucleus, intense HCN4-immunoreactive cell bodies and processes were observed. The locus coeruleus showed moderate HCN3-LI.

## **Raphe**

In the raphe nuclei, HCN3-LI was generally strong whereas other three HCN-LIs were moderate to weak (Fig. 21). In the median raphe nucleus, moderate HCN4-LI of cell bodies and processes were found. In the raphe pallidus nucleus, immunoreactivity in neuropil was intense to moderate for HCN3.

## **Interpeduncular nucleus**

The interpeduncular nuclei exhibited the strongest immunoreactivity for HCN3 in the brain (Fig. 19). At the electron microscopic level, HCN3-LI was observed in axon terminals as well as preterminal axons (Fig. 20). In the apical and caudal subnuclei, immunoreactivity in neuropil was intense for HCN2 as well as for HCN3. In caudal and dorsomedial subnuclei, HCN4-immunoreactive cell bodies and processes were found.

## **Reticular formation**

Diffuse immunoreactivity for HCN2 was observed throughout neuropil of pontine and medullary reticular formation (Figs. 21 and 23-25) In the lateral reticular nucleus, intense immunoreactivity was observed for HCN2, and moderate for HCN1 and HCN4 (Fig. 25). The retrorubral field and intermediate reticular nucleus had intense HCN3-LI (Fig. 25). The cuneiform nucleus showed intense HCN3-LI and moderate HCN2-LI (Fig. 21).

## **Pre- and postcerebellar nuclei**

The pontine nuclei showed intense immunoreactivity for HCN1 and HCN2 (Fig. 21). In the inferior olivary complex, very intense immunoreactivity for HCN1 and HCN3, and moderate for HCN2 were observed (Figs. 29 and 30). In the medial inferior olivary nucleus, intense HCN2-LI as well as HCN1- and HCN3-LIs were observed. In the red nucleus, intense labeling for HCN2 was observed in neuropil of the magnocellular and parvicellular parts, while cell bodies and processes showed moderate HCN4-LI (Fig. 19).

## Cerebellum

### Cerebellar cortex

In the molecular layer of the cerebellar cortex, immunoreactivity was intense for HCN1, and moderate for HCN2 and HCN4 (Fig. 26). In the Purkinje cell layer, intense HCN1-LI was observed in ponceau-like structures around Purkinje cells (arrows in Fig. 26). At the electron microscopic level, immunogold particles for HCN1 were mainly found along plasma membrane of GAD-positive basket cell axons but only rarely in basket cell terminals with symmetrical synapses (Fig. 27). In the molecular layer, HCN1-LI was observed in both axons and dendrites making symmetrical synapses, which presumably originate from stellate cells (data not shown). As same in other brain regions, HCN2-immunopositive cells were observed in the granule cell layer (arrowheads in Fig. 26). Interestingly, these cells were not found in the molecular layer. HCN3-LI in the granule cell layer was selectively found very intense in the flocculus followed by the lobule 10 (Figs. 23 and 28). This immunostaining pattern for HCN3 in the flocculus was similar to that of projections from cholinergic neurons (Ojima et al., 1989). Thus, localization of vesicular acetylcholine transporter (VAChT), which is expressed in cholinergic terminals (Gilmor et al., 1996; Yao and Godfrey, 1999) was compared with that of HCN3-LI by double immunofluorescence (Fig. 13). Immunoreactivity for HCN3 and VAChT was extensively overlapped in axonal processes and boutons (Fig. 13). At the electron microscopic level (Fig. 29a), HCN3-labeled boutons contained small round vesicles and had no clear synapses consistent with the previous reports for cholinergic axon terminals (Yao and Godfrey, 1999; Mechawar et al., 2002). These observations suggest that HCN3 is localized to cholinergic projection in the flocculus. In addition, HCN3-labeled terminals with asymmetrical synapses were rarely found in the flocculus but their identity was unknown (Fig. 29b).

### **Deep cerebellar nuclei**

In the cerebellar nuclei, intense HCN1-, HCN2- and HCN4-LIs were observed in neuropil of the interposed and lateral nuclei (Fig. 30). In the medial cerebellar nucleus, immunoreactivity was intense for HCN1 and HCN4, and moderate for HCN2.

### **Fiber tracts**

Some fiber tracts in the brain selectively showed strong immunoreactivity for distinct HCNs. In the internal capsule, cerebral peduncle, pyramidal tract, fornix, precommissural fornix and stria terminalis, HCN1-LI was found intense in some axon bundles (Figs. 16-18). The dorsal fornix had intense immunoreactivity for HCN1 and HCN2. In the fasciculus retroflexus, entire fiber tracts were intensely immunoreactive for HCN3 and HCN4. In the stria medullaris of the thalamus, intense HCN3-LI and moderate HCN2-LI were found in some axon bundles.

At the electron microscopic level, immunoreactivity for HCNs was widely found in myelinated axons (Fig. 31) as well as in unmyelinated axons in various regions. Immunogold particles in the myelinated axons were mainly found along axonal plasma membrane (Fig. 31b)

### **HCN2-immunopositive cells**

To identify HCN2-immunopositive small cells (Fig. 32), we performed double immunofluorescence for HCN2 and various cell markers (Figs. 33 and 34). Firstly, we used the guinea pig antibody for HCN2 and a mouse monoclonal antibody for the neuronal nuclei (NeuN), which is a marker for matured neurons. Cells labeled for HCN2 and NeuN were completely different. Then, anti- GFAP, NG2, IbaI and GST- $\pi$  antibodies were used to identify astrocytes, oligoprogenitors (Dawson et al., 2000), microglia-macrophages (Imai and Kohsaka, 2002) and oligodendrocytes (Tansey and Cammer, 1991; Taniike et al., 2002), respectively. I found colocalization of HCN2 only with GST- $\pi$  throughout the brain, except for some regions such as the cingulate cortex, perirhinal cortex,

periamygdaloid cortex (a caudal part of the piriform cortex), lateral entorhinal cortex, molecular layer of the cerebellum and amygdaloid area (Fig. 34). In these regions, very few HCN2-immunopositive cells were found and most of GST- $\Pi$ -immunopositive cells were single labeled. In other regions, all HCN2-labeled cells were also labeled for GST- $\Pi$ , making a subpopulation of the GST- $\Pi$ -labeled cells. In addition, some of them were particularly close to neuronal cell bodies (Figs. 32 and 34), which looked like perineuronal oligodendrocytes. In the white matter, we found only a few double labeled cells. At the electron microscopic level, immunogold particles for HCN2 were localized along plasma membrane of cell bodies and in endoplasmic reticulum (Fig. 35). HCN2-immunopositive cells close to neurons had some clumps of heterochromatin along nuclear membrane and their nuclei were eccentrically located in soma, having similar morphological properties to those of previously described perineuronal oligodendrocytes (Mori and Leblond, 1970; Miyake and Kitamura, 1992). These results suggest that HCN2-immunopositive small cells are a subpopulation of oligodendrocytes, including perineuronal oligodendrocytes.

## **Discussion**

### **General Remarks**

The present study provides a detailed description of the subtype-specific distribution of HCN-LI in the adult rat brain. In general, HCN1-LI shows predominantly cortical distribution, whereas HCN3- and HCN4-LIs exhibit mainly subcortical distributions especially abundant in the hypothalamic and thalamic regions, respectively. Immunoreactivity for HCN2 has a very widespread distribution throughout the brain. The distribution of HCN-LI is more extensive than that of their mRNAs indicated by previous *in situ* hybridization studies (Moosmang et al., 1999; Monteggia et al., 2000; Santoro et al., 2000). In many regions, we found a strong overlap among the distribution patterns of HCNs. These results suggest that combination of different HCN subtypes supports the various physiological functions of  $I_h$  in the brain. Further, we observed colocalization and very similar ultrastructural distribution of HCN1- and HCN2-LIs in distal dendrites of pyramidal cells in the hippocampal CA1 area and neocortex, suggesting that HCN1 and HCN2 could form heteromeric channels to regulate the dendritic integration (Magee, 1999). In addition, HCN-LI was localized in glutamatergic, GABAergic and cholinergic neurons, suggesting that HCN could work in various kinds of neurons. Ultrastructural examination indicates that HCNs are located not only in somato-dendritic compartments, but also in axonal compartments of neurons. All HCN subtypes are present in various types of presynaptic elements including glutamatergic, GABAergic and cholinergic projections, suggesting a general role of presynaptic HCNs. In addition, we found HCN2-positive subpopulation of oligodendrocytes including perineuronal oligodendrocytes suggesting an unexpected role of  $I_h$  in glial cells.

### **Correlation between localization of HCN mRNAs and HCN-LIs**

High levels of HCN1 mRNA signals were found in the layer V of the neocortex, pyramidal cell layer of the hippocampal CA areas, hilus of the dentate gyrus, Purkinje cell layer of the cerebellum, optic layer of the

superior colliculus, oculomotor nuclei, and hypoglossal nucleus (Monteggia et al., 2000; Santoro et al., 2000). Present results of HCN1-LI localization are in good agreement with those results, except for Purkinje cells where we did not find strong immunoreactivity (data not shown). In some regions, HCN1-LI was intense in dendritic fields such as the layer I of the neocortex, stratum lacunosum moleculare of the CA1 area and superficial gray layer of the superior colliculus, suggesting that the HCN1 protein is mainly transported to the distal apical dendrites.

Immunoreactivity for HCN2 was extensively distributed throughout the brain similar to the distribution of HCN2 mRNA. The HCN2 encoding mRNA was strongly expressed in the mitral cell layer of the olfactory bulb, nucleus of the diagonal band, hippocampal CA3 area, thalamic region, subthalamic nucleus, mammillary nuclei, hypoglossal nucleus, trapezoid body and cochlear nuclei (Monteggia et al., 2000; Santoro et al., 2000). In the present study, we found intense HCN2-LI in neuropil of all of these regions.

Expression of HCN3 mRNA was generally weak in the brain but prominent in restricted nuclei such as the glomerular layer of the main olfactory bulb, paraventricular supraoptic and mammillary nuclei of the hypothalamus and paraventricular thalamic nucleus (Monteggia et al., 2000). In the present study, HCN3-LI was very strong in these nuclei as well as in the piriform cortex, inferior olivary complex and interpeduncular nuclei. Since intense HCN3-LI was often found in regions where other three HCNs were not expressed or only weakly expressed, HCN3 may have a unique role among HCN subunits.

The HCN4 mRNA is strongly expressed in the mitral cell layer of the olfactory bulb, anterodorsal, laterodorsal, ventroposterior nuclei of the thalamus, and medial habenular nucleus (Monteggia et al., 2000; Santoro et al., 2000; Ludwig et al., 2003). Consistent with these studies, we found very

intense HCN4-LI in the thalamic nuclei, but not in the mitral cell layer and medial habenular nucleus. Instead, very strong HCN4-LI was observed in an external part of the external plexiform layer of the olfactory bulb and fasciculus retroflexus. As described above, HCN-LI was not observed in some regions where the respective HCN mRNAs are strongly expressed. This discrepancy can be partly due to transport of HCN proteins to axons as discussed later.

### **Relationships between HCN localization and electrophysiological function**

$I_h$  has been identified in numerous cell types in the brain, including neurons in the olfactory bulb (Cadetti and Belluzzi, 2001), neocortex (Berger et al., 2001), hippocampus (Magee, 1999), caudate putamen (Momiyama and Koga, 2001), amygdala (Womble and Moises, 1993), nucleus of accumbens (Uchimura et al., 1990), thalamus (Ludwig et al., 2003), hypothalamus (Kamondi and Reiner, 1991), ventral tegmental area (Jiang et al., 1993), superior colliculus (Saito and Isa, 1999), substantia nigra (Washio et al., 1999), mesencephalic trigeminal nucleus (Khakh and Henderson, 1998), inferior olivary complex (Bal and McCormick, 1997), dorsal raphe (Jolas et al., 2000), lateral lemniscus (Fu et al., 1997), area postrema (Funahashi et al., 2002), nucleus of the solitary tract (Iwahori et al., 2002), hypoglossal nucleus (Parkis and Berger, 1997) and cerebellum (Li et al., 1993; Dieudonne, 1998). In the present study, all of these regions showed one or more HCN-LIs.

The importance of  $I_h$  for neuronal rhythmic activity has been well investigated in the thalamic region (McCormick and Bal, 1997; Robinson and Siegelbaum, 2002), where it contributes to spindling, a form of synchronized network activity during slow wave sleep. The slow decay of  $I_h$  over several seconds determines the duration of the interburst interval. Recently, it is reported that in the dorsal lateral geniculate nucleus, thalamocortical neurons of HCN2-deficient mice show a strong reduction of  $I_h$ , suggesting that  $I_h$  in thalamocortical cells is predominantly generated by

HCN2 (Ludwig et al., 2003). In the present study, prominent immunoreactivity for HCN4 as well as HCN2 was detected in most thalamic nuclei including the lateral geniculate nucleus. Furthermore, immunoreactivity for HCN2 and HCN4 was localized to postsynaptic elements in the dorsal lateral geniculate nuclei as confirmed with electron microscopic observation (data not shown). I do not have a good reason why HCN2 but not HCN4 mainly contributes to the rhythmic firing potential. One reason for this might be more hyperpolarized potentials required for the activation of HCN4 compared with HCN2 in these neurons. In fact, the residual  $I_h$  in HCN2-deficient mice was activated at more hyperpolarized potentials in contrast to that in wild type mice (Ludwig et al., 2003). In the ventrobasal thalamic region, vasoactive intestinal polypeptide (VIP) and pituitary adenylate cyclase-activating polypeptide (PACAP) activate  $I_h$  mediated by cAMP (Sun et al., 2003), similar to the effects of 5-HT and noradrenaline on  $I_h$  (McCormick and Pape, 1990). These effects might be another possibility for the increase of HCN4 activation, since HCN4 shows the strongest response to cAMP among all HCNs in a heterologous expression system (Moosmang et al., 2001).

### **HCN in presynaptic elements (axons and axon terminals)**

Previously, electrophysiological studies have demonstrated the presence of  $I_h$  in a number of presynaptic terminals, including crayfish neuromuscular junction (Beaumont and Zucker, 2000), cerebellar basket cell terminals (Southan et al., 2000), and the calyx of Held in the medial nucleus of the trapezoid body (Cuttle et al., 2001). My findings are somewhat different from these electrophysiological results. I hardly observed HCN-LIs in both the terminals of cerebellar basket cells and the calyx of Held, though immunoreactivity for HCN1 and HCN2 could be often found in preterminal axons. Although sensitivity of the present immunohistochemical method might be not enough to detect presynaptic HCNs in these terminals, my results may suggest that HCNs are not directly involved in

neurotransmitter release but rather involved in the regulation of efficiency in action potential conduction into the terminals.

In these unmyelinated axons, the presence of HCNs could contribute to quick recovery from hyperpolarization through  $I_h$  activation resulting in the axonal resetting of resting potential for conduction of high frequency firing in these axons. On the contrary, the axonal HCN might work to increase the failure of transmission. A recent report describes that the inhibitory effect of  $I_h$  upregulation in action potential firing from dendritic depolarization results from an increased membrane conductance at the resting potential owing to enhanced opening of  $I_h$  channels in dendrites (Poolos et al., 2002). This leads to a decrease in both the input resistance and length constant of the dendrite. In the preterminal, HCNs could have the same function to reduce efficiency of action potential conduction. Present results also indicate that HCN is localized to myelinated axons in various regions such as the pyramidal tracts, fornix and fasciculus retroflexus. It is not easy at present to explain the effects of HCNs localized in these myelinated axons. The axonal HCNs might work to increase the efficiency of saltatory conduction because of the depolarizing shifts of resting membrane potential due to  $I_h$  activation.

In this study, no immunoreactivity for all four HCNs was found in the stratum lucidum where the mossy fiber terminals contact with the dendrites of CA3 pyramidal cells. In these terminals, presynaptic  $I_h$  has been proposed to mediate LTP onto postsynaptic CA3 neurons (Mellor et al., 2002), though the role of  $I_h$  has been questioned by another report that showed a reduction in baseline synaptic transmission by side effects of  $I_h$  blockers (Chevaleyre and Castillo, 2002).

### **Distance-dependent localization and subunit assembly**

Previous studies describe that HCN1 and HCN2 can coassemble and function as a heteromeric complex in the hippocampal CA1 area (Chen et al., 2001; Ulens and Tytgat, 2001). In hippocampal and cortical pyramidal

cells, immunogold labeling for HCN1 showed a remarkable increase from somatic to distal apical dendritic membrane (Lorincz et al., 2002). In the present study, we found that HCN1 and HCN2 are colocalized in distal dendrites and had similar ultrastructural distribution patterns in dendritic shafts of pyramidal cells in both the CA1 area of the hippocampus and the layer I of the neocortex. These results support that HCN2 can coassemble with HCN1 and contribute to the distance-independent temporal summation of EPSPs in pyramidal cells (Magee, 1999). In HCN2-deficient CA1 pyramidal cells,  $I_h$  was reduced by only one-third as compared with wild-type animals (Ludwig et al., 2003). This observation also supports my findings. Similar distant-dependent distribution patterns may occur in other neuronal cell types and for other HCN subtypes. For example, in the superior colliculus (HCN1-LI) and external plexiform layer of the main olfactory bulb (HCN4-LI), neurons strongly expressing HCN1 and HCN4 mRNA are distributed in the optic nerve layer and mitral cells, respectively (Santoro et al., 2000). In the present study, intense HCN1-LI was found in the superficial gray layer but not in the optic nerve layer having a concentration gradient towards the surface, suggesting that the HCN1-expressing neurons have higher density of the channel in distal dendrites. In mitral cells of the main olfactory bulb, HCN4-LI also increases from proximal to distal parts of the external plexiform layer. In addition, HCN4-LI was found more intense in dendrites in layer I than cell layers of the nucleus of the lateral olfactory tract as confirmed at the electron microscopic level (data not shown).

I also found colocalization of HCN1 and HCN2 in basket cell axons and their terminals in the hippocampal CA3 area and in cell bodies of mesencephalic trigeminal neurons. However, in other various regions expressing both HCN1 and HCN2 such as hypoglossal nucleus, lateral lemniscus and lateral mammillary nucleus, clear colocalization was not detected at least at the light microscopic level. These results suggest that heteromers of HCN1 and HCN2 may be mainly restricted to pyramidal cells

in the cortical regions in the brain and most  $I_h$  channels would function as homomeric channels in other cell types. For HCN2 and HCN4 combination, no supportive evidence has been found for heteromeric channels (Ludwig et al., 1999). The heteromers of HCN1 and HCN4 are also similarly questioned (Altomare et al., 2003). Thus, it remains unclear whether the other combinations of the HCN channel isoforms can occur to form heteromers. However, since my immunohistochemical results showed that more than three HCN subunits are predominantly expressed in some regions including the ventral pallidum, cochlear nuclei, superior and inferior olive, periolivary nucleus, and area postrema, HCN subunits could have a potential to form functional heteromers in these regions.

### **HCN2-immunopositive oligodendrocytes**

In this study, we found many HCN2-immunopositive small cells double labeled for GST- $\pi$ , indicating that they are a subpopulation of oligodendrocytes. Some of these cells were perineuronal oligodendrocytes. Only a few reports have proposed functions of perineuronal oligodendrocytes. Ludwin (Ludwin, 1984) found that these cells remyelinate axons in trauma-induced demyelination and have function same as myelinating oligodendrocytes. Recently, Taniike et al. (Taniike et al., 2002) suggested that perineuronal oligodendrocytes immunopositive for GST- $\pi$  protect neurons from apoptosis by upregulation of Lipocalin-type prostaglandin D synthase. Although the presence of HCN2 in these cells should result in setting resting membrane potential more positive than that in other cell types of glial cells, it is unclear at present whether the depolarized resting membrane potential may have any relevance to these functions or to any other interactions between perineuronal oligodendrocytes and neurons. The presence of HCN2, however, clearly indicates further heterogeneity of oligodendrocytes even in the GST- $\pi$ -positive cell population.

## **Conclusion**

In conclusion, the distribution patterns of HCN immunoreactive neuropil and neuronal cell bodies were revealed in accordance with the reported patterns of distribution of HCN mRNAs. My results indicated that HCNs are located not only in somato-dendritic compartments but also in axonal compartments of neurons. The HCN1 and HCN2 are colocalized in the distal dendrites of pyramidal cells in the hippocampus and neocortex having a similar ultrastructural distribution. Interestingly, a new type of HCN2-immunopositive oligodendrocytes including perineuronal oligodendrocytes was revealed throughout the brain. The present results will be useful for elucidating yet unidentified functions of  $I_h$  channels in the brain.

## **Acknowledgments**

I thank Drs. Hirohide Takebayashi and Akiko Momiyama, National Institute for Physiological Sciences, for helpful discussion. This work was supported in part by Grants in Aid from the Japanese Ministry of Education, Science, Sports and Culture.

## Literature Cited

- Altomare C, Terragni B, Brioschi C, Milanesi R, Pagliuca C, Viscomi C, Moroni A, Baruscotti M, DiFrancesco D. 2003. Heteromeric HCN1-HCN4 channels: a comparison with native pacemaker channels from the rabbit sinoatrial node. *J Physiol* 549:347-359.
- Bal T, McCormick DA. 1997. Synchronized oscillations in the inferior olive are controlled by the hyperpolarization-activated cation current I(h). *J Neurophysiol* 77:3145-3156.
- Beaumont V, Zucker RS. 2000. Enhancement of synaptic transmission by cyclic AMP modulation of presynaptic I<sub>h</sub> channels. *Nat Neurosci* 3:133-141.
- Bender RA, Brewster A, Santoro B, Ludwig A, Hofmann F, Biel M, Baram TZ. 2001. Differential and age-dependent expression of hyperpolarization-activated, cyclic nucleotide-gated cation channel isoforms 1-4 suggests evolving roles in the developing rat hippocampus. *Neuroscience* 106:689-698.
- Berger T, Larkum ME, Luscher HR. 2001. High I(h) channel density in the distal apical dendrite of layer V pyramidal cells increases bidirectional attenuation of EPSPs. *J Neurophysiol* 85:855-868.
- Brauer AU, Savaskan NE, Kole MH, Plaschke M, Monteggia LM, Nestler EJ, Simburger E, Deisz RA, Ninnemann O, Nitsch R. 2001. Molecular and functional analysis of hyperpolarization-activated pacemaker channels in the hippocampus after entorhinal cortex lesion. *Faseb J* 15:2689-2701.
- Brewster A, Bender RA, Chen Y, Dube C, Eghbal-Ahmadi M, Baram TZ. 2002. Developmental febrile seizures modulate hippocampal gene expression of hyperpolarization-activated channels in an isoform- and cell-specific manner. *J Neurosci* 22:4591-4599.

- Cadetti L, Belluzzi O. 2001. Hyperpolarisation-activated current in glomerular cells of the rat olfactory bulb. *Neuroreport* 12:3117-3120.
- Chapman CA, Lacaille JC. 1999. Intrinsic theta-frequency membrane potential oscillations in hippocampal CA1 interneurons of stratum lacunosum-moleculare. *J Neurophysiol* 81:1296-1307.
- Chen S, Wang J, Siegelbaum SA. 2001. Properties of hyperpolarization-activated pacemaker current defined by coassembly of HCN1 and HCN2 subunits and basal modulation by cyclic nucleotide. *J Gen Physiol* 117:491-504.
- Chevaleyre V, Castillo PE. 2002. Assessing the role of  $I_h$  channels in synaptic transmission and mossy fiber LTP. *Proc Natl Acad Sci U S A* 99:9538-9543.
- Cuttle MF, Rusznak Z, Wong AY, Owens S, Forsythe ID. 2001. Modulation of a presynaptic hyperpolarization-activated cationic current ( $I(h)$ ) at an excitatory synaptic terminal in the rat auditory brainstem. *J Physiol* 534:733-744.
- Dawson MR, Levine JM, Reynolds R. 2000. NG2-expressing cells in the central nervous system: are they oligodendroglial progenitors? *J Neurosci Res* 61:471-479.
- Dieudonne S. 1998. Submillisecond kinetics and low efficacy of parallel fibre-Golgi cell synaptic currents in the rat cerebellum. *J Physiol* 510 ( Pt 3):845-866.
- DiFrancesco D. 1993. Pacemaker mechanisms in cardiac tissue. *Annu Rev Physiol* 55:455-472.
- Fu XW, Brezden BL, Wu SH. 1997. Hyperpolarization-activated inward current in neurons of the rat's dorsal nucleus of the lateral lemniscus in vitro. *J Neurophysiol* 78:2235-2245.

- Funahashi M, Mitoh Y, Matsuo R. 2002. Electrophysiological properties of the rat area postrema neurons displaying both the transient outward current and the hyperpolarization-activated inward current. *Brain Res Bull* 58:337-343.
- Gasparini S, DiFrancesco D. 1999. Action of serotonin on the hyperpolarization-activated cation current (I<sub>h</sub>) in rat CA1 hippocampal neurons. *Eur J Neurosci* 11:3093-3100.
- Gilmor ML, Nash NR, Roghani A, Edwards RH, Yi H, Hersch SM, Levey AI. 1996. Expression of the putative vesicular acetylcholine transporter in rat brain and localization in cholinergic synaptic vesicles. *J Neurosci* 16:2179-2190.
- Holderith NB, Shigemoto R, Nusser Z. 2003. Cell type-dependent expression of HCN1 in the main olfactory bulb. *Eur J Neurosci* 18:344-354.
- Imai Y, Kohsaka S. 2002. Intracellular signaling in M-CSF-induced microglia activation: role of Iba1. *Glia* 40:164-174.
- Ishii TM, Takano M, Xie LH, Noma A, Ohmori H. 1999. Molecular characterization of the hyperpolarization-activated cation channel in rabbit heart sinoatrial node. *J Biol Chem* 274:12835-12839.
- Iwahori Y, Ikegaya Y, Matsuki N. 2002. Hyperpolarization-activated current I<sub>h</sub> in nucleus of solitary tract neurons: regional difference in serotonergic modulation. *Jpn J Pharmacol* 88:459-462.
- Jiang ZG, Pessia M, North RA. 1993. Dopamine and baclofen inhibit the hyperpolarization-activated cation current in rat ventral tegmental neurones. *J Physiol* 462:753-764.
- Jolas T, Nestler EJ, Aghajanian GK. 2000. Chronic morphine increases GABA tone on serotonergic neurons of the dorsal raphe nucleus: association with an up-regulation of the cyclic AMP pathway. *Neuroscience* 95:433-443.

- Kamondi A, Reiner PB. 1991. Hyperpolarization-activated inward current in histaminergic tuberomammillary neurons of the rat hypothalamus. *J Neurophysiol* 66:1902-1911.
- Kawaguchi Y. 1992. Large aspiny cells in the matrix of the rat neostriatum in vitro: physiological identification, relation to the compartments and excitatory postsynaptic currents. *J Neurophysiol* 67:1669-1682.
- Khakh BS, Henderson G. 1998. Hyperpolarization-activated cationic currents (I<sub>h</sub>) in neurones of the trigeminal mesencephalic nucleus of the rat. *J Physiol* 510 ( Pt 3):695-704.
- Li SJ, Wang Y, Strahlendorf HK, Strahlendorf JC. 1993. Serotonin alters an inwardly rectifying current (I<sub>h</sub>) in rat cerebellar Purkinje cells under voltage clamp. *Brain Res* 617:87-95.
- Lorincz A, Notomi T, Tamas G, Shigemoto R, Nusser Z. 2002. Polarized and compartment-dependent distribution of HCN1 in pyramidal cell dendrites. *Nat Neurosci* 5:1185-1193.
- Ludwig A, Budde T, Stieber J, Moosmang S, Wahl C, Holthoff K, Langebartels A, Wotjak C, Munsch T, Zong X, Feil S, Feil R, Lancel M, Chien KR, Konnerth A, Pape HC, Biel M, Hofmann F. 2003. Absence epilepsy and sinus dysrhythmia in mice lacking the pacemaker channel HCN2. *Embo J* 22:216-224.
- Ludwig A, Zong X, Jeglitsch M, Hofmann F, Biel M. 1998. A family of hyperpolarization-activated mammalian cation channels. *Nature* 393:587-591.
- Ludwig A, Zong X, Stieber J, Hullin R, Hofmann F, Biel M. 1999. Two pacemaker channels from human heart with profoundly different activation kinetics. *Embo J* 18:2323-2329.

- Ludwin SK. 1984. The function of perineuronal satellite oligodendrocytes: an immunohistochemical study. *Neuropathol Appl Neurobiol* 10:143-149.
- Luthi A, McCormick DA. 1998. H-current: properties of a neuronal and network pacemaker. *Neuron* 21:9-12.
- Magee JC. 1998. Dendritic hyperpolarization-activated currents modify the integrative properties of hippocampal CA1 pyramidal neurons. *J Neurosci* 18:7613-7624.
- Magee JC. 1999. Dendritic Ih normalizes temporal summation in hippocampal CA1 neurons. *Nat Neurosci* 2:508-514.
- McCormick DA, Bal T. 1997. Sleep and arousal: thalamocortical mechanisms. *Annu Rev Neurosci* 20:185-215.
- McCormick DA, Pape HC. 1990. Noradrenergic and serotonergic modulation of a hyperpolarization-activated cation current in thalamic relay neurones. *J Physiol* 431:319-342.
- Mechawar N, Watkins KC, Descarries L. 2002. Ultrastructural features of the acetylcholine innervation in the developing parietal cortex of rat. *J Comp Neurol* 443:250-258.
- Mellor J, Nicoll RA, Schmitz D. 2002. Mediation of hippocampal mossy fiber long-term potentiation by presynaptic Ih channels. *Science* 295:143-147.
- Miyake T, Kitamura T. 1992. Glutamine synthetase immunoreactivity in two types of mouse brain glial cells. *Brain Res* 586:53-60.
- Momiyama T, Koga E. 2001. Dopamine D(2)-like receptors selectively block N-type Ca(2+) channels to reduce GABA release onto rat striatal cholinergic interneurons. *J Physiol* 533:479-492.
- Monteggia LM, Eisch AJ, Tang MD, Kaczmarek LK, Nestler EJ. 2000. Cloning and localization of the hyperpolarization-activated cyclic

- nucleotide-gated channel family in rat brain. *Brain Res Mol Brain Res* 81:129-139.
- Moosmang S, Biel M, Hofmann F, Ludwig A. 1999. Differential distribution of four hyperpolarization-activated cation channels in mouse brain. *Biol Chem* 380:975-980.
- Moosmang S, Stieber J, Zong X, Biel M, Hofmann F, Ludwig A. 2001. Cellular expression and functional characterization of four hyperpolarization-activated pacemaker channels in cardiac and neuronal tissues. *Eur J Biochem* 268:1646-1652.
- Mori S, Leblond CP. 1970. Electron microscopic identification of three classes of oligodendrocytes and a preliminary study of their proliferative activity in the corpus callosum of young rats. *J Comp Neurol* 139:1-28.
- Muller F, Scholten A, Ivanova E, Haverkamp S, Kremmer E, Kaupp UB. 2003. HCN channels are expressed differentially in retinal bipolar cells and concentrated at synaptic terminals. *Eur J Neurosci* 17:2084-2096.
- Ojima H, Kawajiri S, Yamasaki T. 1989. Cholinergic innervation of the rat cerebellum: qualitative and quantitative analyses of elements immunoreactive to a monoclonal antibody against choline acetyltransferase. *J Comp Neurol* 290:41-52.
- Pape HC. 1996. Queer current and pacemaker: the hyperpolarization-activated cation current in neurons. *Annu Rev Physiol* 58:299-327.
- Parkis MA, Berger AJ. 1997. Clonidine reduces hyperpolarization-activated inward current (I<sub>h</sub>) in rat hypoglossal motoneurons. *Brain Res* 769:108-118.

- Paxinos G, Watson C. 1998. The rat brain in stereotaxic coordinates, 4th ed. San Diego: Academic Press.
- Poolos NP, Migliore M, Johnston D. 2002. Pharmacological upregulation of h-channels reduces the excitability of pyramidal neuron dendrites. *Nat Neurosci* 5:767-774.
- Robinson RB, Siegelbaum SA. 2002. Hyperpolarization-Activated Cation Currents: From Molecules to Physiological Function. *Annu Rev Physiol*.
- Saito Y, Isa T. 1999. Electrophysiological and morphological properties of neurons in the rat superior colliculus. I. Neurons in the intermediate layer. *J Neurophysiol* 82:754-767.
- Santoro B, Chen S, Luthi A, Pavlidis P, Shumyatsky GP, Tibbs GR, Siegelbaum SA. 2000. Molecular and functional heterogeneity of hyperpolarization-activated pacemaker channels in the mouse CNS. *J Neurosci* 20:5264-5275.
- Santoro B, Grant SG, Bartsch D, Kandel ER. 1997. Interactive cloning with the SH3 domain of N-src identifies a new brain specific ion channel protein, with homology to eag and cyclic nucleotide-gated channels. *Proc Natl Acad Sci U S A* 94:14815-14820.
- Santoro B, Liu DT, Yao H, Bartsch D, Kandel ER, Siegelbaum SA, Tibbs GR. 1998. Identification of a gene encoding a hyperpolarization-activated pacemaker channel of brain. *Cell* 93:717-729.
- Sefton JA, Dreher B. 1995. Visual System. In: Paxinos G, Editor. *The Rat Nervous System*. Sandiego: Academic Press. p 833-898.
- Seifert R, Scholten A, Gauss R, Mincheva A, Lichter P, Kaupp UB. 1999. Molecular characterization of a slowly gating human hyperpolarization-activated channel predominantly expressed in thalamus, heart, and testis. *Proc Natl Acad Sci U S A* 96:9391-9396.

- Shigemoto R, Kinoshita A, Wada E, Nomura S, Ohishi H, Takada M, Flor PJ, Neki A, Abe T, Nakanishi S, Mizuno N. 1997. Differential presynaptic localization of metabotropic glutamate receptor subtypes in the rat hippocampus. *J Neurosci* 17:7503-7522.
- Sloviter RS, Ali-Akbarian L, Horvath KD, Menkens KA. 2001. Substance P receptor expression by inhibitory interneurons of the rat hippocampus: enhanced detection using improved immunocytochemical methods for the preservation and colocalization of GABA and other neuronal markers. *J Comp Neurol* 430:283-305.
- Southan AP, Morris NP, Stephens GJ, Robertson B. 2000. Hyperpolarization-activated currents in presynaptic terminals of mouse cerebellar basket cells. *J Physiol* 526 Pt 1:91-97.
- Sun QQ, Prince DA, Huguenard JR. 2003. Vasoactive intestinal polypeptide and pituitary adenylate cyclase-activating polypeptide activate hyperpolarization-activated cationic current and depolarize thalamocortical neurons in vitro. *J Neurosci* 23:2751-2758.
- Taniike M, Mohri I, Eguchi N, Beuckmann CT, Suzuki K, Urade Y. 2002. Perineuronal oligodendrocytes protect against neuronal apoptosis through the production of lipocalin-type prostaglandin D synthase in a genetic demyelinating model. *J Neurosci* 22:4885-4896.
- Tansey FA, Cammer W. 1991. A pi form of glutathione-S-transferase is a myelin- and oligodendrocyte-associated enzyme in mouse brain. *J Neurochem* 57:95-102.
- Thoby-Brisson M, Telgkamp P, Ramirez JM. 2000. The role of the hyperpolarization-activated current in modulating rhythmic activity in the isolated respiratory network of mice. *J Neurosci* 20:2994-3005.

- Uchimura N, Cherubini E, North RA. 1990. Cation current activated by hyperpolarization in a subset of rat nucleus accumbens neurons. *J Neurophysiol* 64:1847-1850.
- Ulens C, Tytgat J. 2001. Functional heteromerization of HCN1 and HCN2 pacemaker channels. *J Biol Chem* 276:6069-6072.
- Vasilyev DV, Barish ME. 2002. Postnatal development of the hyperpolarization-activated excitatory current ih in mouse hippocampal pyramidal neurons. *J Neurosci* 22:8992-9004.
- Washio H, Takiguchi-Hayashi K, Konishi S. 1999. Early postnatal development of substantia nigra neurons in rat midbrain slices: hyperpolarization-activated inward current and dopamine-activated current. *Neurosci Res* 34:91-101.
- Womble MD, Moises HC. 1993. Hyperpolarization-activated currents in neurons of the rat basolateral amygdala. *J Neurophysiol* 70:2056-2065.
- Yao W, Godfrey DA. 1999. Vesicular acetylcholine transporter in the rat cochlear nucleus: an immunohistochemical study. *J Histochem Cytochem* 47:83-90.

## Figures and Table

**Fig. 1 Immunoblot analysis of rat brain with HCN antibodies**

Crude membrane preparations from whole rat brains were reacted with HCN antibodies. Immunoreactive products of 120kDa are detected for HCN1 and HCN2, and those of 85 and 140kDa for HCN3 and HCN4, respectively. No immunoreactivity was detected after adsorption of each HCN antibody with the corresponding antigens (Ads). Molecular mass markers are indicated on the left in kDa. F, gel front.

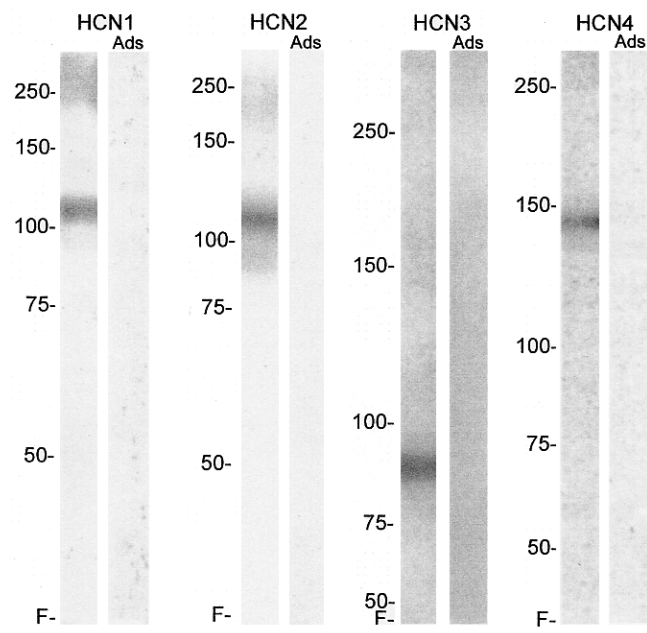


**Fig. 2 HCN-expressing COS-7 cells**

The COS-7 cells were transiently transfected with the cDNAs of HCNs. Each HCN antibody strongly reacted with COS-7 cells expressing the respective HCN. No cross-reactivity of the antibodies among four HCNs was detected. Horizontal lines show cells transfected with each HCN cDNA (Transfection). Vertical lines show cells labeled with each HCN antibody (Antibody). Note: In each experiment, the signal to noise ratio was very high. To clearly show immunonegative COS-7 cells, the laser power was increased to a saturating level for immunopositive cells.

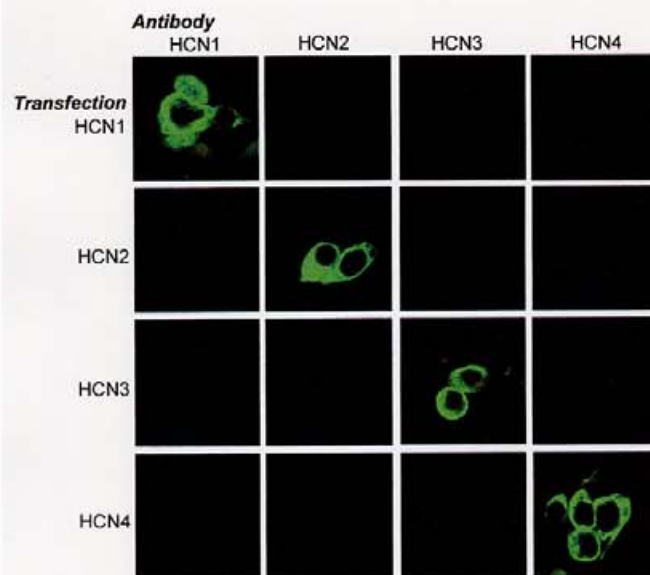


**Fig. 3 Distribution of immunoreactivity for HCNs in the rat brain**

Parasagittal sections of the rat brain were immunostained with HCN1, HCN2, HCN3 and HCN4 antibodies.

12, hypoglossal nucleus; AON, anterior olfactory nuclei; AP, area postrema; Cb, cerebellar cortex; CC, cerebral cortex; CL10, cerebellar cortex lobule 10; fr, fasciculus retroflexus; Gr, gracile nucleus; Hb, habenular nucleus; Hy, hypothalamus; Hi, hippocampus; IC, inferior colliculus; IO, inferior olive; IP, interpeduncular nucleus; LOT, nucleus of the lateral olfactory tract; LL, lateral lemniscus; LS, lateral septum nucleus; MB, mammillary body; PA, preoptic area; Pir, piriform cortex; Pn, pontine nuclei; SC, superior colliculus; SOC, superior olivary complex; Tg, tegmental nuclei; Th, thalamus. Scale bar, 1mm.

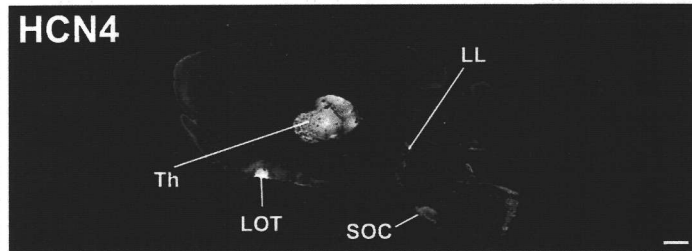
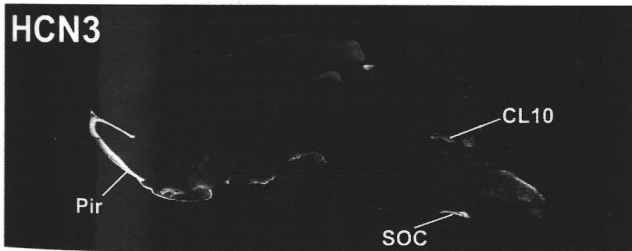
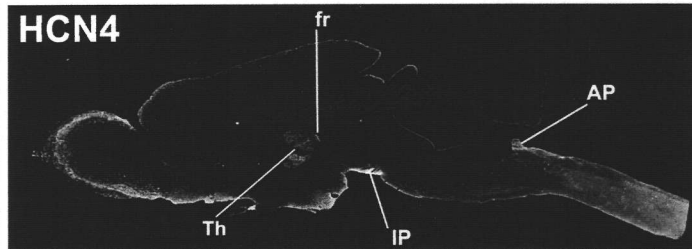
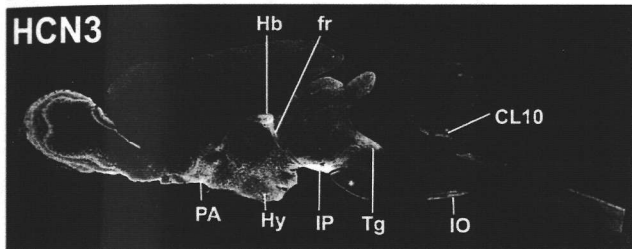
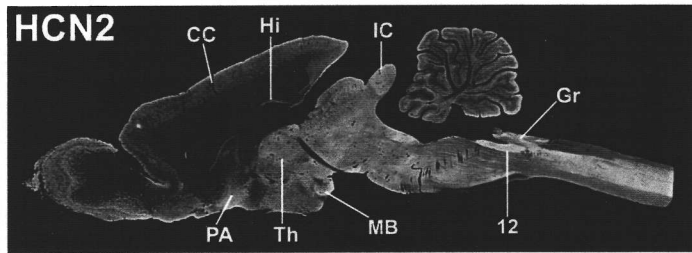
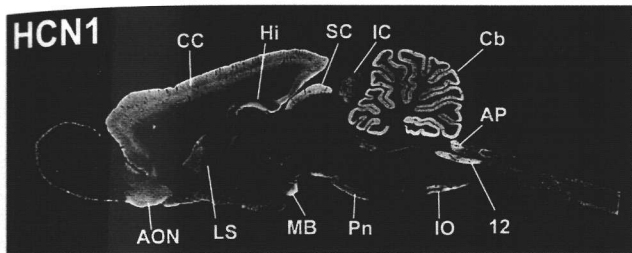


**Fig. 4 HCN-like immunoreactive (LI) cell bodies, processes and neuropil**

(a) HCN1-LI neuropil in the CA1 stratum lacunosum moleculare (LM) of the hippocampus and molecular layer (Mo) of the dentate gyrus, (b) HCN2-LI neuropil in the dorsal lateral geniculate nucleus, (c) HCN3-LI neuronal cells in the anterior pretectal nucleus, ventral part, (d) HCN4-LI neuronal cells in the anterior pretectal nucleus, dorsal part.

(a) and (b) Immunoreactivity for HCN1 and HCN2 mainly exhibits neuropil labeling in the brain. Only a few regions have clearly visible neuronal cell bodies and processes, except for HCN2-immunopositive small cells (arrows in b). (c) and (d): Large number of HCN3- and HCN4-LI neuronal cell bodies and processes are observed in some brain regions including the anterior pretectal nucleus. Scale bar, 20 $\mu$ m.

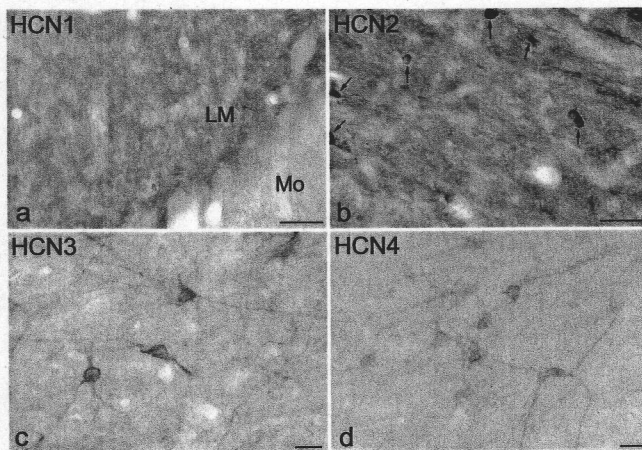
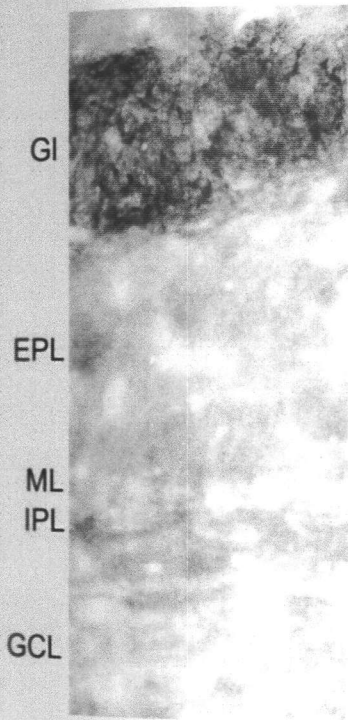


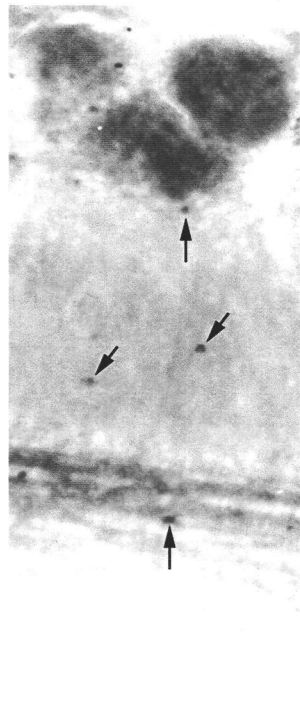
**Fig. 5 Distribution of HCN-LI in the main olfactory bulb**

In the glomerular layer (Gl), intense immunoreactivity for HCN1, HCN2 and HCN3 are observed. In the external plexiform layer (EPL), HCN4-LI increases towards the glomerular layer. In the internal plexiform layer (IPL), intense HCN2- and HCN3-LIs are observed. Arrows indicate HCN2-immunopositive small cells. Arrowheads show axon bundles immunopositive for HCN3. ML, mitral cell layer; GCL, granule cell layer. Scale bar, 200µm.

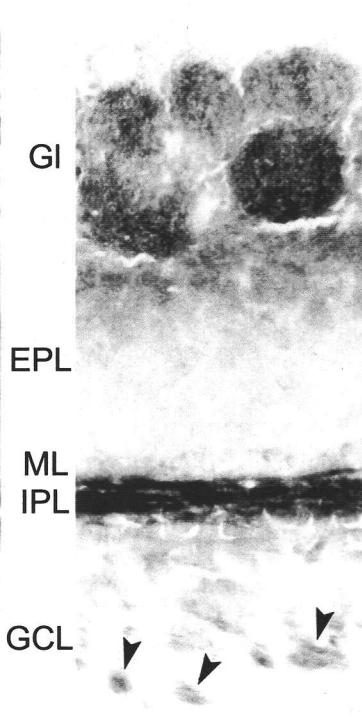
HCN1



HCN2



HCN3



HCN4

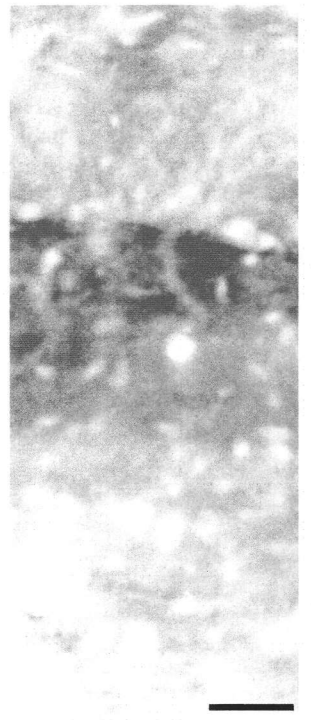


**Fig. 6 Distribution of HCN-LI in the anterior olfactory nuclei.**

HCN1-LI is extensively observed in neuropil throughout the anterior olfactory nuclei (AON) and piriform cortex (Pir), whereas strong HCN2- and HCN3-LI are restricted to layer Ia (Ia) of the piriform cortex. DP, dorsal peduncular cortex; ICj, islands of Calleja; Pir, piriform cortex; TT, tenia tecta; lot, lateral olfactory tract; ri, rhinal incisula. Scale bar, 1000 $\mu$ m.

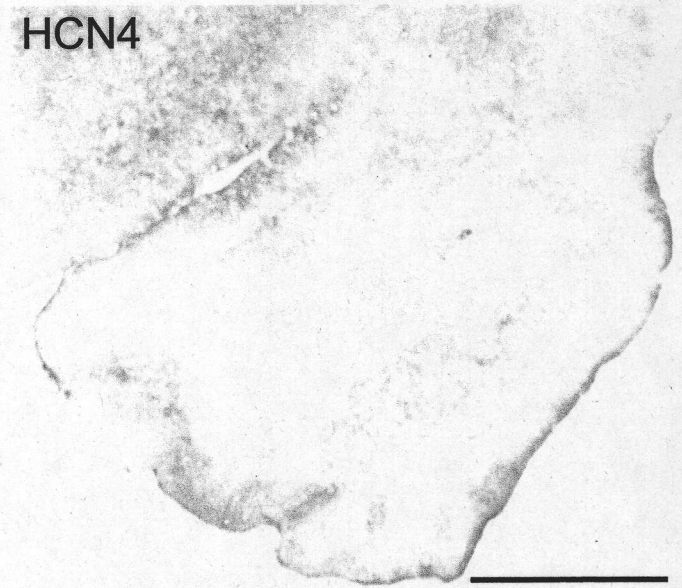
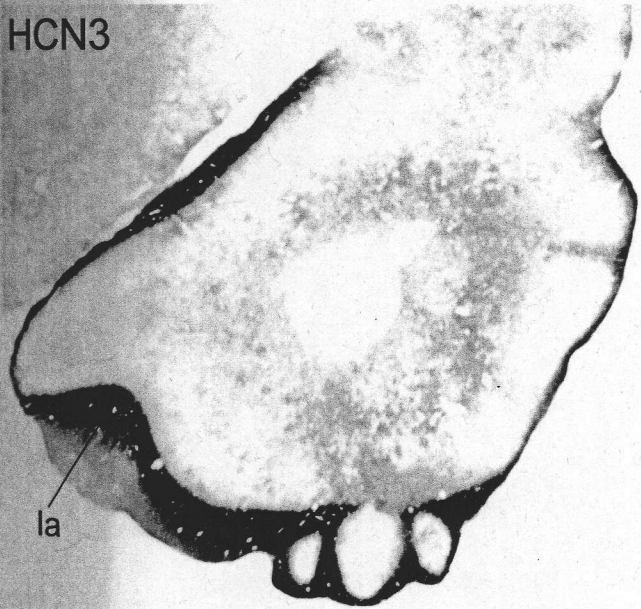
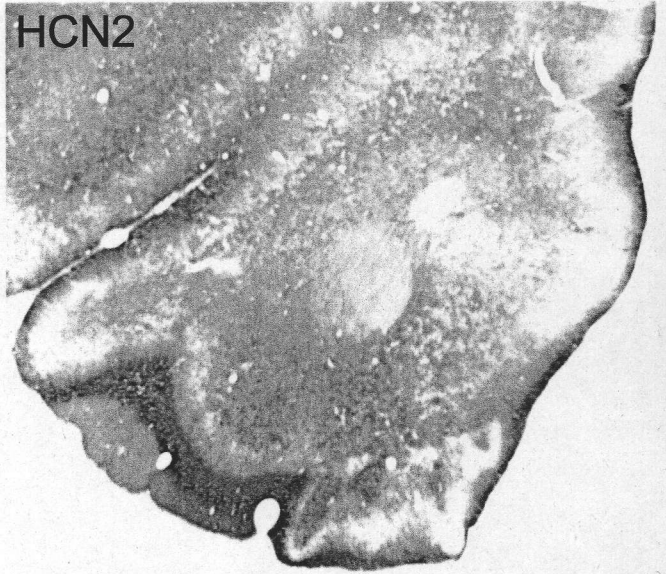
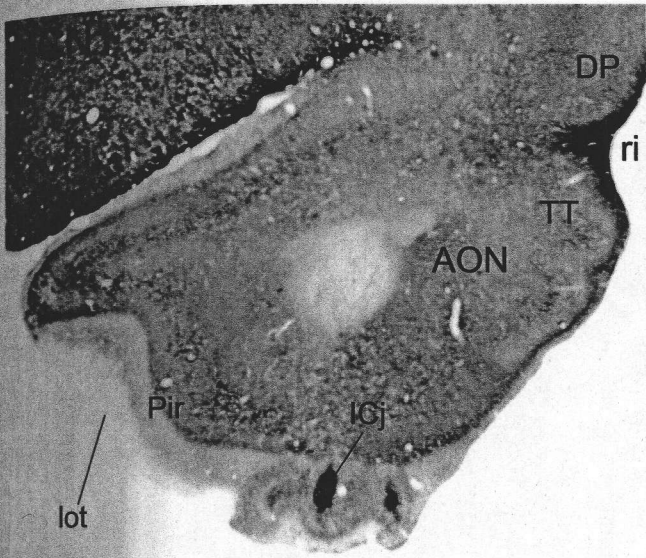


**Fig. 7 Distribution of HCN-LI in the primary somatosensory cortex**

Both HCN1- and HCN2-LIs increase towards layer I of the somatosensory cortex. HCN2-immunopositive small cells are scattered throughout cortical layers, except for layer I. Scale bar, 500 $\mu$ m.

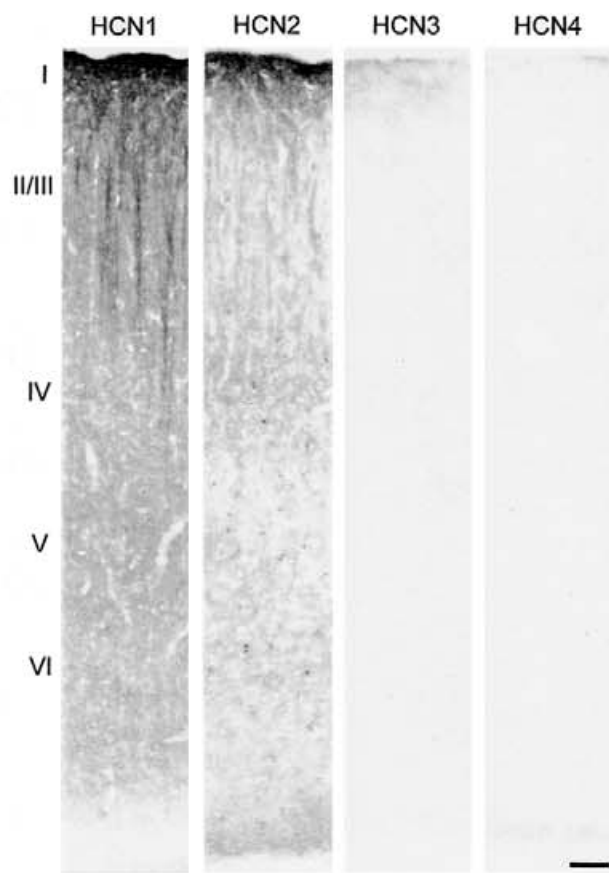


**Fig. 8 Double-immunofluorescence labeling for HCN1 and HCN2**

In distal dendrites in the somatosensory cortex, basket cell terminals in the hippocampal CA3 area and neuronal cell bodies in the mesencephalic trigeminal nucleus (V), HCN1- and HCN2-LIs are extensively overlapped. In the hypoglossal nucleus, however, no clear colocalization is detected. White arrows indicate small cells single labeled for HCN2. Scale bar, 50 $\mu$ m.

HCN1

HCN2

Overlay

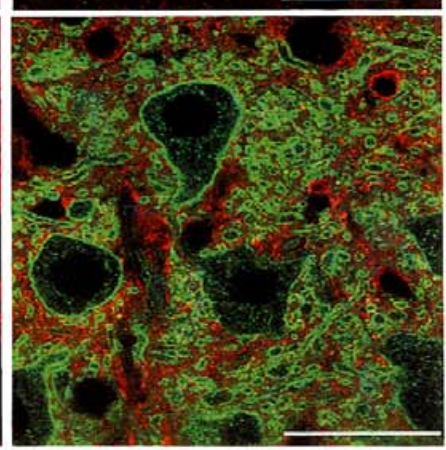
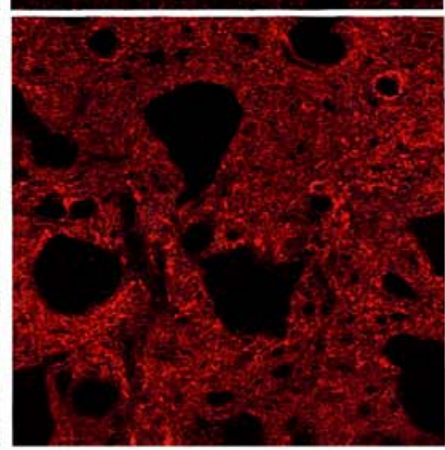
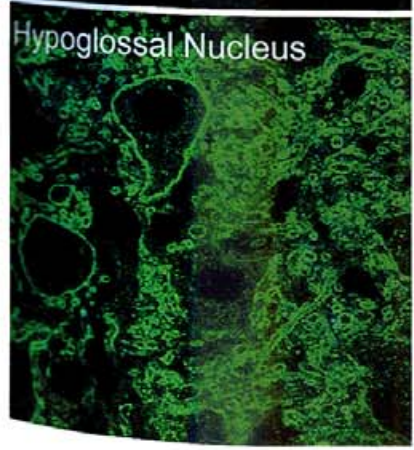
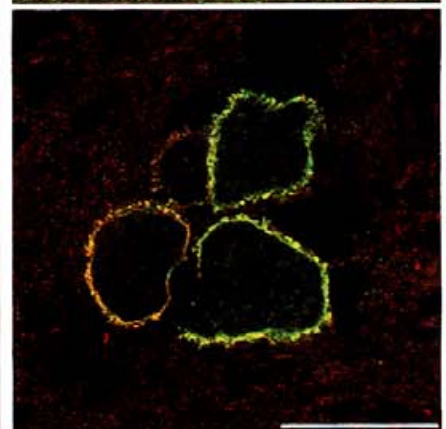
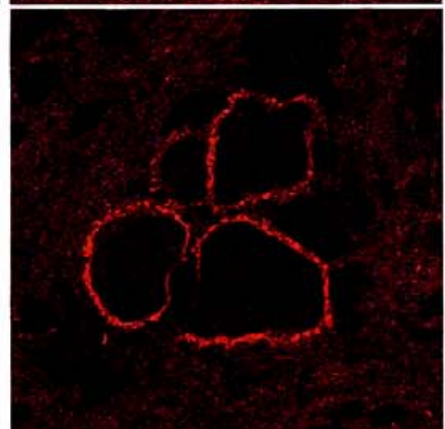
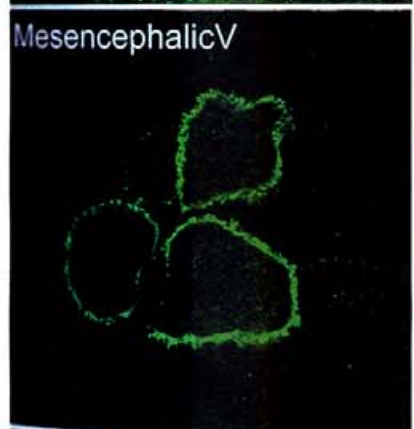
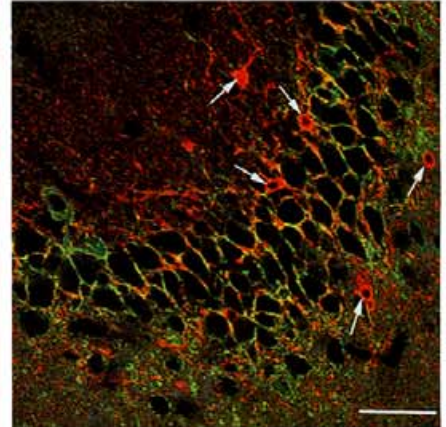
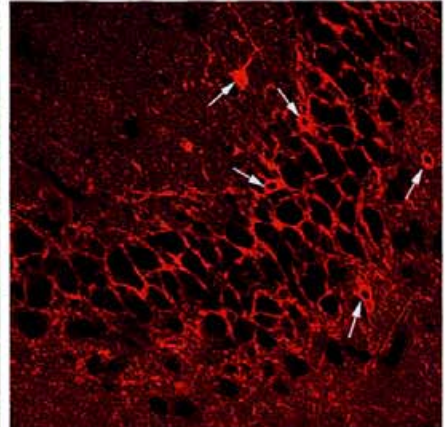
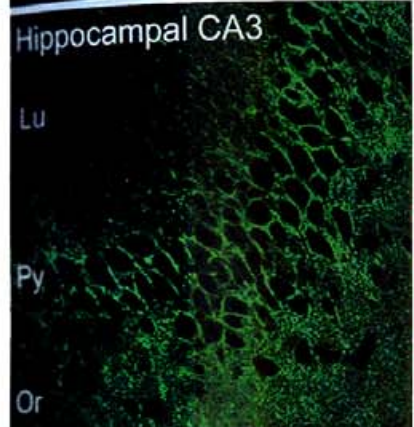
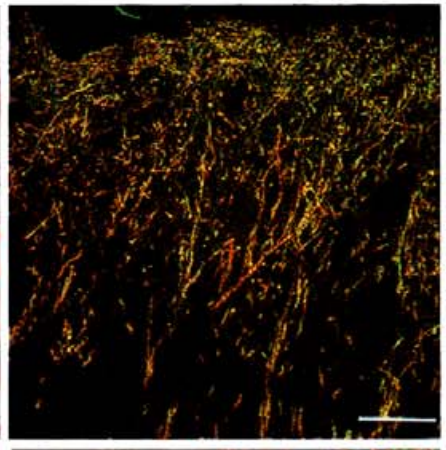
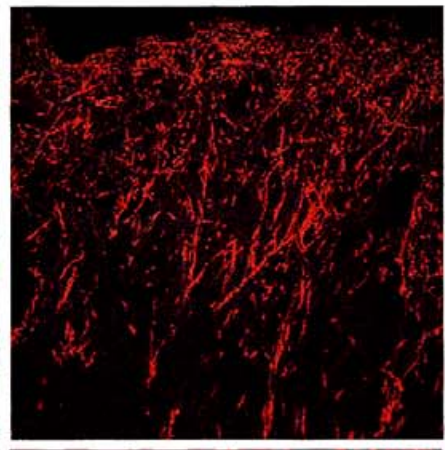
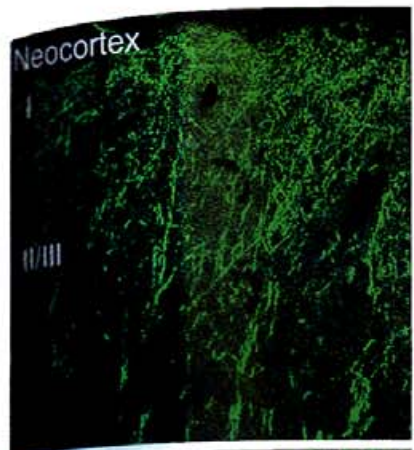


**Fig. 9 Electronmicroscopic immunogold labeling for HCN2 in the neocortex and hippocampus**

Immunogold particles for HCN2 are mainly observed along plasma membrane of dendritic shafts of presumed pyramidal cells in layer I of the neocortex (a, c) and stratum lacunosum moleculare of the hippocampal CA1 area (b, d). No gold particles are found in asymmetrical synapses (arrows). Some particles are present in cytoplasm of dendrites and spines (arrow heads). Asterisk indicate GAD-labeled (peroxidase reaction) profiles, which are immunonegative for HCN2. Scale bar, 0.2 $\mu$ m.

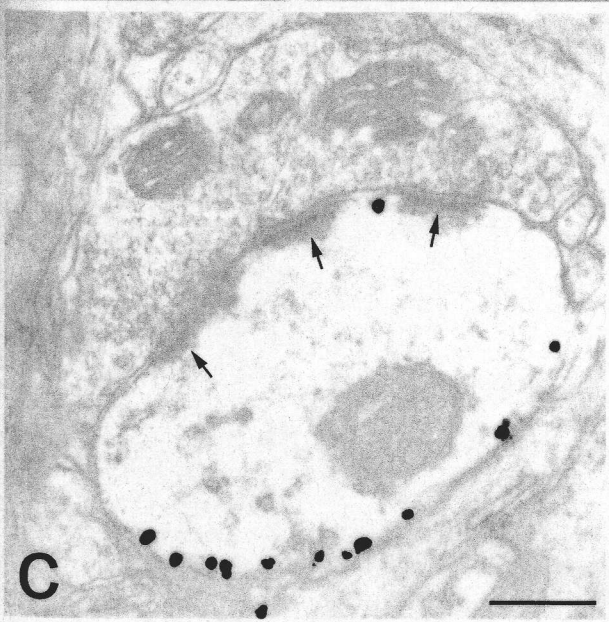
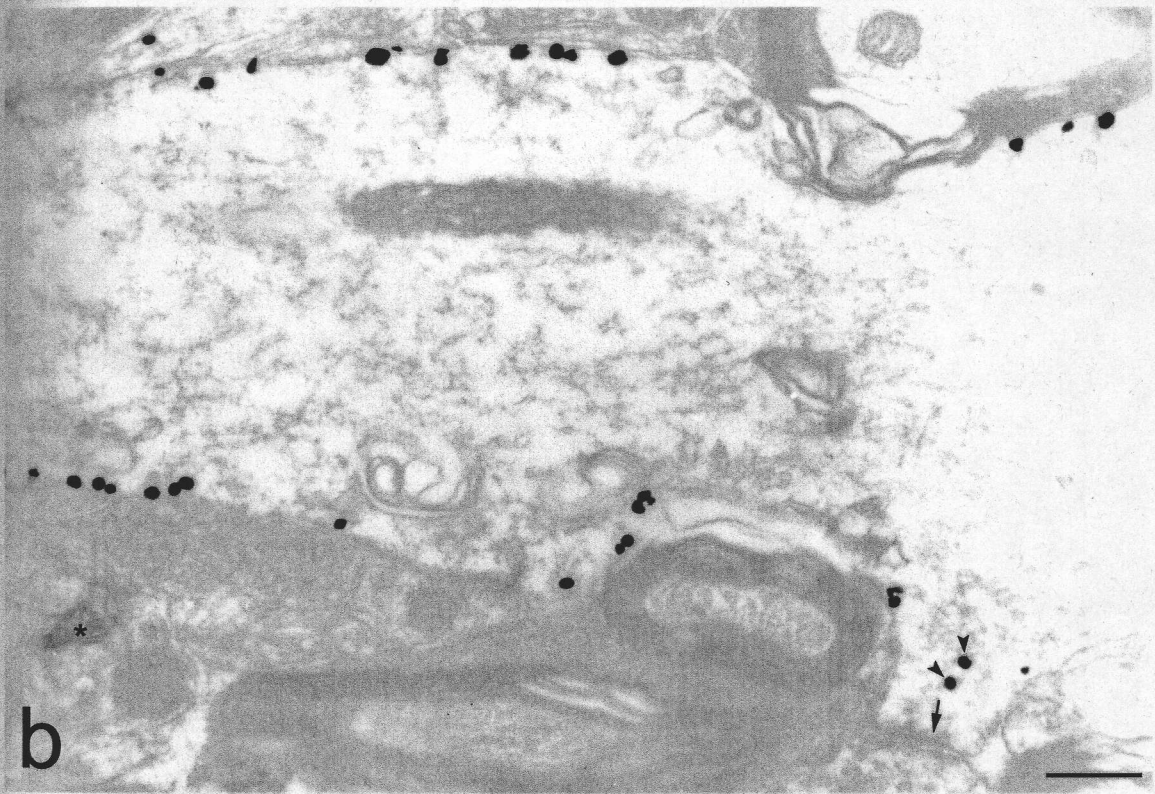
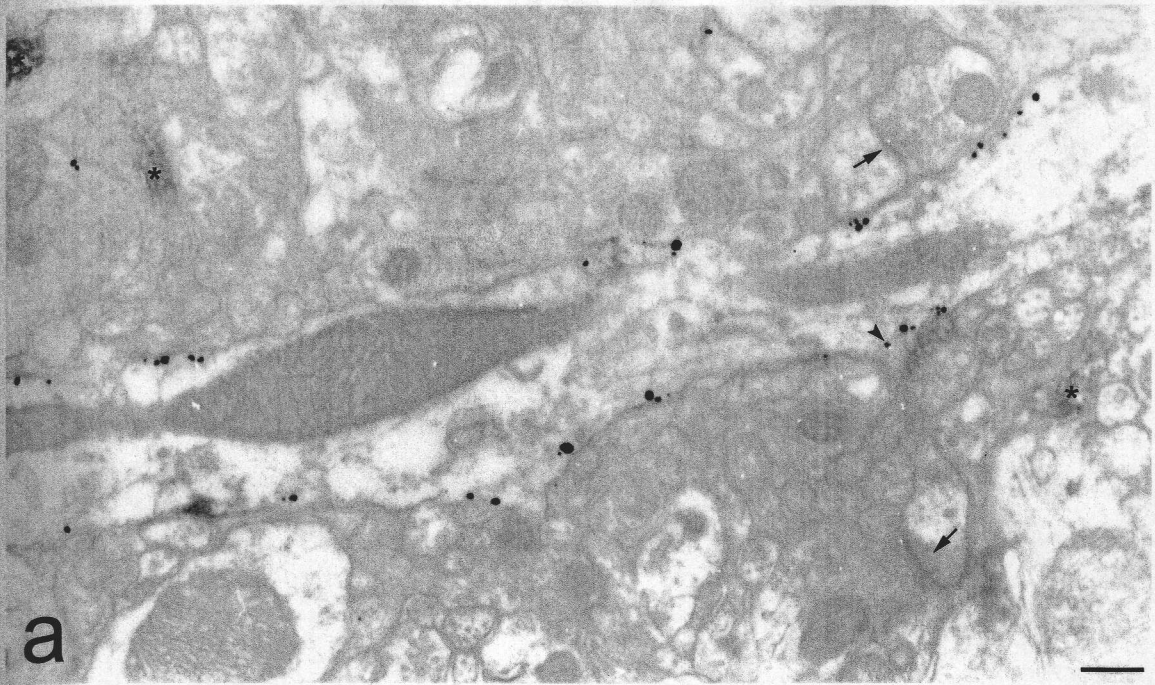


**Fig. 10 Distribution of HCN-LI in the hippocampus**

Intense immunoreactivity for HCN1 and HCN2 are observed in the stratum lacunosum moleculare (LM) of the CA1 area and stratum pyramidale (Py) of the CA3 area. Arrowheads indicate moderate HCN3-LI in the inner one third of the dentate molecular layer (Mo). Arrow shows patches of intense HCN1-LI in the border zone between the medial and lateral habenula. Or, stratum oriens; Ra, stratum radiatum; Gr, granular layer of the dentate gyrus; Lu, stratum lucidum; MHb, medial habenula; LHb, lateral habenula. Scale bar, 500 $\mu$ m.

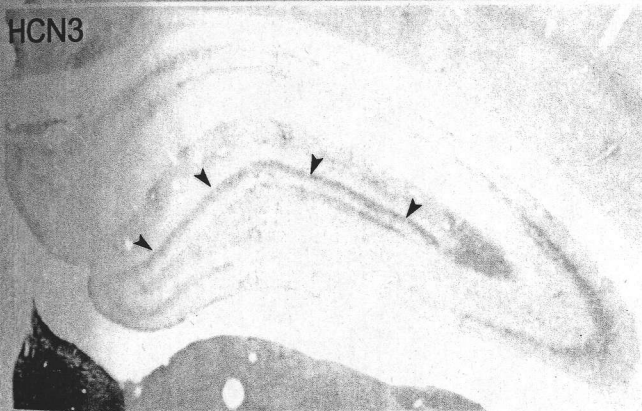
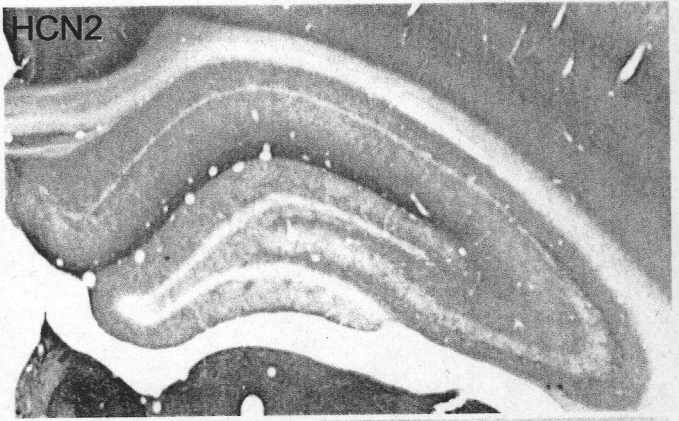
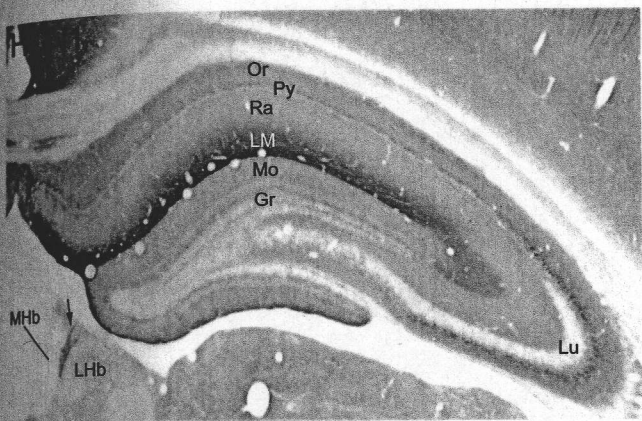


**Fig. 11 Presynaptic localization of HCN1- and HCN2-LIs in the CA3 pyramidal cell layer of the hippocampus**

Peroxidase reaction products for HCN1 (a) and HCN2 (c) are observed in axons and axon terminals making symmetrical synapses (arrows) with soma (S) of pyramidal cells. Immunogold particles for HCN1 (b) are found along axonal plasma membrane but localized apart from synaptic sites (arrow). Scale bar, 0.2 $\mu$ m.

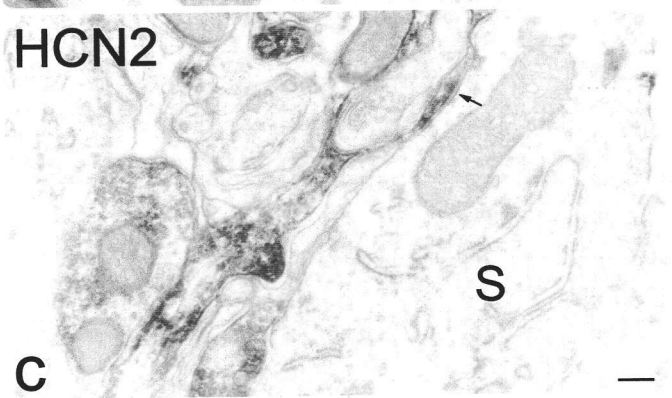
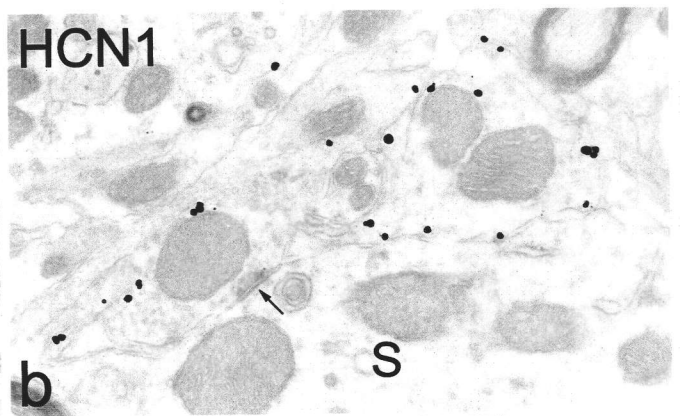
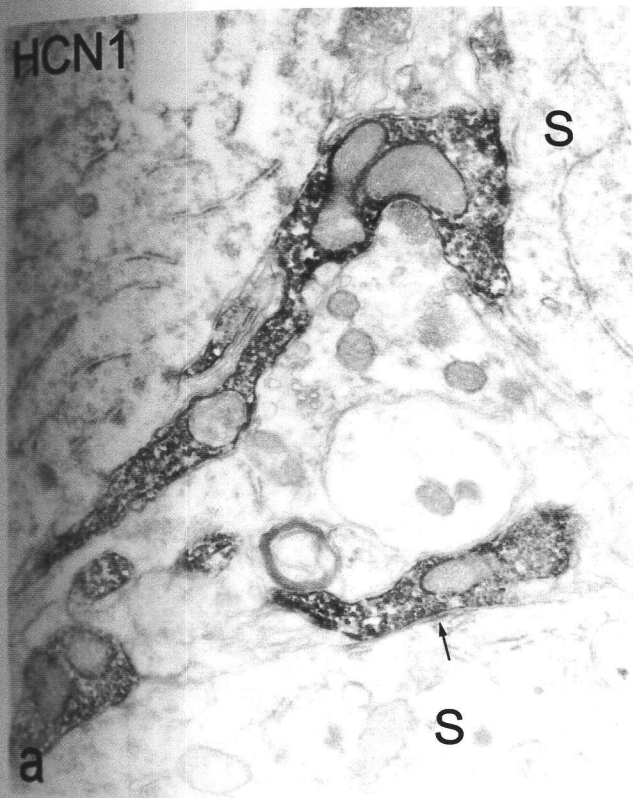


**Fig. 12 Distribution of HCN-LI in the telencephalic region**

Intense HCN1-LI is observed in the lateral septal nucleus (LS), whereas HCN2- and HCN3-LIs are prominent in the medial septal nucleus (MS) and nucleus of the diagonal band (DB). In the caudate putamen (CPu) diffuse immunoreactivity in neuropil is observed for HCN1 and HCN2. Arrow indicates axon bundles strongly immunostained for HCN1.

BST, bed nucleus of the stria terminalis; ICj, islands of Calleja; IG, indusium griseum; SHi, septohippocampal nucleus; Tu, olfactory tubercle; VP, ventral pallidum; ac, anterior commissure; cg, cingulum; ox, optic chiasm. Scale bar, 1000µm.

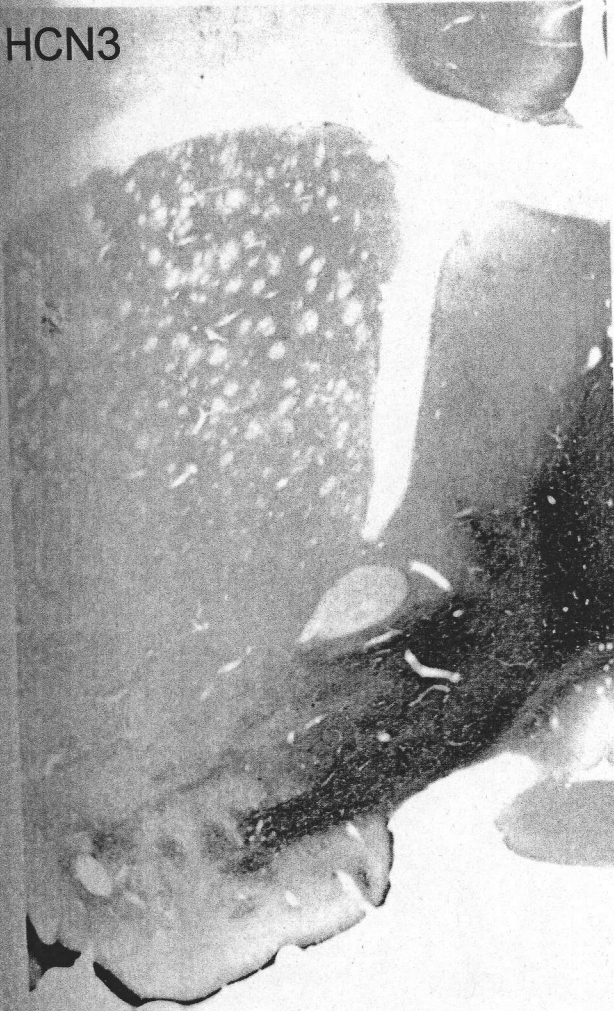
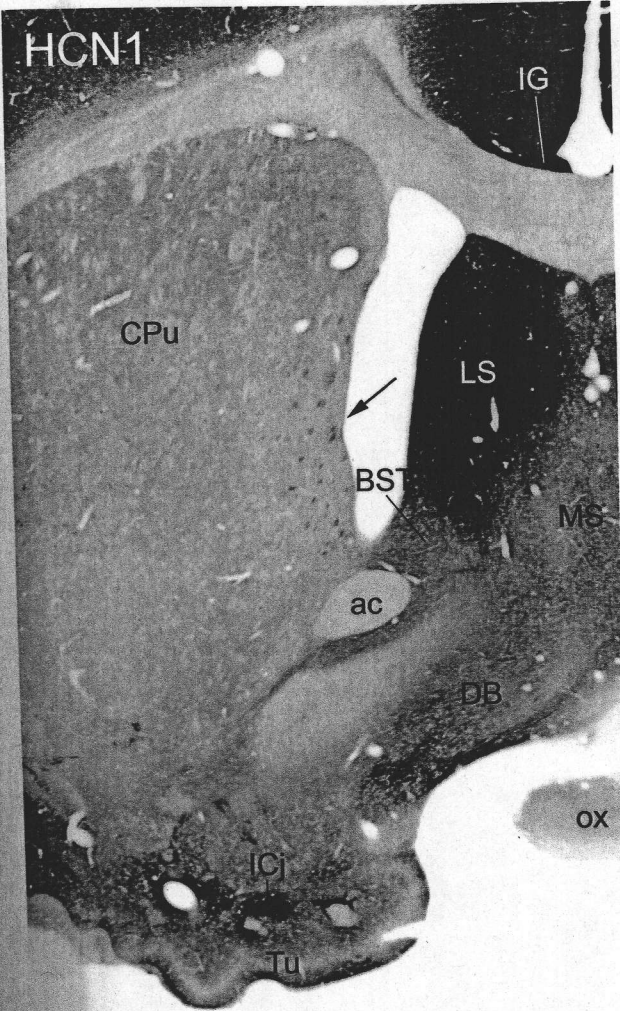


**Fig. 13 Immunoreactivity for HCN3 in cholinergic neurons**

In the caudate putamen, all ChAT-positive cell bodies are immunolabeled for HCN3 (upper figures). Presumed medial spiny neurons are moderately labeled for HCN3. In the flocculus of the cerebellum, immunoreactivity for HCN3 and VAcHt are extensively overlapped in bouton-like structures (lower figures). Scale bars, 50 $\mu$ m.

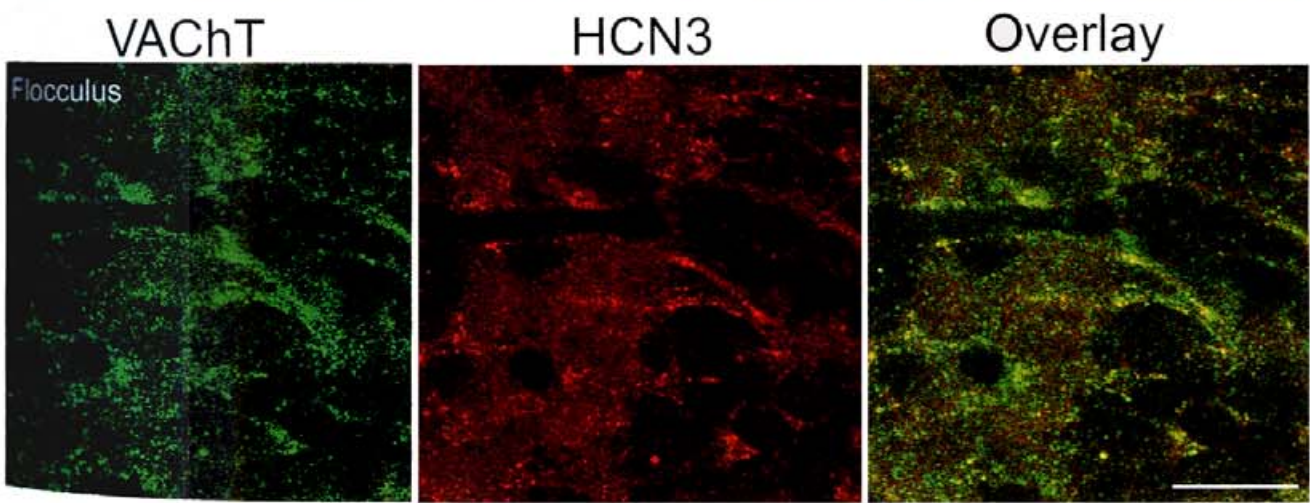
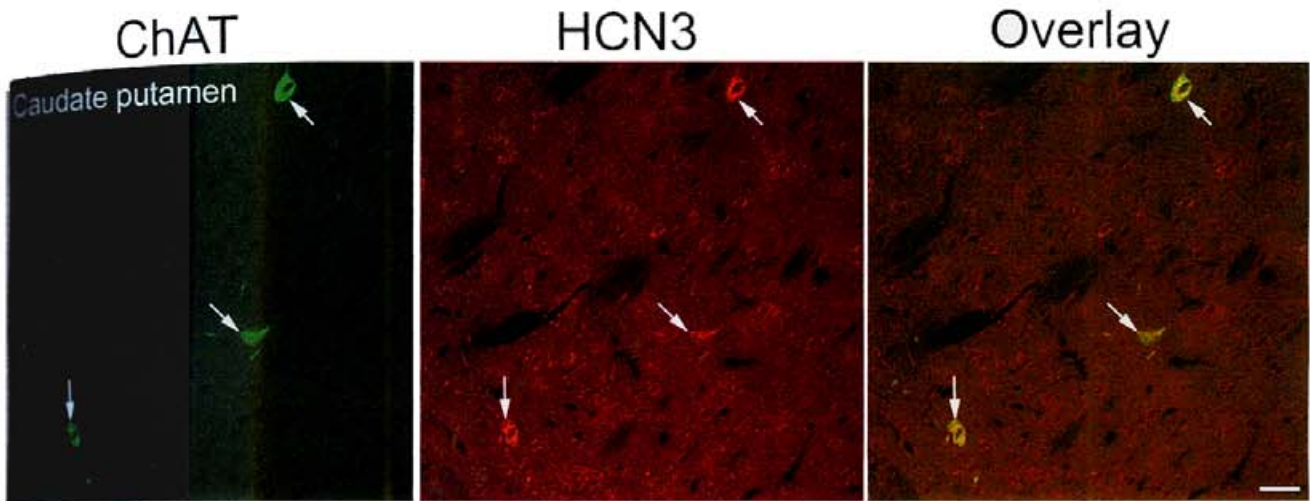


**Fig. 14 Distribution of HCN3- and HCN4-LIs in the hypothalamus and nucleus of the lateral olfactory tract**

Intense HCN3-LI is observed in the lateral hypothalamic area (LH), magnocellular preoptic nucleus (MCPO) and superficial layers (arrow, terminal zone of projections from the main olfactory bulb) of the amygdaloid area and nucleus of the lateral olfactory tract (LOT), whereas intense HCN4-LI is restricted to layer I of the LOT. SCh, suprachiasmatic nucleus; SO, supraoptic nucleus. Scale bar, 1000 $\mu$ m.

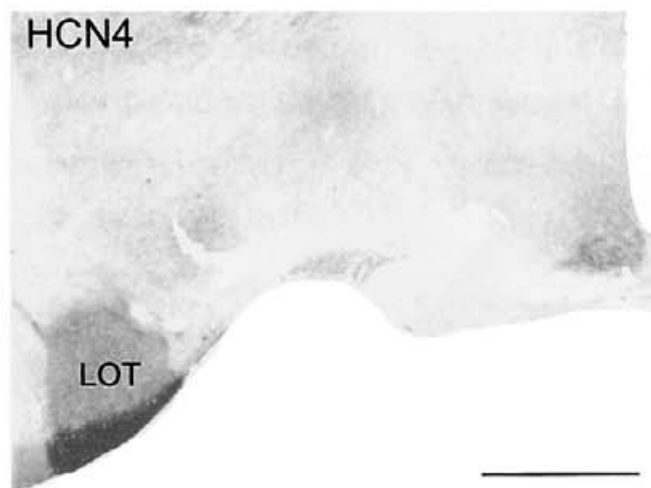
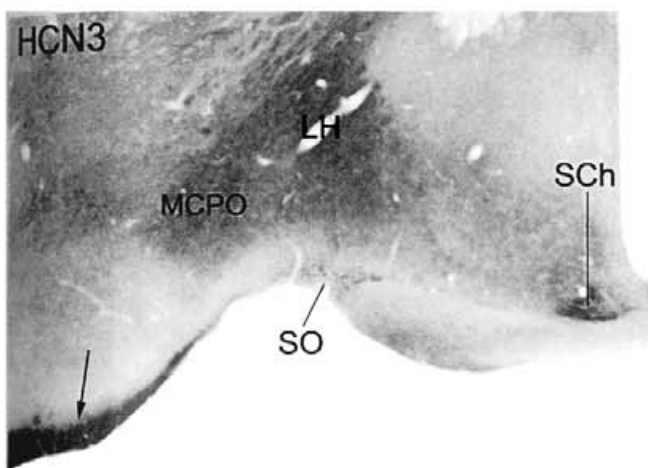


**Fig. 15 Distribution of HCN-LI in the diencephalic region**

Distinct distribution patterns are apparent for the four HCN subtypes in the diencephalon. Immunoreactivity for HCN2 is extensively observed throughout the thalamus and hypothalamus, whereas those for HCN3 and HCN4 are mainly localized to the hypothalamic and thalamic regions, respectively, looking largely complementary to each other. AD, anterodorsal thalamic nucleus; AM, anteromedial thalamic nucleus; AMV, anteromedial thalamic nucleus, ventral part. AV, anteroventral thalamic nucleus; AH, anterior hypothalamic area; Amy, amygdaloid area; GP, globus pallidus; LD, laterodorsal thalamic nucleus; LH, lateral hypothalamic area; Pa, paraventricular hypothalamic nucleus; PT, paratenial thalamic nucleus; PV, paraventricular thalamic nucleus; Re, reuniens thalamic nucleus; Rh, rhomboid thalamic nucleus; Rt, reticular thalamic nucleus; VA, ventral anterior thalamic nucleus; f, fornix; ic, internal capsule; st, stria terminalis. Scale bar, 1000µm.

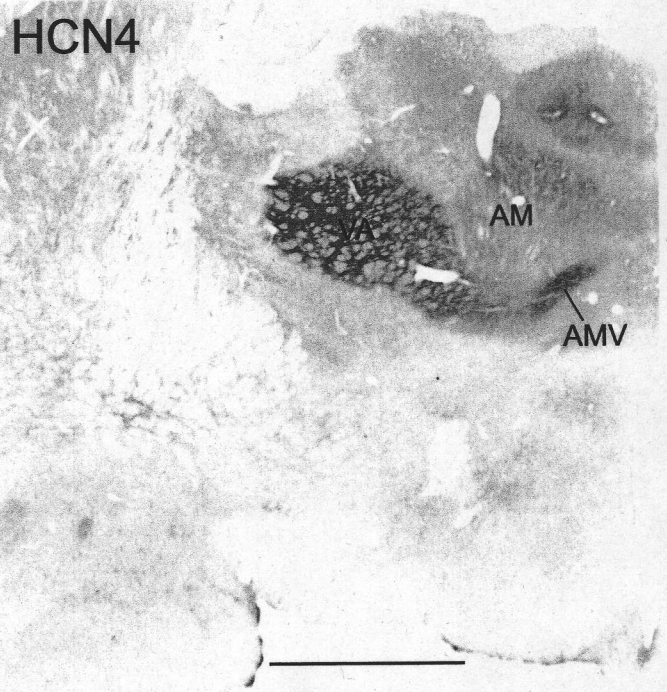
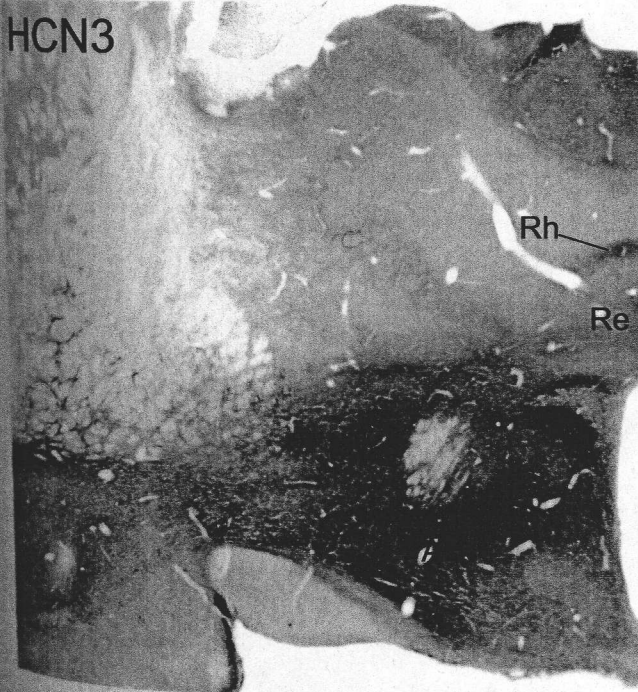
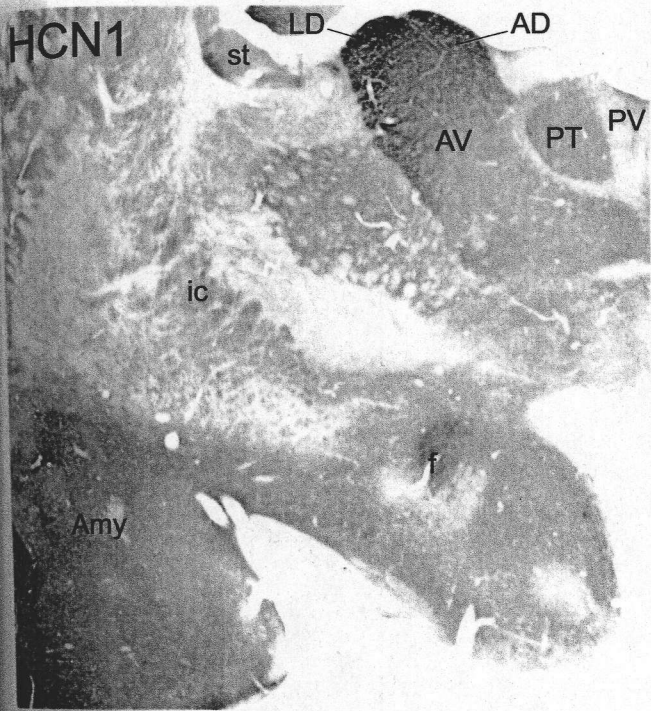


**Fig. 16 Distribution of HCN-LI in the diencephalic region**

CM, central medial thalamic nucleus; DM, dorsomedial hypothalamic nucleus, Hb, habenular nuclei; LD, laterodorsal thalamic nucleus; LH, lateral hypothalamic area; MD, mediodorsal thalamic nucleus; PV, paraventricular thalamic nucleus; Rt, reticular thalamic nucleus; Sub, submedius thalamic nucleus; VL, ventrolateral thalamic nucleus; VM, ventromedial thalamic nucleus; VPL, ventral posterolateral thalamic nucleus; VPM, ventral posteromedial thalamic nucleus, ZI, zona incerta; aot, accessory olfactory tract; f, fornix; mt, mammillothalamic tract. Scale bar, 1000 $\mu$ m.

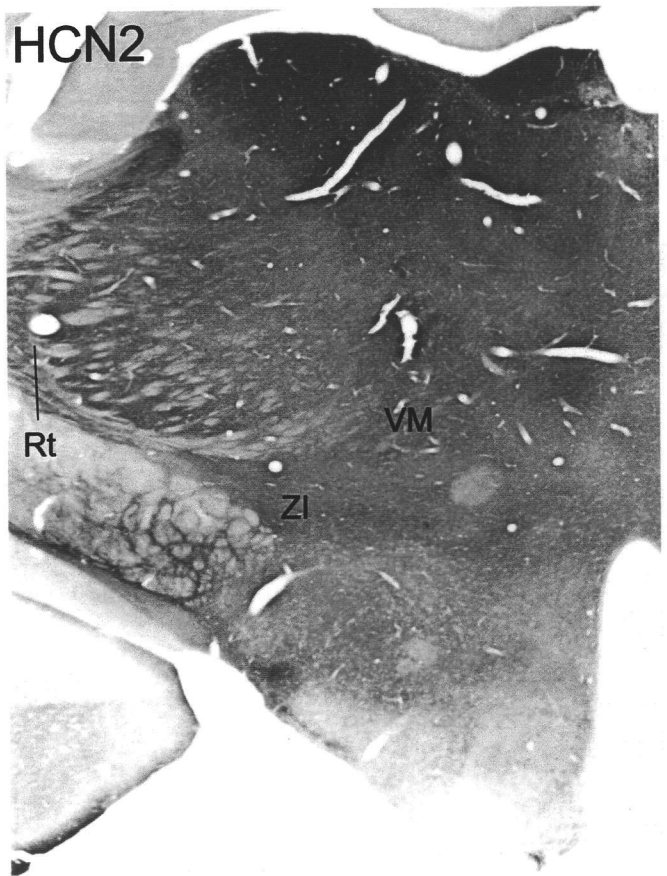
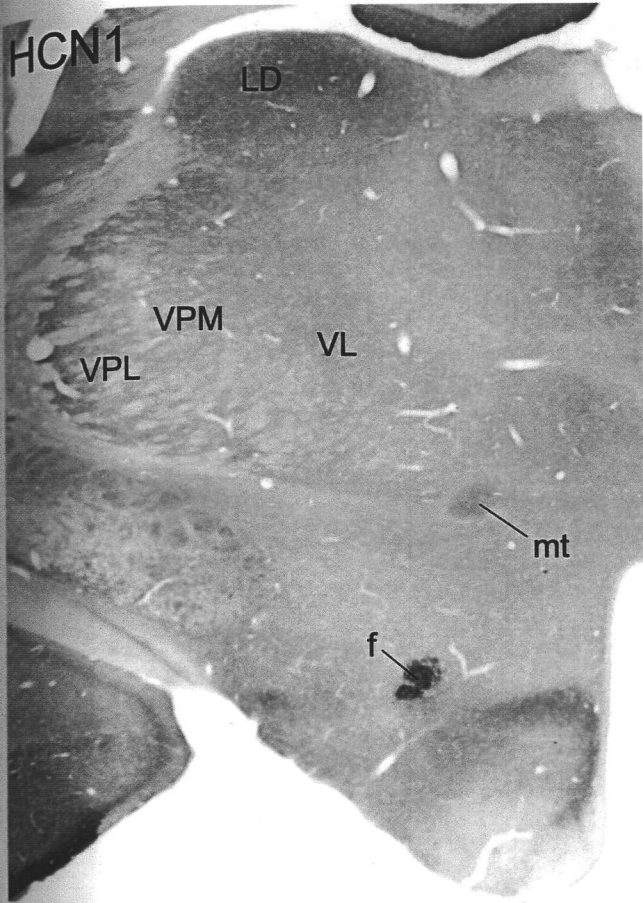


**Fig. 17 Distribution of HCN-LI in the diencephalic region**

Arrow shows patches of intense HCN1-LI in the border zone between the medial (MHb) and lateral habenula (LHb). Intense immunolabeling in axonal bundles is observed for HCN1 in the fornix (f) and internal capsule (ic), and that for HCN3 and HCN4 in the fasciculus retroflexus (fr). DLG, dorsal lateral geniculate nucleus; LH, lateral hypothalamic area; LP, lateral posterior thalamic nucleus; PF, parafascicular thalamic nucleus; PH, posterior hypothalamic area; PM, premammillary nucleus; Po, posterior thalamic nuclear group; STh, subthalamic nucleus; VLG, ventral lateral geniculate nucleus; VPL, ventral posterolateral thalamic nucleus; VPM, ventral posteromedial thalamic nucleus; VPPC, ventral posterior thalamic nucleus, parvicellular part; VTM, ventral tuberomammillary nucleus; ZI, zona incerta. Scale bar, 1000µm.

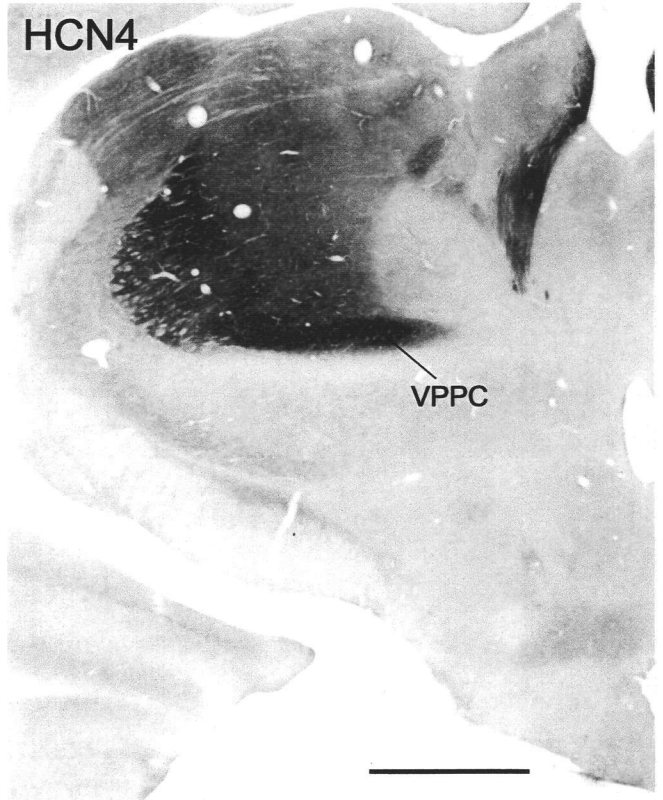
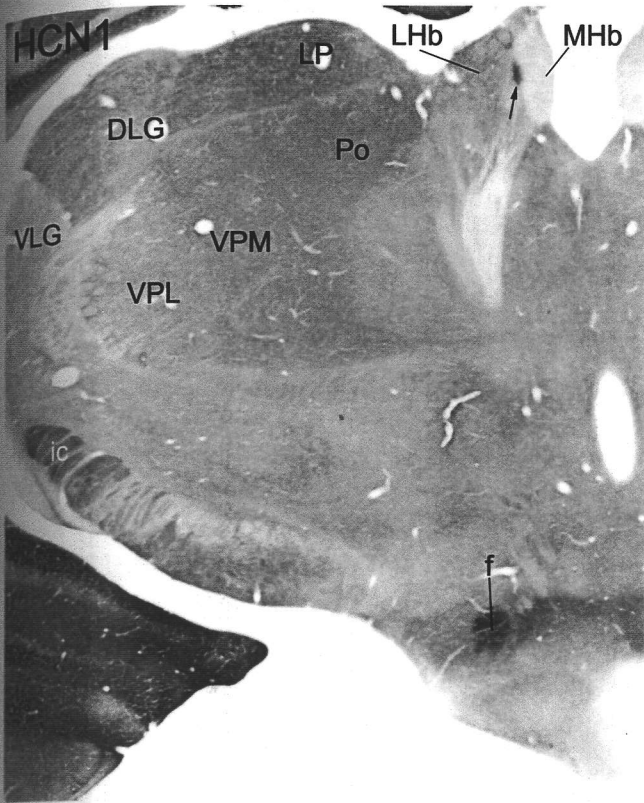


**Fig. 18 Distribution of HCN-LI in the diencephalic region**

Distinct immunolabeling patterns for HCNs are apparent in the geniculate nuclei. HCN2-LI is extensively distributed in the medial and lateral geniculate nuclei, whereas intense immunolabeling for HCN3 is restricted to the intergeniculate leaflet (IGL), and that for HCN4 to the dorsal lateral geniculate nucleus (DLG) and medial geniculate nucleus (MG). In the substantia nigra, immunolabeling for HCN3 is strong in the compact part (SNC), and that for HCN2 in the reticular part (SNR). APTD, anterior pretectal nucleus, dorsal part; APTV, anterior pretectal nucleus, ventral part; LH, lateral hypothalamic area; LMN, lateral mammillary nucleus; LP, lateral posterior thalamic nucleus; MG, medial geniculate nucleus; MM, medial mammillary nucleus; MPT, medial pretectal nucleus; OPT, olivary pretectal nucleus; SNM, substantia nigra medial part; VLG, ventral lateral geniculate nucleus; cp, cerebral peduncle; fr, fasciculus retroflexus. Scale bar, 1000 $\mu$ m.

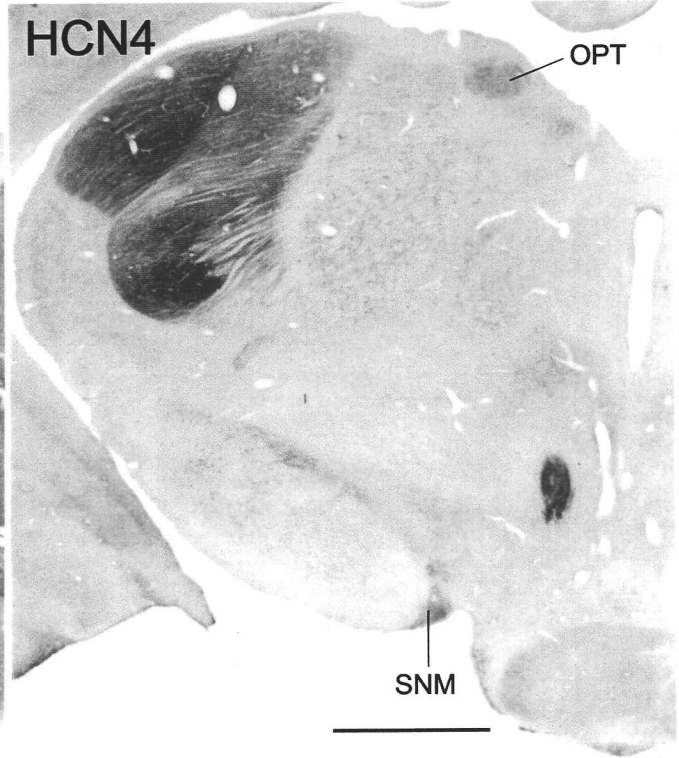
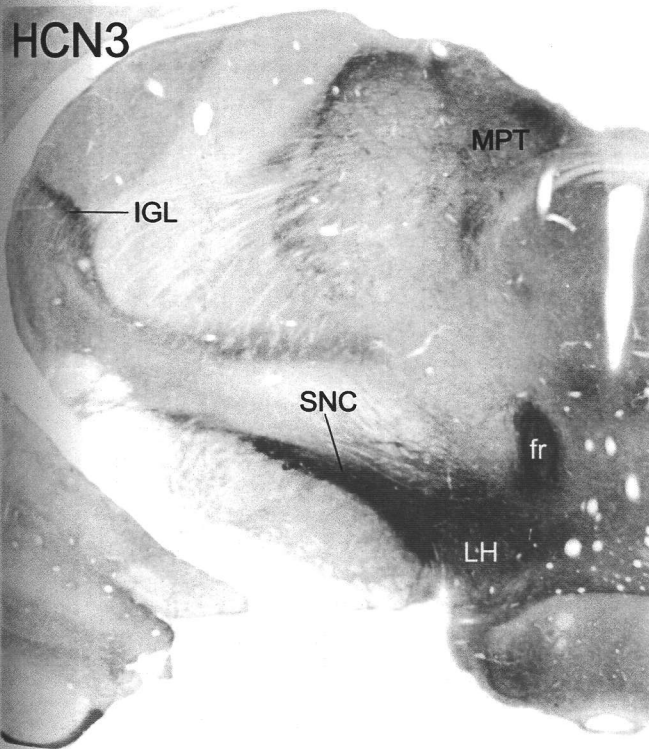
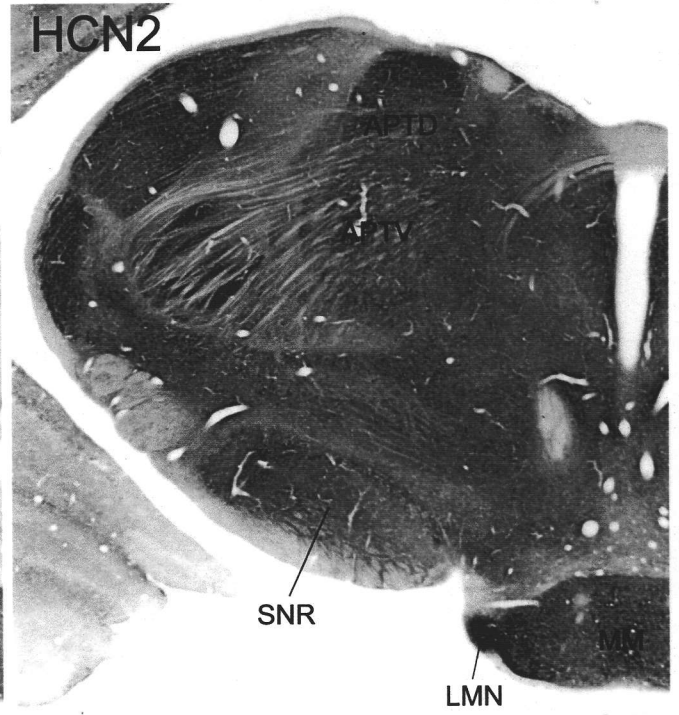
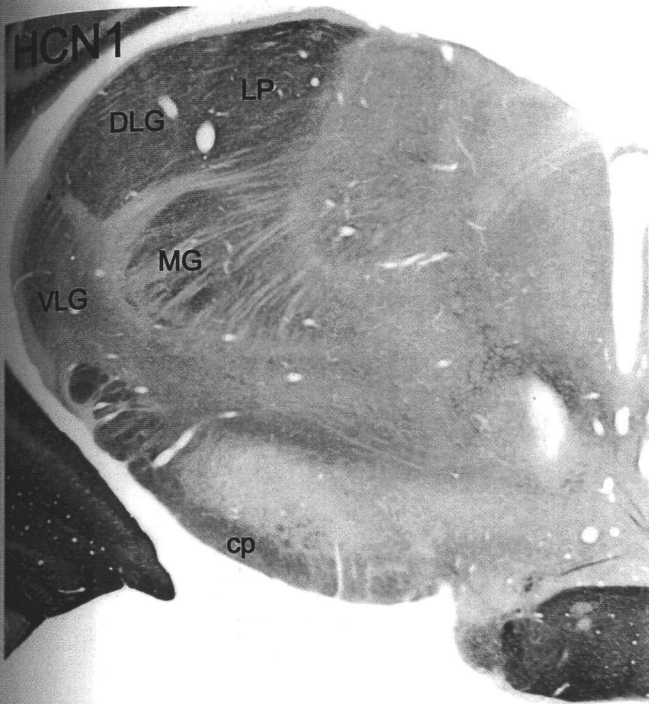


**Fig. 19 Distribution of HCN-LI in the midbrain**

Intense immunolabeling for HCN1 and HCN3 is observed in the superficial gray layer of the superior colliculus (SuG). Arrows indicate HCN3-positive dense network processes penetrating the intermediate layers of the superior colliculus. The most intense HCN3-LI in the brain is found in the interpeduncular nuclei (IP). 3, oculomotor nucleus; DLPAG, dorsolateral periaqueductal gray; DMPAG, dorsomedial periaqueductal gray, InG, intermediate gray layer of the superior colliculus; InWh, intermediate white layer of the superior colliculus; LPAG, lateral periaqueductal gray; MG, medial geniculate nucleus; Op, optic nerve layer of the superior colliculus; R, red nucleus; SNCD, substantia nigra, compact part, dorsal tier; SNL, substantia nigra lateral part; SNR, substantia nigra, reticular part. Scale bar, 1000 $\mu$ m.

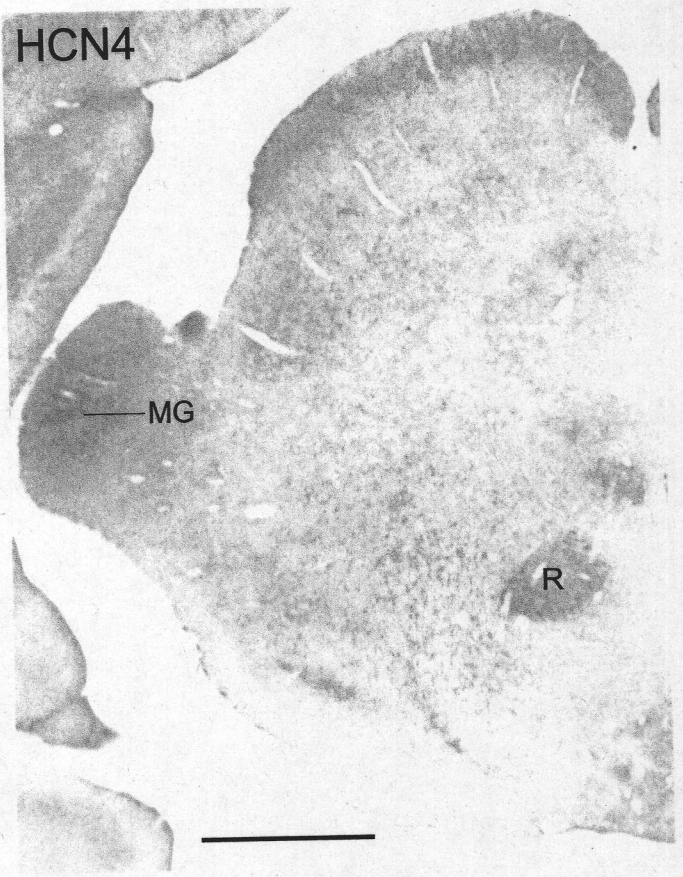
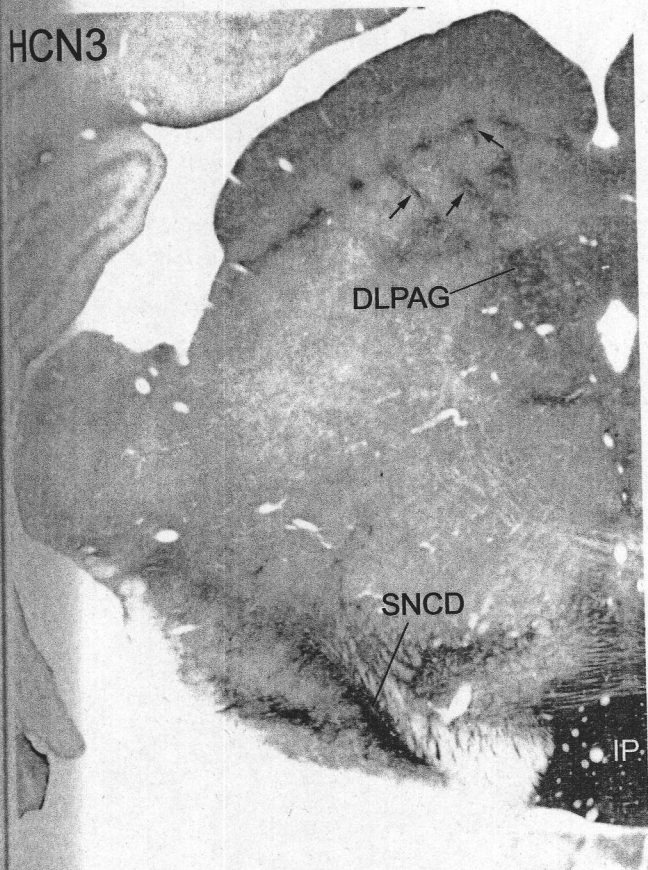
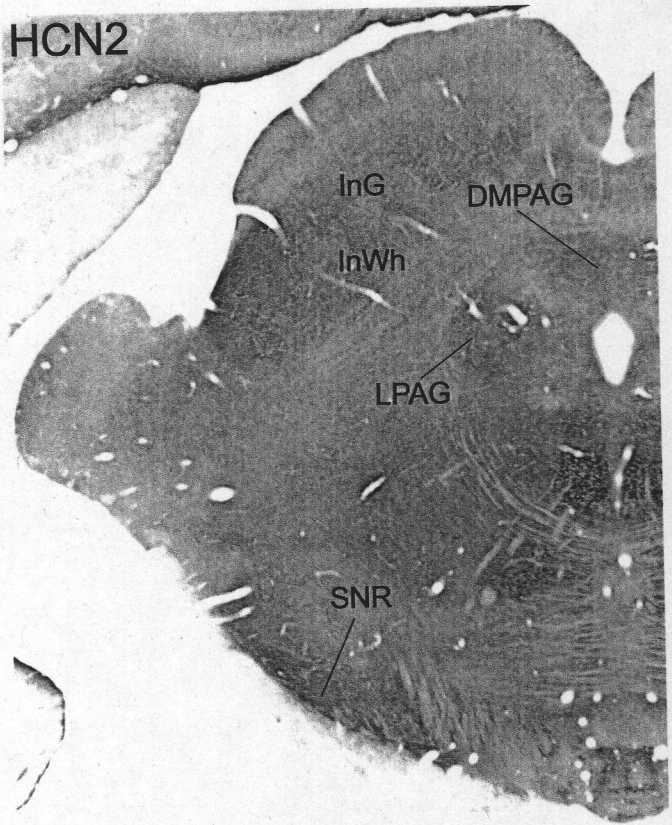


**Fig. 20 Presynaptic localization of HCN3 in the interpeduncular nucleus**

In the interpeduncular nucleus, HCN3-LI is localized to preterminal and terminal portions of axons. Arrows indicate asymmetrical synapses. Scale bar, 0.2 $\mu$ m.

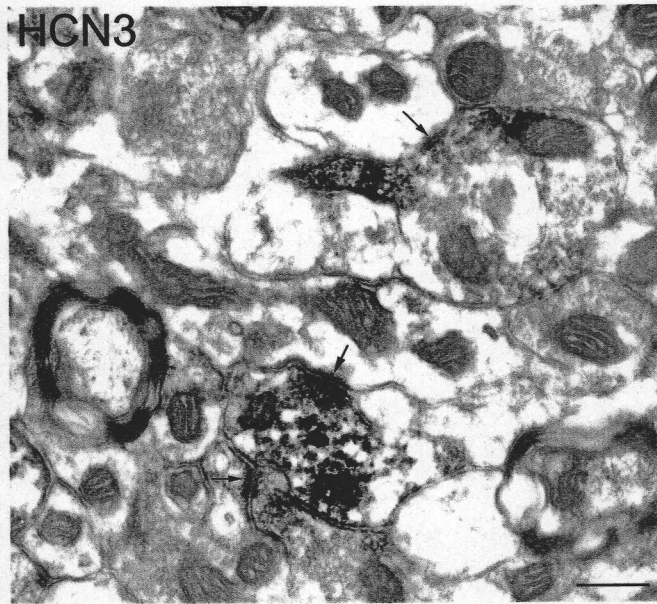


**Fig. 21 Distribution of HCN-LI in the pons**

Intense immunolabeling for HCN1 and HCN2 is observed in the inferior colliculus (IC) and that for HCN3 in the dorsal raphe (DR), median raphe (MnR) and cuneiform (CnF) nuclei. The nucleus of the lateral lemniscus (LL) has intense immunoreactivity for all HCNs. PAG, periaqueductal gray; Pn, pontine nuclei; PnO, pontine reticular nucleus, oral part; PPTg, pedunclopontine tegmental nuclei; VTg, ventral tegmental nucleus; lfp, longitudinal fasciculus of the pons. Scale bar, 1000µm.

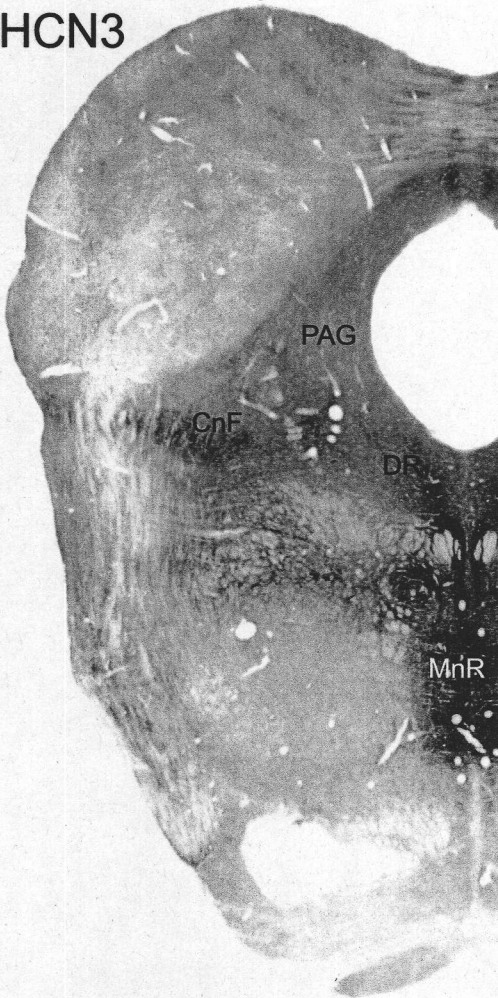
HCN1



HCN2



HCN3



HCN4

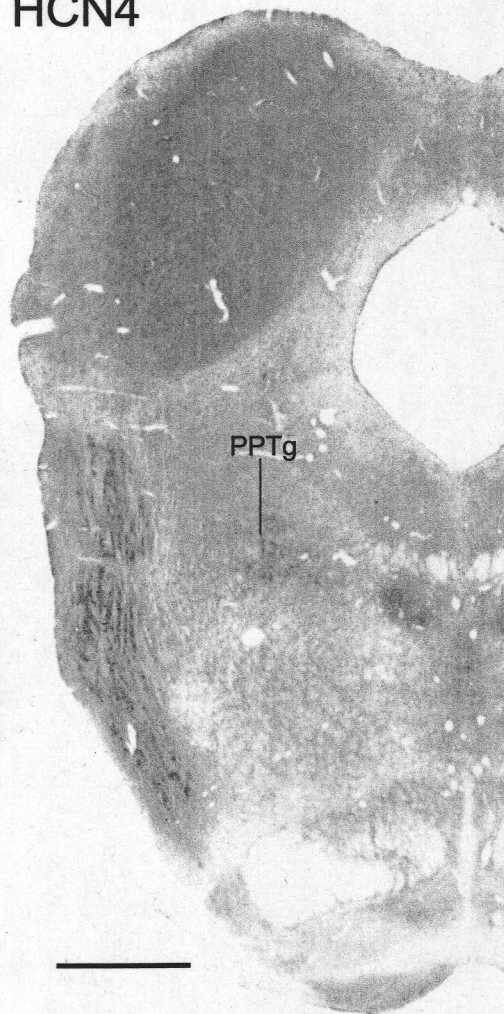


**Fig. 22 Distribution of HCN-LI in the medulla oblongata**

The superior olivary complex (SOC) and anterior part of the ventral cochlear nucleus (VCA) show intense immunolabeling for all HCNs. Pr5, principal sensory trigeminal nucleus; Tz, nucleus of the trapezoid body; SuVe, superior vestibular nucleus; VPO, ventral periolivary nucleus; py, pyramidal tract. Scale bar, 1000 $\mu$ m.

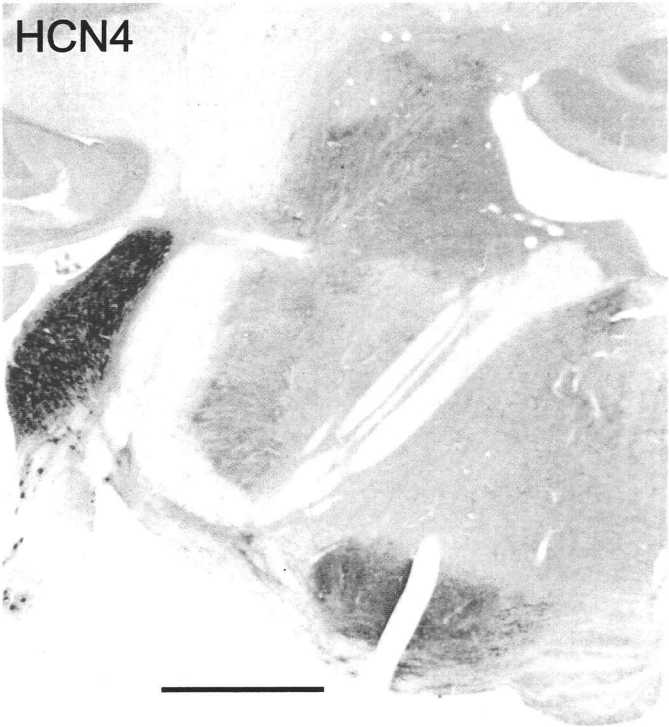
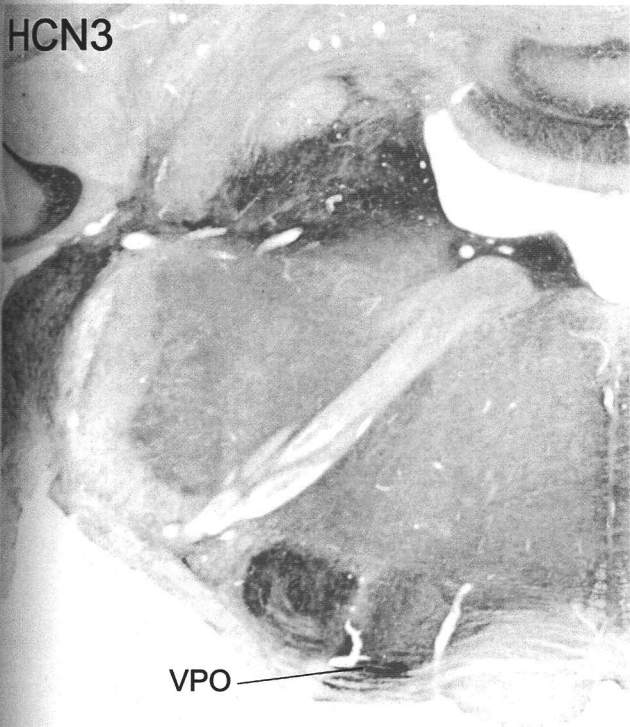
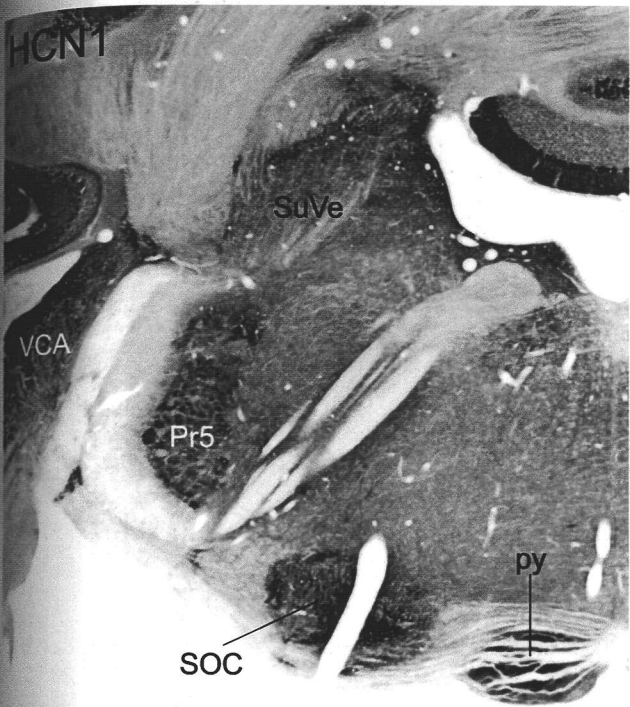
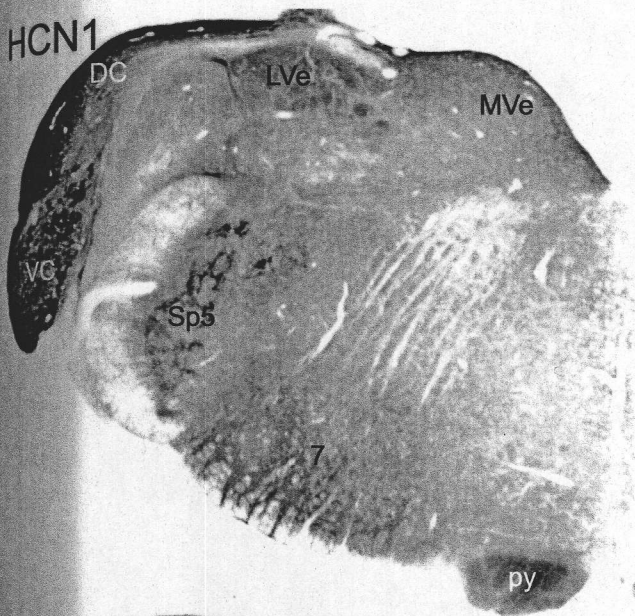


**Fig. 23 Distribution of HCN-LI in the medulla oblongata**

The dorsal cochlear nucleus (DC) shows intense immunolabeling for HCN1, HCN2 and HCN3. HCN2-LI is extensively observed throughout the medulla oblongata. 7, facial nucleus; LVe, lateral vestibular nucleus; MVe, medial vestibular nucleus; Sp5, spinal trigeminal nucleus; VC, ventral cochlear nucleus; py, pyramidal tract. Scale bar, 1000µm.

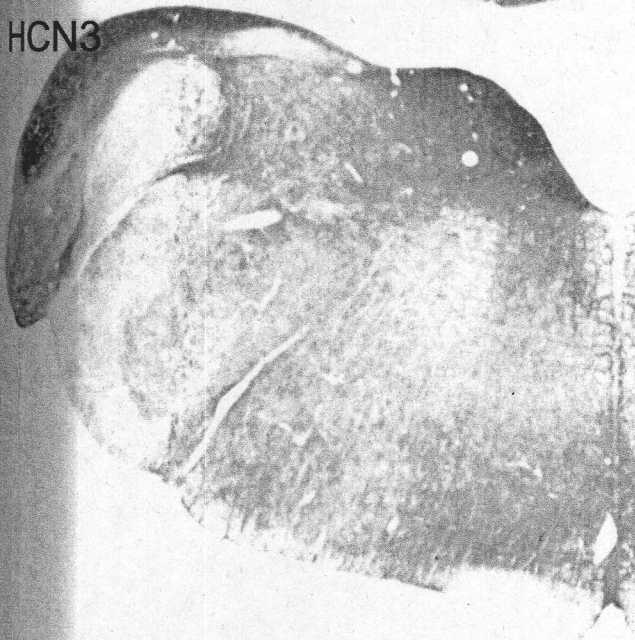
HCN1



HCN2



HCN3



HCN4

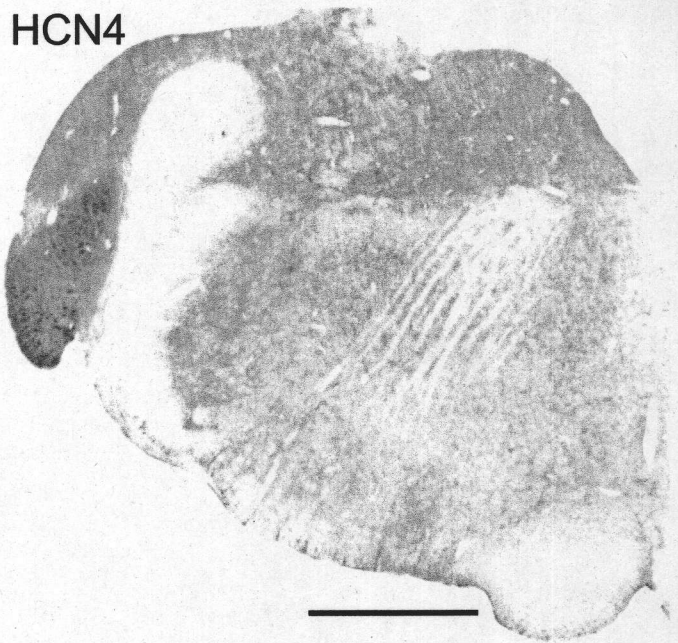
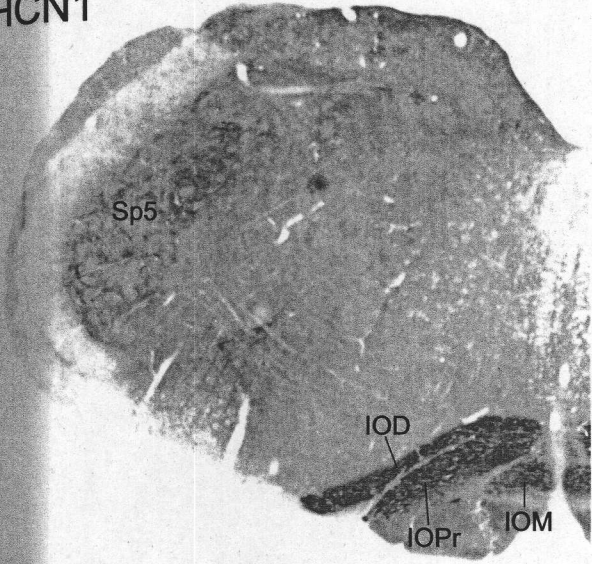


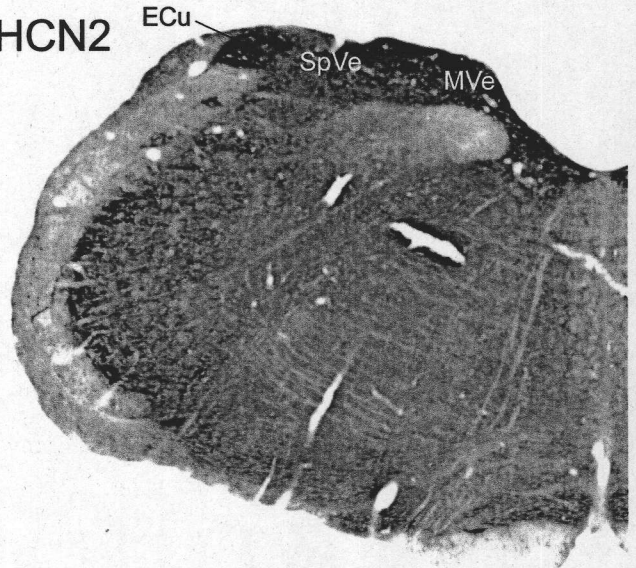
**Fig. 24 Distribution of HCN-LI in the medulla oblongata**

The inferior olivary complex shows intense immunolabeling for HCN1 and HCN3. Amb, ambiguus nucleus; ECu, external cuneate nucleus; IOD, inferior olive, dorsal nucleus; IOM, inferior olive, medial nucleus; IOPr, Inferior olive, principal nucleus; MVe, medial vestibular nucleus; Sol, nucleus of the solitary tract; Sp5, spinal trigeminal nucleus; SpVe, spinal vestibular nucleus. Scale bar, 1000 $\mu$ m.

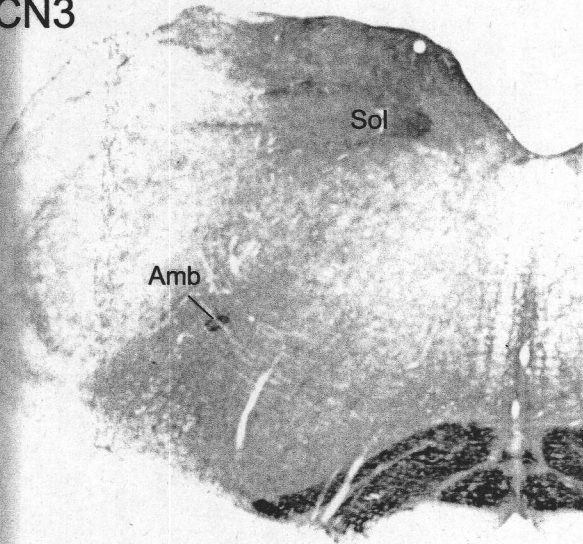
HCN1



HCN2



HCN3



HCN4

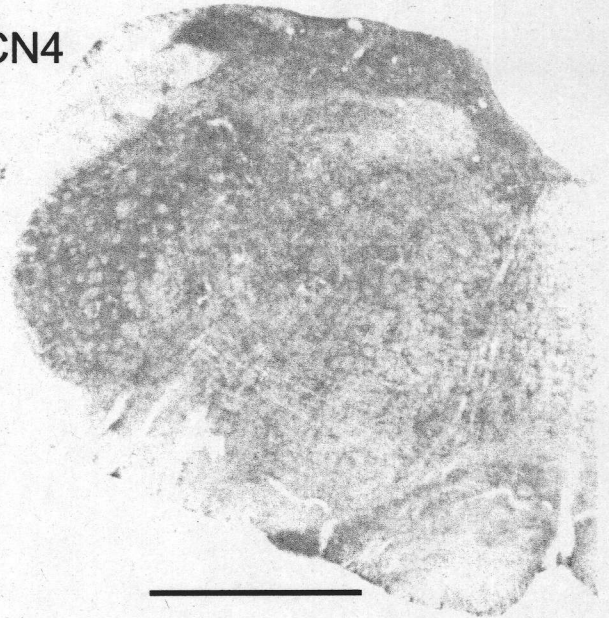
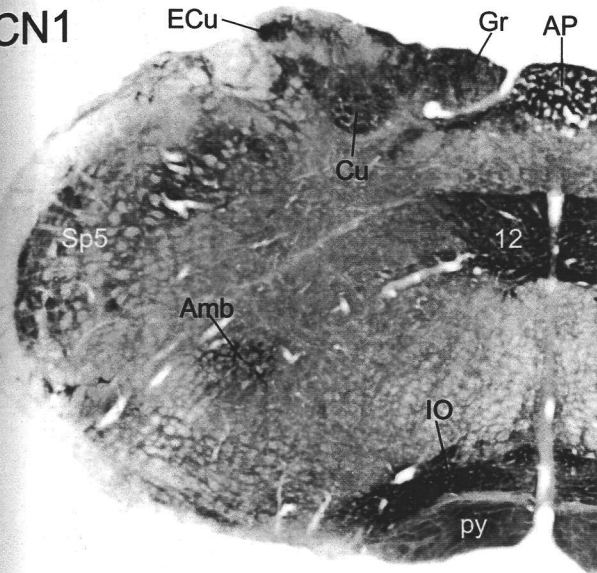


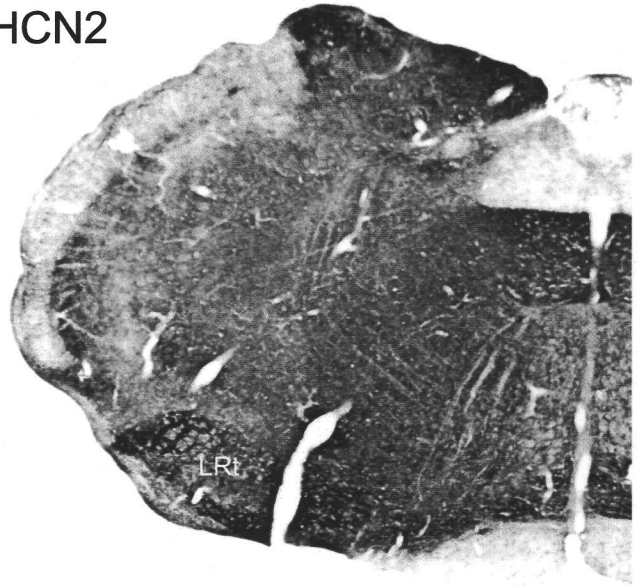
**Fig. 25 Distribution of HCN-LI in the medulla oblongata**

The hypoglossal nucleus (12) shows intense immunolabeling for HCN1 and HCN2, but with little colocalization (see Fig. 8). The nucleus of the solitary tract (Sol) is labeled for HCN3 but devoid of HCN2-LI. The area postrema (AP) shows intense immunolabeling for HCN1, HCN3 and HCN4. 10, dorsal motor nucleus of vagus; Amb, ambiguus nucleus; Cu, cuneate nucleus; ECu, external cuneate nucleus; Gr, gracile nucleus; IO, inferior olivary complex; IRt, intermediate reticular nucleus; LRt, lateral reticular nucleus; Sp5, spinal trigeminal nucleus; py, pyramidal tract. Scale bar, 1000 $\mu$ m.

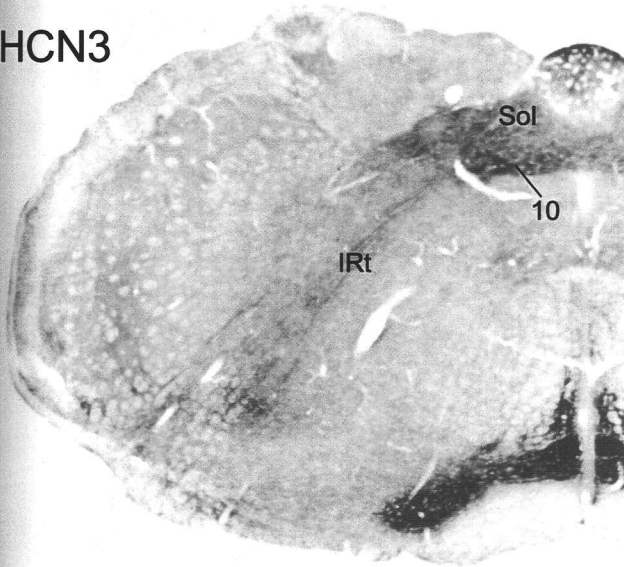
HCN1



HCN2



HCN3



HCN4

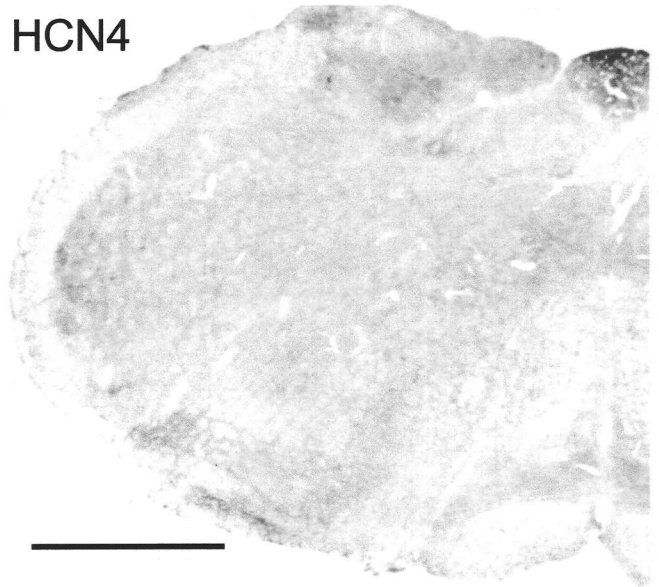


**Fig. 26 Distribution of HCN-LI in the cerebellar cortex**

Arrows indicate HCN1-positive ponceau-like structures basket cell axons. HCN2-immunopositive small cells are observed (arrow heads) in the granule cell layer (GC). MO, molecular layer; PC, Purkinje cell layer. Scale bar, 20µm.

HCN1

HCN2

HCN3

HCN4

MO

PC

GC

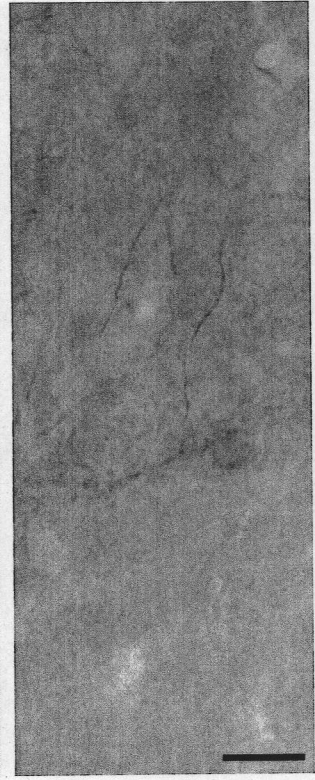
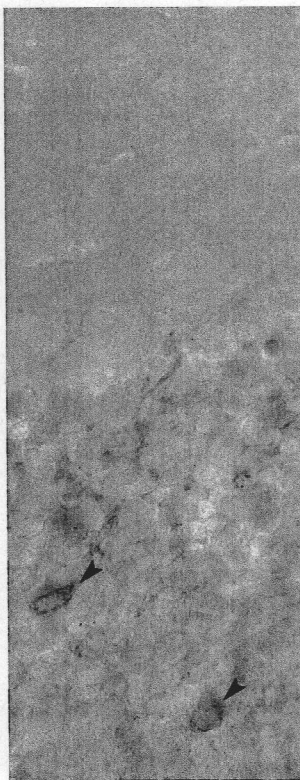


**Fig. 27 Presynaptic localization of HCN1-LI in the Purkinje cell layer of the cerebellum**

Most immunogold particles for HCN1 are observed in GAD-positive (peroxidase reaction) axons of basket cells (a). In basket cell terminals, immunogold particles for HCN1 are rarely found (b), being distant from symmetrical synapses (arrow). Pur, Purkinje cell body. Scale bar, 0.2 $\mu$ m.

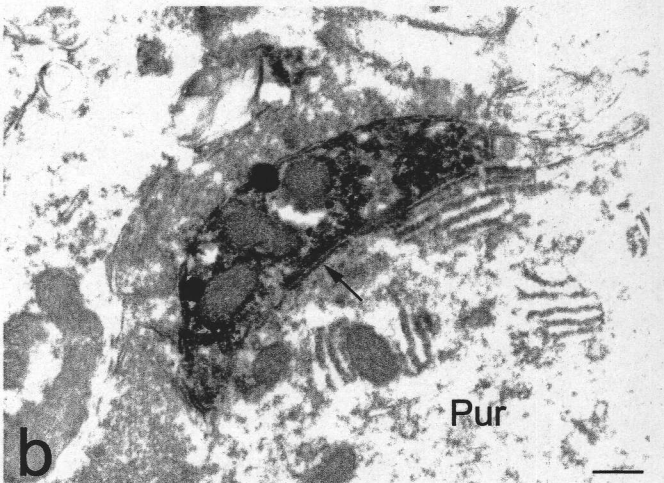
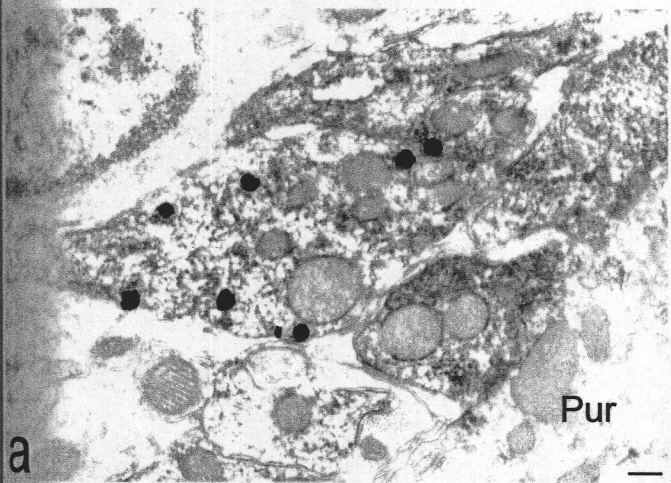


**Fig. 28 Distribution of HCN3-LI in the flocculus**

Immunolabeling for HCN3 is selectively strong in the granule cell layer of the flocculus (Fl). PFl, paraflocculus; VCA, ventral cochlear nucleus, anterior part. Scale bar, 1000 $\mu$ m.

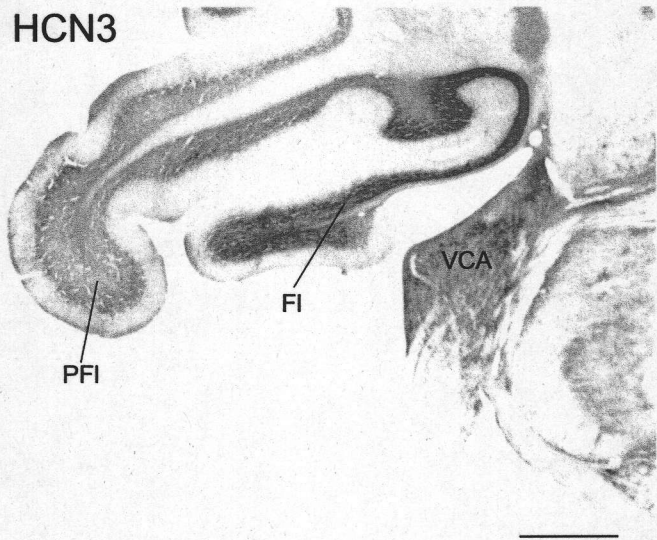


**Fig. 29 Electron microscopic localization of HCN3-LI in the flocculus**

(a) HCN3-labeled boutons (arrow) contain small round vesicles and have no clear synapses. (b) A rare example of the HCN3-labeled bouton that has an asymmetrical synapse (arrow). Scale bar, 0.2 $\mu$ m

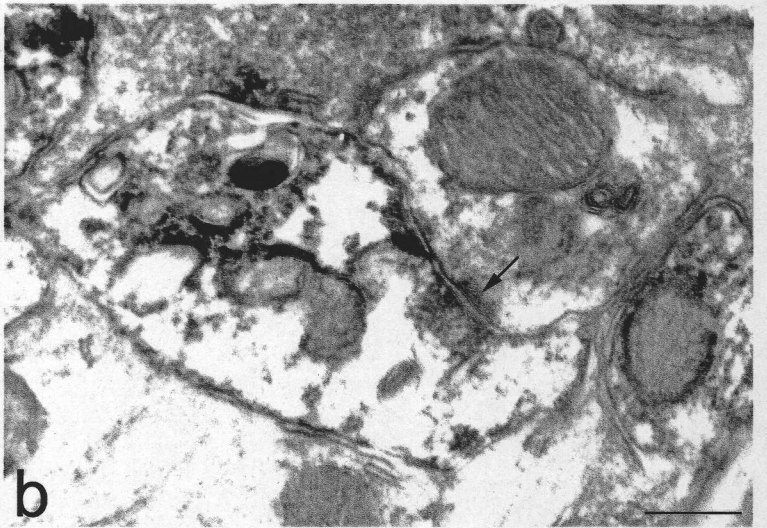


**Fig. 30 Distribution of HCN-LI in the deep cerebellar nuclei**

The deep cerebellar nuclei and lateral vestibular nucleus (LVe) show intense immunolabeling for HCN1 and HCN2. Int, interposed cerebellar nucleus; Lat, lateral cerebellar nucleus; Med, medial cerebellar nucleus; MVe, medial vestibular nucleus. Scale bar, 1000 $\mu$ m.

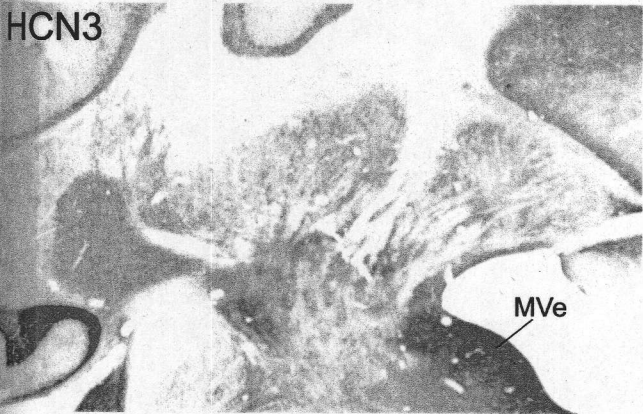
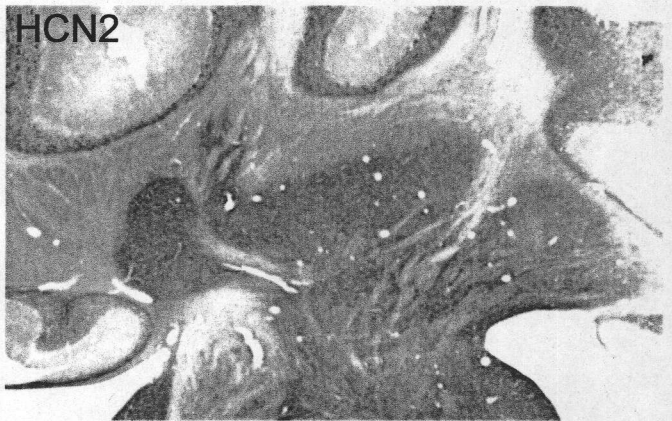
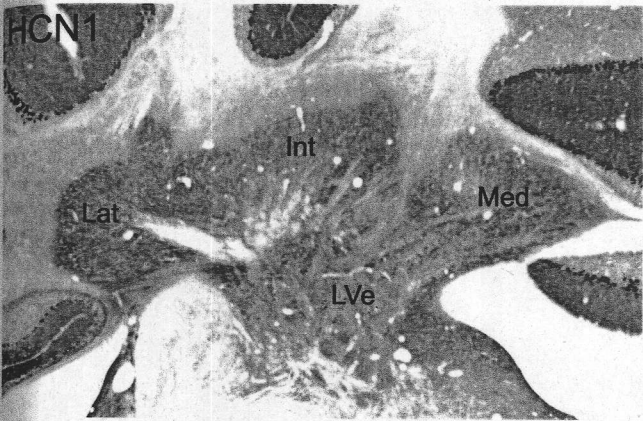


**Fig. 31 Localization of HCNs in myelinated axons**

Peroxidase reaction products for HCN4 (a) and immunogold particles for HCN2 (b) are seen in myelinated axons in the medial habenular nucleus and hippocampal CA3 area, respectively. Scale bar, 0.2 $\mu$ m.

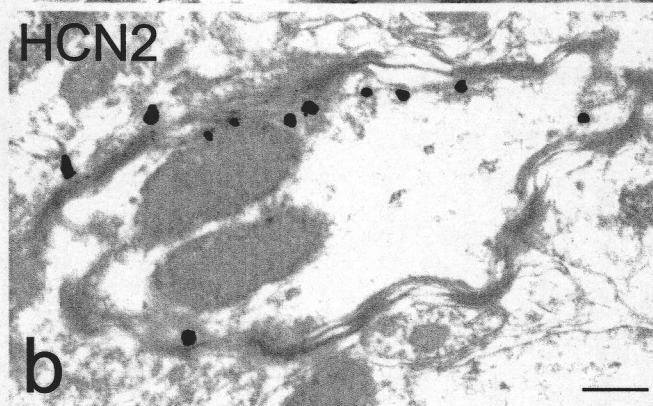
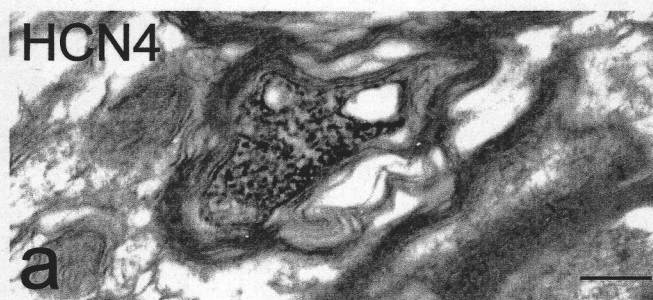
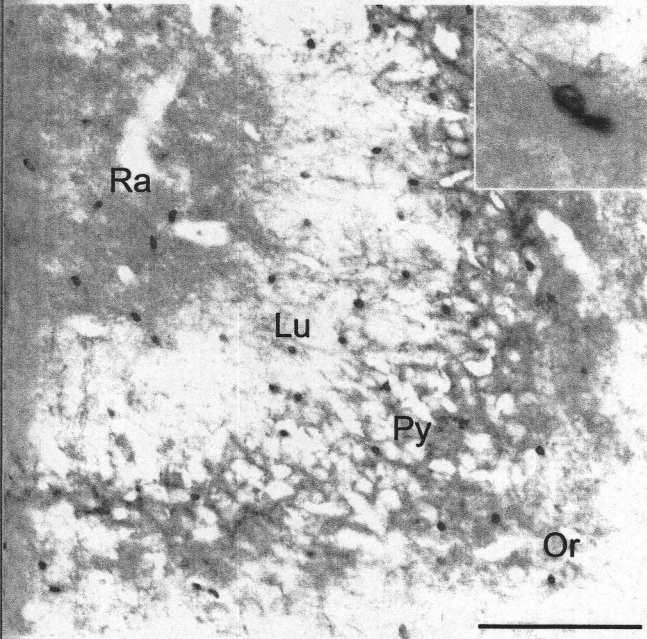


**Fig. 32 HCN2-immunopositive small cells**

HCN2-immunopositive small cells are extensively found in most brain regions, being densest in neuronal cell layers such as the CA3 pyramidal cell layer (Py) of the hippocampus and cerebellar granule cell layer (GC). Inset: Cell bodies with fine processes are shown. Or, stratum oriens; Lu, stratum lucidum; Ra, stratum radiatum; MO, molecular layer; PC, Purkinje cell layer. Scale bars, 100 $\mu$ m.

Hippocampus



Cerebellar Cortex

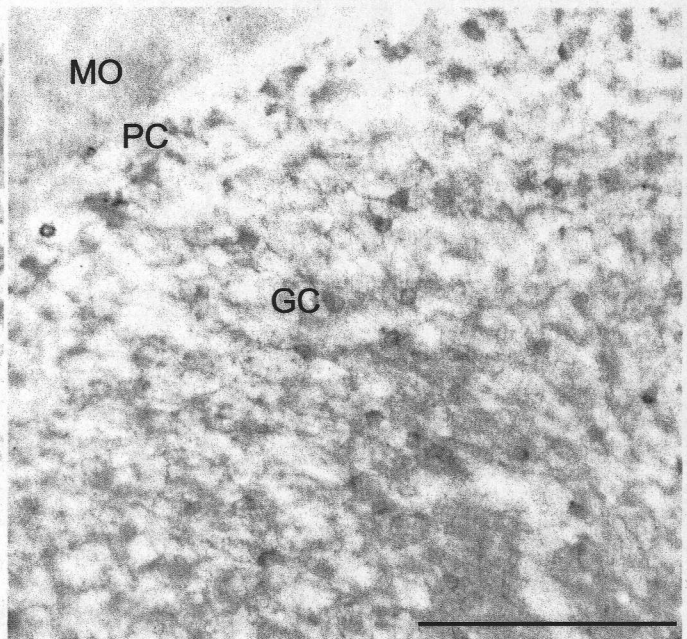


**Fig. 33 Double-immunofluorescence for identification of HCN2-immunopositive small cells in the hippocampus**

Markers for matured neurons (NeuN), astrocytes (GFAP), microglia (Iba-1) and oligodendrocyte progenitors (NG2) are negative for HCN2-immunopositive small cells (arrows). Scale bars, 50 $\mu$ m.

Marker

HCN2

Overlay

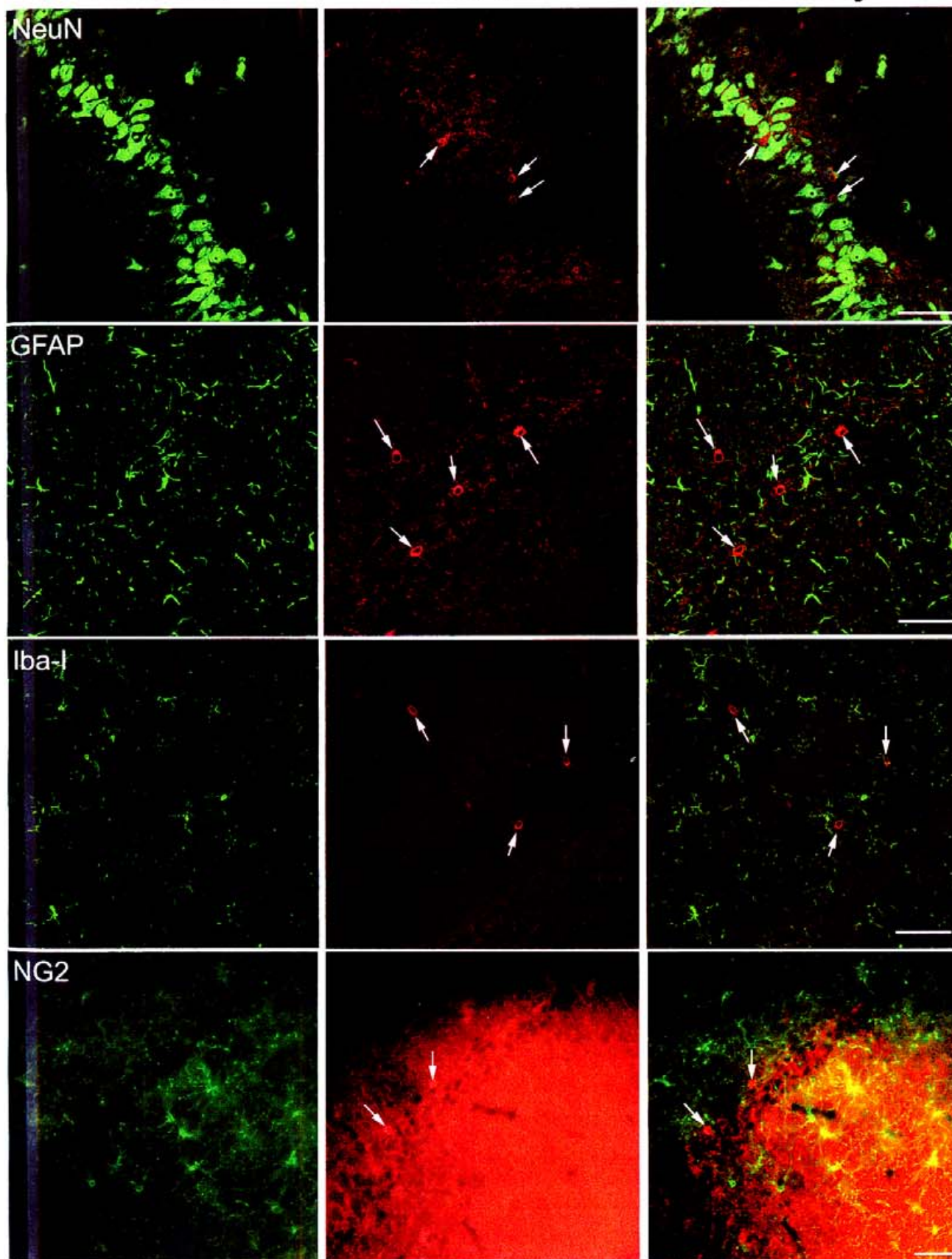


**Fig. 34 Double-immunofluorescence for HCN2 and GST- $\pi$**

GST- $\pi$ , a marker for oligodendrocytes, is positive in all HCN2-immunopositive cells (arrows) throughout the brain (upper figures). In some regions such as the cingulate cortex, perirhinal cortex, periamygdaloid cortex (a caudal part of the piriform cortex), lateral entorhinal cortex and amygdaloid area (lower figures), where very few HCN2-immunopositive cells are present, cells single labeled for GST- $\pi$  are found. Scale bars, 50 $\mu$ m.

GST- $\pi$

HCN2

Overlay

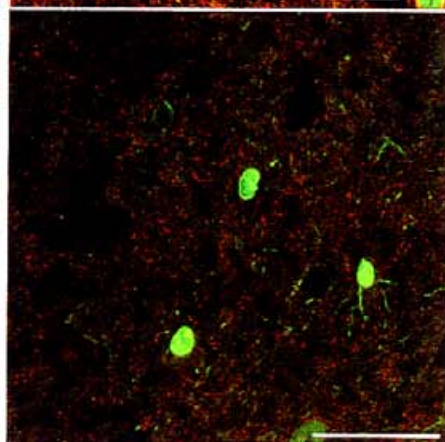
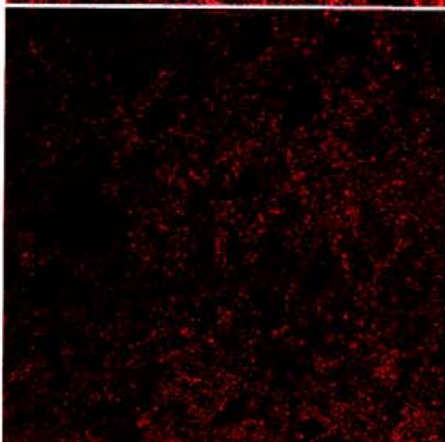
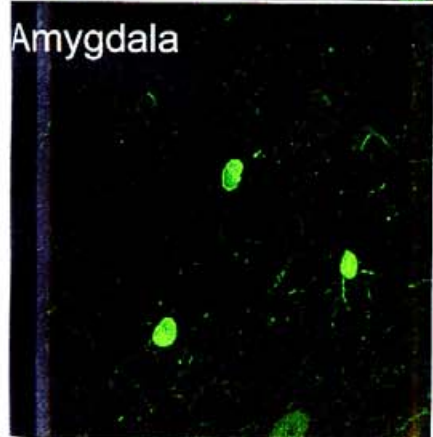
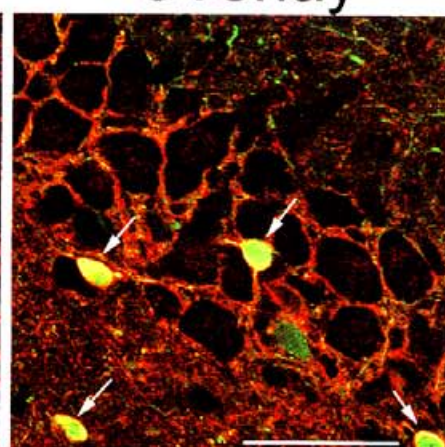
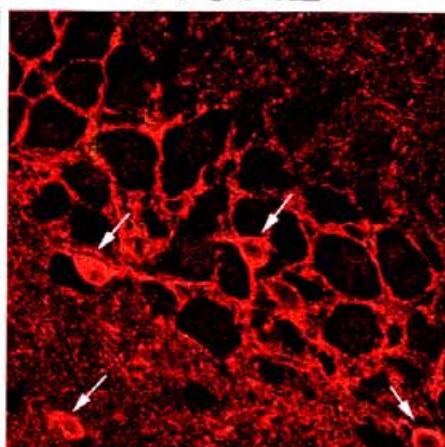
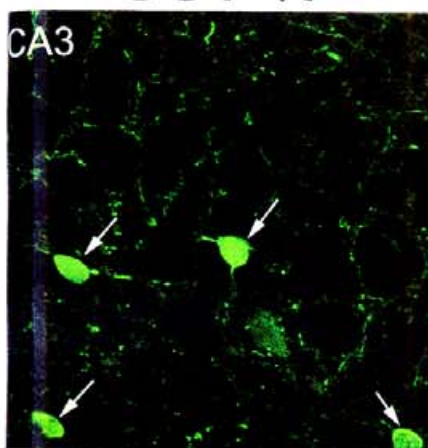
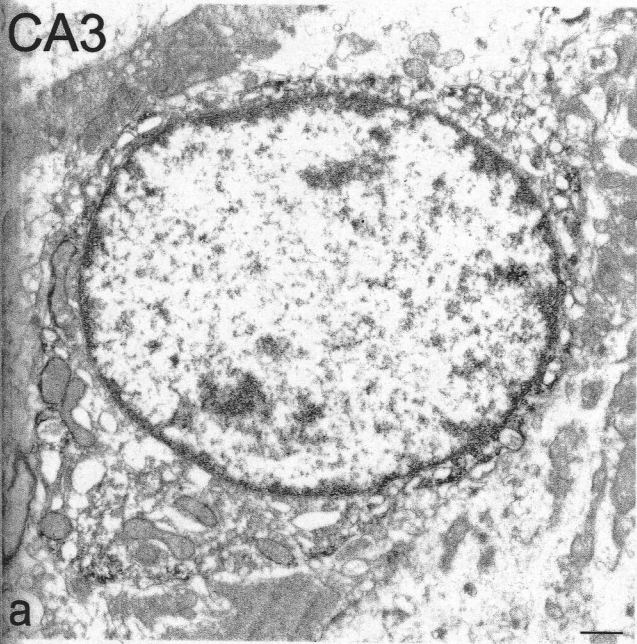


**Fig. 35 Electron microscopic localization of HCN2 in oligodendrocytes**

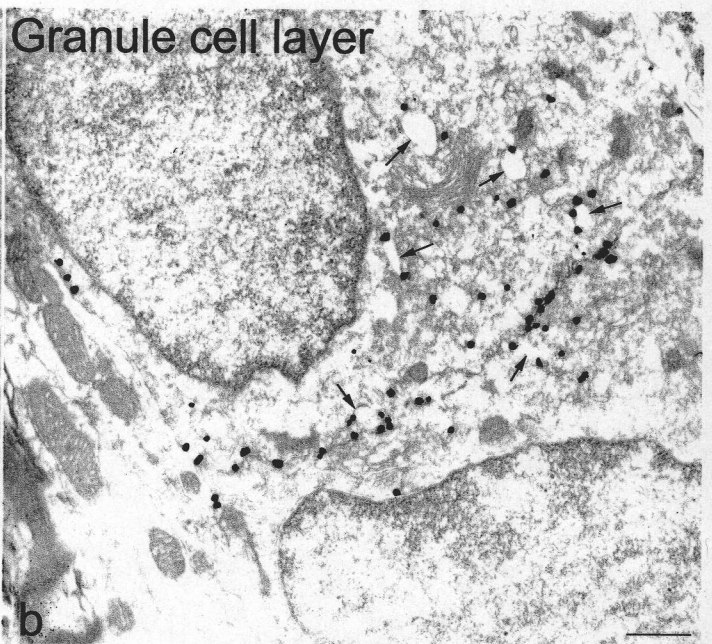
(a), Peroxidase reaction products for HCN2 are found in small cells having some clumps of heterochromatin along nuclear membrane. (b), Immunogold particles for HCN2 are localized along plasma membrane and endoplasmic reticulum (arrows). Scale bar, 0.4 $\mu$ m

CA3



a

Granule cell layer



b

**Table. 1 Density of HCN-LI in neuropil of the rat brain regions**

Intensity of HCN-LI was evaluated very intense (4), intense (3), moderate (2), weak (1) or back ground level (0) by comparing with internal standards as follows:

HCN1; stratum lacunosum moleculare in the CA1 area of the hippocampus (4), granular layer of the cochlear nuclei (3) and paraventricular thalamic nucleus (2).

HCN2; stratum lacunosum moleculare in the CA1 area of the hippocampus (4), granular layer of the cochlear nuclei (3) and caudate putamen (2).

HCN3; piriform cortex (4), anterior hypothalamic area (3) and granular layer of the cochlear nuclei (2).

HCN4; ventral lateral thalamic nucleus (4), paratenial thalamic nucleus (3) and granular layer of the cochlear nuclei (2).

C indicates presence of immunostained neuronal cell bodies and processes clearly visible at the light microscpic level as shown in Figs. 4c and 4d.

Note: The internal standards of the same grade do not necessarily have the same intensity of immunostaining among four HCN-LIs.

Names of the structure	HCN1	HCN2	HCN3	HCN4
<b>Olfactory bulb and associated region</b>				
<b>Main olfactory bulb</b>				
Glomerular layer	4	4	3	1
External plexiform layer	1	2	1	3
Mitral cell layer	1	1	0	1
Internal plexiform layer	2	4	4	2
Granular cell layer	1	2	1	1
<b>Accessory olfactory bulb</b>				
Glomerular layer	1	0	1	1
External plexiform layer	1	1	1	2
Mitral cell layer	1	1	1	0
Internal plexiform layer	1	1	4	1
Granule cell layer	2	0	1	1
<b>Anterior olfactory nucleus</b>				
External part	2-3	2	1	1
Dorsal part	2-3	2	1	0
Lateral part	2-3	2	1	1
Medial part	2-3	2	1	0
Posterior part	2-3	3	1	0
Ventral part	2-3	3	1	1
<b>Olfactory tubercle</b>				
Plexiform layer	3	3	3	2
Densocellular layer	1	1	0	0
Polymorph layer	2	1	1	2
Piriform cortex	3	4	4	2-3
Islands of Calleja	4	2	1	2
Indusium griseum	3	1	0	0
Tenia tecta	2-3	1	0	0
Dorsal endopiriform nucleus	2	2	2	1
Ventral endopiriform nucleus	2	1	1	1
Amygdalopiriform transition area	2	1	2	0
Bed nucleus of the accessory olfactory tract	1	0	0	1
Nucleus of the lateral olfactory tract	2	2	1	4
Semilunar nucleus	0	3	4	0
Cingulate cortex	3	2-3	1	1
Retrosplenial cortex	3	2-3	2	1
Lateral entorhinal cortex	3	1	1	0-1
Medial entorhinal cortex	3	1	1	0
Subiculum	4	2-3	0	0
Parasubiculum	3	2	2	1
Presubiculum	3	2-3	1	0-1
<b>Cerebral neocortex</b>				
Layer I	4	4	1	0
Layer II	3	2-3	1	1
Layer III	3	2-3	1	1
Layer IV	1	3	1	0
Layer V	2	1	0	0
Layer VI	1	2	0	0
<b>Hippocampus</b>				
<b>CA1</b>				
Stratum lacunosum moleculare	4	4	1	1
Stratum radiatum	1	1	0	0
Stratum pyramidale	2	1	1	1
Stratum oriens	2	2	0	0
<b>CA3</b>				
Stratum lacunosum moleculare	3	2	2	1
Stratum radiatum	2	1	0	0
Stratum lucidum	0	0	0	0
Stratum pyramidale	3	3	2	2
Stratum oriens	3	3	1	1
<b>Dentate gyrus</b>				
Molecular layer	2	2	2	0
Granule cell layer	3	1	0	0
Hilus	1	2	1	1
<b>Septal, preoptic and amygdaloid regions</b>				
<b>Septal nucleus</b>				
Lateral septal nucleus, dorsal part	3-4	1	1	0
Lateral septal nucleus, ventral part	3-4	2	1	0
Medial septal nucleus	2	3	2	2
Triangular septal nucleus	3	2	2	1
Bed nucleus of the stria terminalis	2-3	1	1	0
Nucleus of the diagonal band	2	3	3	1
Substantia innominata	2	1	2	0
Septohippocampal nucleus	1	3	0	1

<b>Preoptic nucleus</b>				
Medial preoptic area	1	0	1	1
Antero dorsal preoptic nucleus	2	1	3	1
Lateral preoptic area	1	2	2-3	1
Magnocellular preoptic nucleus	1	3	3	2
<b>Amygdala</b>				
Medial amygdaloid nucleus	2-3	1	1, C	1
Cortical amygdaloid nucleus	2-3	1	1	1
Anterior amygdaloid area	2-3	1	1, C	0
Central amygdaloid nucleus	2-3	1	0	0
Lateral amygdaloid nucleus	2-3	1	1, C	2
Basolateral amygdaloid nucleus	2-3	1	1	2
Basomedial amygdaloid nucleus	2-3	1	1	0
<b>Basal ganglia</b>				
Caudate putamen (striatum)	2-3	2	1, C	1
Accumbens nucleus	2	1	1	0
Ventral pallidum	1	3-4	3, C	2-3, C
Lateral globus pallidus	1	4	1-2	1-2
Medial globus pallidus	1	4	2-3	1
Clastrum	3	1	0	0
Substantia nigra pars compacta	2	2	4	2
Substantia nigra pars reticulata	0	3-4	2	2
Substantia nigra, lateral and medial parts	2	3	2	2, C
Ventral tegmental area	0	1-2	0	0
Subthalamic nucleus	1	3	4	2
<b>Thalamus</b>				
<b>Midline group</b>				
Paraventricular thalamic nucleus	2	1	3	1
Paratenial thalamic nucleus	2	3	2	3
Reuniens thalamic nucleus	2	3	1	1
<b>Anterior group</b>				
Laterodorsal thalamic nucleus	3	4	1	2
Anteroventral thalamic nucleus	3-4	4	1-2	2-3
Anteromedial thalamic nucleus	2	2	2	2-3
Anteromedial thalamic nucleus, ventral part	2	2	2	4
Anterodorsal thalamic nucleus	3	4	3	2
Intermediodorsal thalamic nucleus	1	1	2	2
Interanteromedial thalamic nucleus	2	2	2	2
Interanterodorsal thalamic nucleus	1	2	1	2
<b>Medial group</b>				
Mediodorsal thalamic nucleus	2	3	2	3-4
Submedius thalamic nucleus	1	3	0	4
<b>Intralaminar nuclei</b>				
Centromedial thalamic nucleus	1	2	3	1
Centrolateral thalamic nucleus	1	2	0	2
Parafascicular thalamic nucleus	1	2	1	2
Rhomboid thalamic nucleus	1	2	3	1
Paracentral thalamic nucleus	1	1	2	0
Rostral interstitial nucleus of medial longitudinal fasciculus	2	1	0	0
Prerubral field	2	1	1	0
<b>Lateral group</b>				
Lateral posterior thalamic nucleus	3	2	1	2
Posterior thalamic nuclear group	2	2	1	3
Suprageniculate thalamic nucleus	1	1	2	1
<b>Ventral group</b>				
Ventral anterior thalamic nucleus	3	3	1	4
Ventral lateral thalamic nucleus	3	3	0	4
Ventral medial thalamic nucleus	2	2	1	4
Ventral posterolateral thalamic nucleus	3	3	1	4
Ventral posteromedial thalamic nucleus	2	4	1	4
Ventral posterior thalamic nucleus, parvicellular part	2	3	0	4
<b>Geniculate complex</b>				
Medial geniculate nucleus	2	4	1	4
Dorsal lateral geniculate nucleus	2-3	4	2	4
Ventral lateral geniculate nucleus	1	4	2-3	1
Intergeniculate leaflet	0	1	4	1
<b>Epithalamus</b>				
Medial habenular nucleus	0	1-2	4	2-4
Lateral habenular nucleus	1	4	4	1
<b>Ventral thalamus</b>				
Reticular thalamic nucleus	0-1	4	2	2, C
Zona incerta	1	2	1	0
Subparafascicular thalamic nucleus, parvicellular part	1	1	2	0
<b>Hypothalamus</b>				
Supraoptic nucleus	0	2	3, C	2, C

Periventricular nucleus	0	1	1	1
Anterior hypothalamic area	1	2	3	1
Suprachiasmatic nucleus	1	0	3	2-3
Paraventricular nucleus	0	0	3-4, C	1, C
Ventromedial hypothalamic nucleus	3	1	2	0
Posterior hypothalamic area	0-1	2	2	1
Dorsomedial hypothalamic nucleus	2	2	3	0
Arcuate hypothalamic nucleus	0	0	1	2-3, C
Ventral tuberomammillary nucleus	0	1	3	1
Lateral hypothalamic area	0-1	1	4	1
Gemini hypothalamic area	2	2-3	2	0
Premammillary nucleus	1	3	4	2
Medial mammillary nucleus	3	3	2	2
Lateral mammillary nucleus	2	4	3	2
Supramammillary nucleus	1	2	3	0
<b>Sensory brain stem systems</b>				
<b>Visual</b>				
Superior colliculus				
Superficial gray layer of the superior colliculus	4	2	3	2
Optic layer of the superior colliculus	1	1	1	1
Intermediate gray layer of the superior colliculus	1	3	2	1
Intermediate white layer of the superior colliculus	1	2	1	0
Parabigeminal nucleus	1	2	2	0
Nucleus of the optic tract	1	0	1	0
Olivary pretectal nucleus	1	0	2	3
Precommissural nucleus	1	2	3, C	2, C
Anterior pretectal nucleus, ventral part	3	3	2	1, C
Anterior pretectal nucleus, dorsal part	2	4	3, C	1, C
Medial pretectal nucleus	1	2	3	1
Medial terminal nucleus of the accessory optic tract	2	0	0	2
<b>Somatosensory</b>				
Mesencephalic trigeminal nucleus	3	4	1	1-2
Principal sensory trigeminal nucleus	3	2	2	2
Spinal trigeminal nuclei, oral part	4	3	1	2
Spinal trigeminal nuclei, interpolar and caudal part	4	4	2-3	2
Paratrigeminal nucleus	4	4	3	2
External cuneate nucleus	3	4	2	2
Cuneate nucleus	3	3	2	2
Gracile nucleus	3-4	4	2	2
<b>Auditory</b>				
Dorsal cochlear nucleus	4	4	4	2-3
Ventral cochlear nucleus, anterior and posterior part	4, C	4	3, C	4, C
Granular layer of the cochlear nuclei	3	3	2	2
Inferior colliculus	4	2-3	1	2, C
Periolivary nucleus	4	4	4	2
Lateral lemniscus	4	4	3	4, C
Superior olivary complex	4	4	4	3, C
Superior paraolivary nucleus	2	3	2	2, C
Nucleus of the trapezoid body	2	3	2	2, C
<b>Vestibular</b>				
Vestibulocerebellar nucleus	3	2	2	2
Lateral vestibular nucleus	3	3	1	2
Spinal vestibular nucleus	1	3	1	2
Medial vestibular nucleus, magnocellular part	2	2	2	2
Medial vestibular nucleus, parvicellular part	3	4	3-4	2
Superior vestibular nucleus	2	3	3	2
Prepositus nucleus	3	3	3-4	1
Nucleus X and Y	3	1	3	0
<b>Gustatory and visceral</b>				
Nucleus of the solitary tract	0-1	0	3	1
Medial parabrachial nucleus	2	1	3	0
Lateral parabrachial nucleus	2	3	4	0
Area postrema	4	0	3	4
<b>Motor brain stem systems</b>				
<b>Eye</b>				
Abducens nucleus	2	3	2	1
Oculomotor nucleus	2	4	2	2
Supraoculomotor cap	2-3	4	3	1
Trochlear nucleus	2	4	2	2
Edinger-Westphal nucleus	0	2	0	1
<b>Jaw and face</b>				
Facial nucleus	2-3	3	1	1
Motor trigeminal nucleus	2	1	1	0
Accessory trigeminal nucleus	2-3	1	1	0
<b>Tongue and viscera</b>				
Hypoglossal nucleus	3	4	2	2

Ambiguous nucleus	3, C	2	3	1
Dorsal motor nucleus of vagus	1	0	4	1
Barrington's nucleus	1	1	2	1
<b>Reticular core</b>				
<b>Periaqueductal gray</b>				
Periaqueductal gray, medial and lateral	2	3	2	0
Dorsolateral periaqueductal gray	2	2	3	0
Anterior tegmental nucleus	2	2	2	4, C
Ventral tegmental nucleus	2	2	3-4	2
Dorsal tegmental nucleus	2-3	3-4	4	1
Laterodorsal tegmental nucleus	2	1	3	1
Microcellular tegmental nucleus	2	1	3	0
Pedunculopontine tegmental nucleus	0	1	2	3, C
Locus coeruleus	1	1	2	1
<b>Raphe</b>				
Dorsal raphe nucleus	2	1	2-3	1
Paramedian raphe nucleus	1	2	4	1
Median raphe nucleus	0	2	4	2, C
Pontine raphe nucleus	2	1	4	1
Raphe pallidus nucleus	1	1	2-3	1
<b>Interpeduncular nucleus</b>				
Apical subnucleus	0	3	4	2
Caudal subnucleus	2	3	4	2, C
Dorsolateral subnucleus	1	2	4	2
Dorsomedial subnucleus	0	1	4	2, C
Intermediate subnucleus	2	2	4	2
Lateral subnucleus	0	2	4	2
Rostral subnucleus	0	1	4	2
Rostrolateral subnucleus	0	1	4	2
<b>Reticular formation</b>				
Lateral reticular nucleus	2	3-4	1	2
Retrorubral nucleus (field)	1	1	3	1
Pontine reticular nucleus	1-2	2	1	0-1
Gigantocellular reticular nucleus	1-2	2	1	0-1
Medullary reticular nucleus	1-2	2	1	0-1
Cuneiform nucleus	1	2	3	1
Intermediate reticular nucleus	1	1	3	0
<b>Pre- and postcerebellar nuclei</b>				
Pontine nuclei	3	3	2	1
Parasolitary nucleus	1	0	4	0
Inferior olive, medial part	4	3	4	1
Inferior olive, other nuclei	4	2	4	1
Red nucleus, magnocellular part	2	3	0	2, C
Red nucleus, parvocellular part	2	3	0	2, C
<b>Cerebellum</b>				
<b>Cortex</b>				
Molecular layer	3	2	1	2
Purkinje cell layer	4	1	1	1
Granule cell layer	2	2	2	1
<b>Flocculus</b>				
Molecular layer	-	-	1	-
Purkinje cell layer	-	-	1	-
Granule cell layer	-	-	4	-
<b>Deep cerebellar nuclei</b>				
Interposed cerebellar nuclei	3	2-3	1	3
Lateral cerebellar nucleus	3	3	2	3
Medial cerebellar nucleus	3	2	1	2
<b>Fiber</b>				
cerebral peduncle, basal part	3	0	0	0
fornix	4	0	0	0
precommissural fornix	3	0	1	1
dorsal fornix	3	3	1	1
stria terminalis	3	1	0	0
internal capsule	2-3	0	0	1
stria medullaris of the thalamus	1	2	4	0
fasciculus retroflexus	0	0	4	4
pyramidal tract	2-3	0	0	0